The 6th ISSMGE McClelland Lecture: Time-dependent vertical bearing behaviour of shallow foundations and driven piles

R. J. Jardine
Imperial College London, UK

ABSTRACT: This paper considers the vertical bearing behaviour of shallow foundations and piles driven at clay, chalk and sand sites. It emphasises the strengths, when studying complex problems and natural geomaterials, of combining field experiments and full-scale monitoring with high quality site characterisation, element testing and representative numerical modelling. The main focus is on reporting and interpreting field observations that provide vital checks and benchmarks for modelling and identify key physical processes that might otherwise remain unrecognized. The latter include the time-dependent impacts on offshore foundation behaviour of consolidation, creep straining, geomaterial micro-to-macro fabric and in-situ chemical reactions. The case studies considered identify the key ageing mechanisms and the circumstances under which they may affect foundation design, service use or decommissioning procedures.

1 Introduction

Renewable energy related studies and projects were already becoming prominent at the 2012 Offshore Site Investigation and Geotechnics (OSIG) Conference at which Murff (2012) delivered the 1st ISSMGE McClelland Honours Lecture on ‘Estimating the capacity of Offshore Foundations’, setting out elegant limit analyses for problems encountered in oil and gas developments. The 2023 ‘Innovative Geotechnologies for Energy Transition’ OSIG theme reflects the increasingly large share of offshore geoscientists’ and geotechnical engineers’ work devoted to the urgent international need for lower carbon energy.

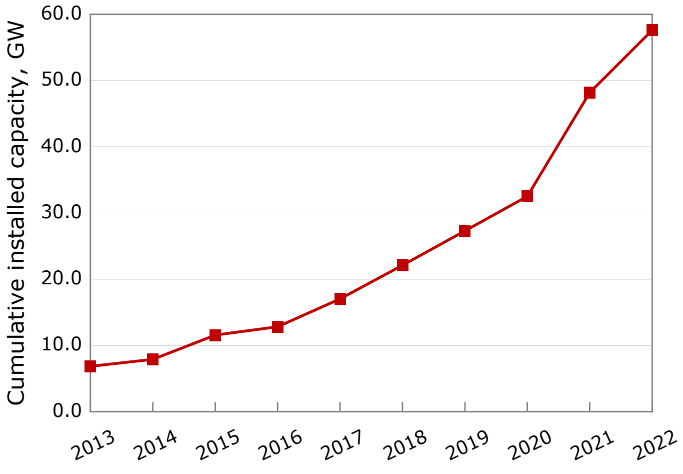

Figure 1. Development of offshore wind worldwide; data from World Forum Offshore Wind (2023).

The 2023 McClelland Lecturer set out his appreciation of geotechnical aspects of the ongoing energy transition in the 2016 Rankine Lecture on ‘Geotechnics, Energy and Climate Change’ (Jardine 2020). Figure 1 shows how total offshore wind capacity has increased since then, through development approaches that continue to flourish worldwide.

However, the questions Murff (2012) raised in relation to oil and gas remain equally relevant to current offshore challenges, and open to further investigation. This paper returns to consider how natural geomaterials’ complex properties, including those that are intrinsically time-dependent, affect offshore foundation behaviour, relying critically on field measurements to support the main arguments made.

Understanding and quantifying how foundation performance varies over time is central to modern whole life cycle project approaches; Gourvenec (2022). The potential benefits of installing foundations in advance of superstructures, or gradually building up maintained loads, may be central to design. The applicability of such strategies depends on the times required to achieve significant benefits and whether a staged construction sequence, and any additional ground movements it might generate, impinge on the foundations’ serviceability. Designers can also consider whether gains may be made by addressing the life cycle stages at which foundations need to cope with specified levels of extreme short-term loading events, such as storms or earthquakes.

Moving to field installation, understanding time-dependency is vital to interpreting, for example, pile driving or suction caisson penetration records. Ageing behaviour is a key issue in any in-service assessment of whether existing foundations can accommodate higher-than-originally specified loads to meet updated reliability, structural, plant, metocean, earthquake, marine growth or scour requirements.

The effects of ageing remain relevant up to the end of the foundations' working lives. Knowing the vertical uplift, pullout or push-over capacities that apply in the field after many years in service can be critically important when selecting the best options and field equipment to undertake foundation decommissioning.

Murff (2012), Randolph (2013) and Clukey (2022) showed in their McClelland Lectures the powerful insights that analysis and physical modelling can offer in complex offshore geotechnical problems. This Lecture emphasises the strengths, when studying complex problems and natural geomaterials, of combining field experiments and full-scale monitoring with high quality site characterisation, element testing and representative numerical modelling. Field observations provide vital checks and benchmarks for modelling and often identify important physical processes that might otherwise remain unrecognised, including the four time-dependent phenomena outlined below, which affect the field bearing behaviour of offshore foundations.

- Consolidation involving effective stresses, strains and states changing over time as pore pressures dissipate from initially out-of-equilibrium conditions towards steady average states. The geomaterials' effective-stress constitutive relationships may themselves be time or strain-rate dependent.
- Changes in geomaterial fabric that result from foundation loading or installation processes. These may involve micro-scale changes such as bonds breaking in cemented geomaterials, residual fabric developing on localised shear bands, sand grains breaking and re-morphing under shock or sustained load in sands, or the response shown by sensitive geomaterials that exist at natural states that cannot be sustained after experiencing large strains. Meso-to-macro scale changes may also apply, such as the time-dependent formation, or closure, of fractures in stiff clays or soft rocks.
- Creep processes in which geomaterial strains and states continue to vary time after reaching pore pressure equilibrium. In-situ effective stress regimes may also change in response, especially in any highly redundant system in which, for example, arching systems may develop or diminish over time.
- Chemical changes, including corrosion between steels and geomaterials, that may occur and influence load carrying capacity over time.

Offshore engineers employ many types of foundation to transmit multi-axial, monotonic and cyclic loads safely into a wide spread of potential seabed geomaterials. This paper focuses on a feasible sub-set of exemplar conditions. While recognising that other components and cyclic actions must be considered in offshore design (Erbrich et al. 2010, Jardine et al. 2012, Andersen 2015, Byrne et al. 2017, Jeanjean 2017), we consider only vertical monotonic loading. The scope is also limited to shallow foundations and driven piles installed at clay, chalk (a silt-sized, lightly cemented, very soft carbonate rock) and finally hard-grained (mainly silica) sand sites.

The main feature examined in Part 1 is how the ground beneath shallow foundations responds to long-term maintained loading. Raft, mat and pad foundations are treated, for simplicity, as though 'wished-in-place'. However, it is known that that dynamic offshore installation procedures can affect shallow foundations' performance in service, just as (for example) extended excavation exposures can lead to greater-than-expected settlements under onshore raft foundations; Hight and Higgins (1995).

Part 2 focuses principally on the effects of pile driving and the in-situ ageing processes it can trigger. The mechanisms that generate axial capacity variations over time are shown to be complex and to present new challenges for representative modelling.

The effects of maintained loading are also considered briefly in the second 'driven pile' part of the paper, although its effects have been investigated less extensively and appear to be more modest, at least for clay sites.

2 Part 1 – Time-dependent behaviour of shallow foundations

The first half of the paper concentrates on long-term field loading experiments involving shallow foundations. It offers insights that apply to offshore gravity base platforms, subsea structures and even pipelines. We consider first the response of a sensitive, 'structured' low apparent OCR, natural marine, clay to prolonged field loading, before moving to discuss stiff clay, chalk and quartz sand cases.

2.1 *Shallow foundations on clays*

2.1.1 *Low OCR clays*

Soft seabed clays are encountered worldwide in offshore engineering projects. While embedded 'skirt piles' are required to support heavy fixed Gravity Base structures at soft clay sites, relatively small subsea templates, pipeline end manifold (PLEM), pipeline end termination (PLET), or in-line tee (ILT) flowline structures, such as that shown in Figure 2, are often founded on mats. Pipelines and export cables also frequently need to rest on soft clay layers.

Natural erosion or mass movement processes can lead to mechanically overconsolidated states, especially on continental shelf or sloping seabed sections. Clays can also be found in geologically normally consolidated, or even under-consolidated, states in settings where deposition rates exceed those of erosion; see for example McClelland (1956), Moore et al. (2007), Kvalstad et al. (2005), Evans (2011), Kovacevic et al. (2012) or Young (2017). In-situ or laboratory testing often indicates finite 'crustal' strengths and apparent 'over-consolidation' related to biological/chemical bonding, or geological ageing; the same factors can augment the clays' shear strength anisotropy. It is common to find large populations of open, isolated, relatively large void spaces in such clays that have been deposited under low energy deep marine environments that lead to high liquidity indices; Skempton (1970), Burland (1990). Such microstructures can render the clays sensitive, brittle in shear, markedly strain rate-dependent and susceptible to sampling or foundation installation disturbance. They also lead to markedly non-linear consolidation and creep behaviour; see Hight et al. (2003).

Figure 2. Example of deepwater seabed, skid-founded, pipeline structure, with person for scale. Photograph from https://nainamania.files.wordpress.com

Wide foundation bearing areas are required to carry heavy facility loads on very soft clays. However, it is instructive to consider whether benefits may be gained from undrained shear strengths growing under imposed loads, as is common in multi-stage onshore flood defence or highway embankment construction; see Tavenas and Leroueil (1980), Nicholson and Jardine (1981), Ladd (1991) or Jardine (2002). Closed-form solutions are not available for undrained stability problems where S_u values vary with depth, location and time. However, staged construction is amenable to numerical analysis with well-formulated Critical State, or other, models that link consolidation and shear strength development; see for example Jardine and Smith (1991). Hydro-dynamically coupled modelling also offers the prospect of predicting rates of change in behaviour over time.

Analyses can be undertaken that recognise natural clays' anisotropy, structural sensitivity and strain rate dependency, and non-linear consolidation behaviour. See for example Zdravkovic et al. (2002), Karstunen et al. (2005), Karstunen and Yin (2010) or Panayides et al. (2012). However, the development, calibration and application of fully representative natural soft clay constitutive models remains a challenge for practice. High quality field tests provide a secure way of assessing potential design approaches and developing robust practical guidance.

2.1.2 *Field experiments on soft, structured, Bothkennar clay*

Jardine et al (1995) and Lehane et al (2003) report experiments, undertaken between 1990 and 2001, on square reinforced concrete pads with 2.2m and 2.4m widths B, at the UK's Bothkennar (then) national soft clay test site, located on the Firth of Forth in east Scotland. The field tests, which were instrumented as shown in Figure 3, started as an adjunct to Lehane's (1992) PhD study of displacement pile behaviour at this and other sites. They followed the extensive characterisation study reported in Geotechnique's June 1992 edition of the very soft-to-soft Holocene silty shallow-marine 'Carse' clays encountered, whose profile is summarised in Figure 4. The clay's high plasticity results in large part from its organic content, expressed here as 'loss on ignition'. The clay's depositional environment and organic activity contribute to high liquidity indices and a lightly biologically cemented sensitive structure which, along with seasonal variations contribute to the plotted profiles of oedometer Yield Stress Ratios (YSR = σ'_{vy}/σ'_{v}) and field vane S_u^{FV}.

Best practice sampling, laboratory trimming and consolidation procedures were developed and applied in comprehensive, high-resolution, stress-path testing on locally instrumented top-quality samples by Hight et al. (1992), Smith (1992), Smith, Jardine and Hight (1992), who characterised the clay's brittle behaviour in triaxial stress space and showed how it 'de-structures' and develops large creep strains when consolidated along 'radial' triaxial effective stress paths covering a wide range of dq/dp' gradients. Their tests showed an ≈3.1 ratio between peak triaxial compression and extension S_u values; Albert et al. (2003) and Jardine et al. (2004) confirmed the clay's anisotropic S_u and stiffness characteristics further through hollow cylinder apparatus and small strain triaxial probing experiments. Leroueil et al. (1992) and Nash et al. (1992) investigated the clay's hydraulic conductivity and strain rate dependent behaviour under oedometer and other conditions.

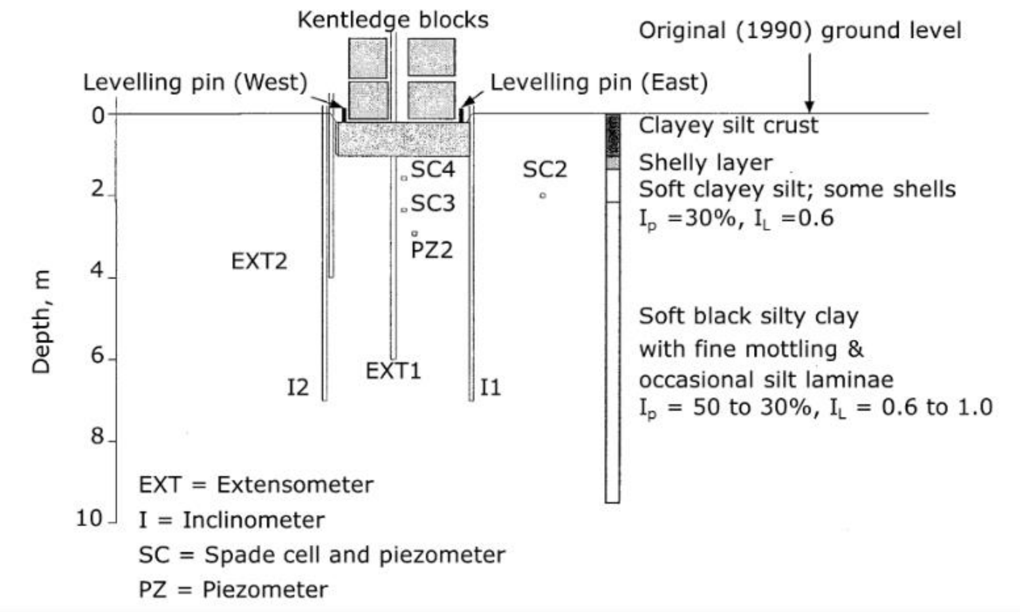

Figure 3. Instrumentation of Bothkennar reinforced concrete pad employed for Tests B and C. Average pad settlements assessed from North, South, East and West levelling targets.

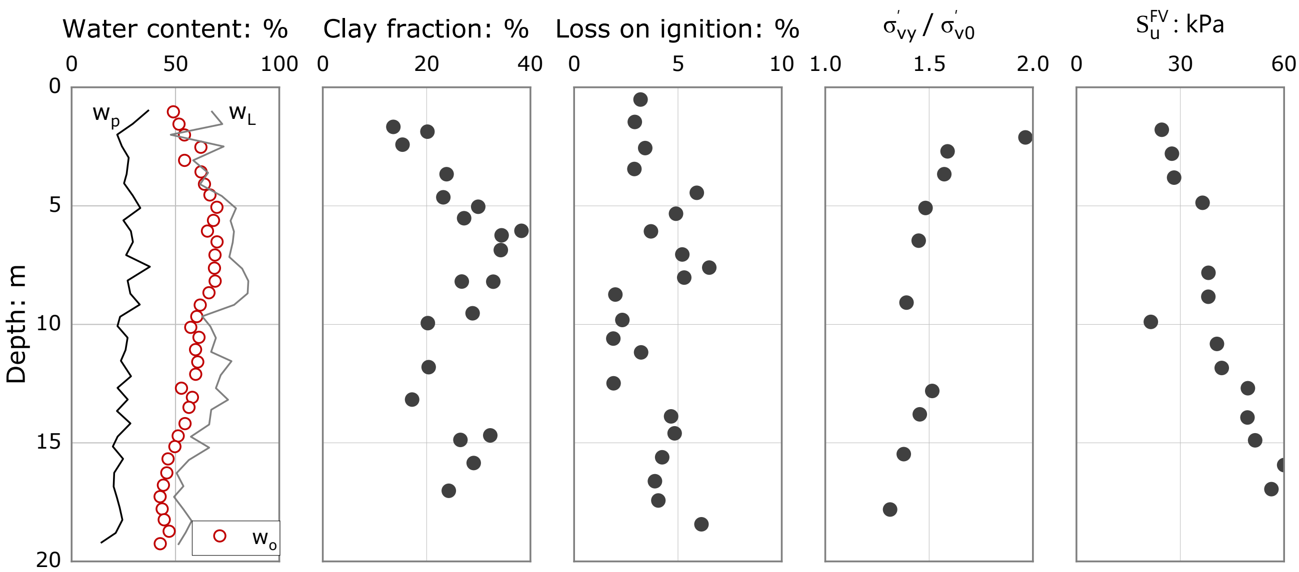

Figure 4. Bothkennar profile, showing Atterberg plastic (w_P) and liquid (w_L) limits, water contents (w), clay fraction, organic content from loss on ignition, oedometer yield stress ratios (YSR = $\sigma'_{vy}/\sigma'_{v0}$) and field vane undrained shear strength S_u^{FV} profile; re-drawn from Leroueil et al. (1992).

The first experimental objective was to establish how the operational foundation S_u values, as back-analysed with Davis and Booker's (1973) solutions from a pad loading test to failure, compared with the wide range of S_u values indicated by alternative in-situ and laboratory approaches. The second aim was to check how bearing capacities might evolve over time under maintained loads. It was recognised that the stresses imposed through the pads would spread radially with depth and that any long-term S_u gains would be localised in the most heavily loaded areas.

The testing sequence involved loading, in Test A, one pad to failure over 2.5 days by carefully applying small increments of deadweight loading. Pause periods were imposed between each load step to ensure that multiple measurements could be made safely until the average short-term pad settlement reached $\approx B/10$. With this 'bearing capacity' known, the second pad was loaded in Test B to 2/3 of the failure bearing pressure and left to settle for 11 years while instrument monitoring and optical surveying continued at a gradually reducing frequency. The excess pore pressures dissipated fully within the first year and approximately 35% of the long-term (post loading) settlement occurred after full hydraulic equilibrium had been achieved. After 11 years of maintained loading, this pad was also brought to failure over $\approx$2.5 days in Test C by adding further kentledge carefully until the foundation developed an additional average settlement of ≈B/10.

The key outcomes are summarised in Figure 5 by plotting the three tests' average vertical load-settlement behaviour, while Figure 6 presents the settlement-log time trend from the 11 year long maintained load stage of Test B. Jardine et al. (1995) noted that the average operational field undrained shear strength back-analysed from Test A amounted to 74% of the peak S_u afforded by undrained triaxial compression tests (conducted at an axial strain rate of 5% per day) on K_0 consolidated specimens, trimmed carefully by thin wire from top quality Sherbrooke 'block' samples. They concluded that the relatively minor 26% shortfall could be ascribed to the sensitivity, anisotropy and modest, brittle, bio-cementation identified in the clay's micro-fabric.

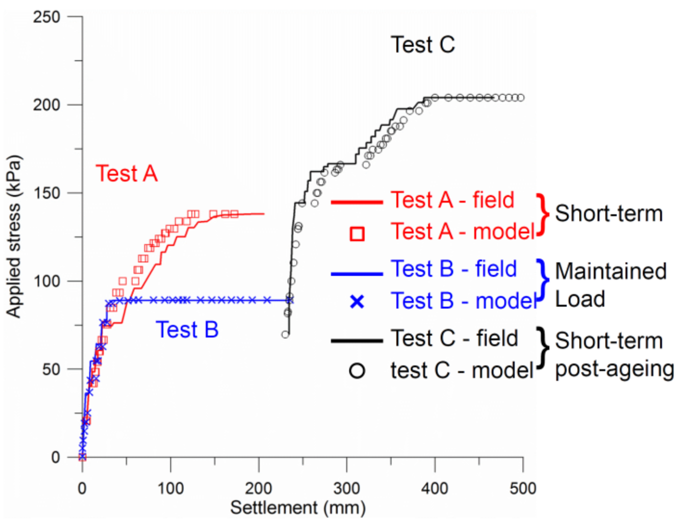

Figure 5. Load-settlement behaviour of Bothkennar rigid pads in Tests A, B and C, field data after Lehane and Jardine (2003) and FEM predictions from Bodas Freitas et al. (2015).

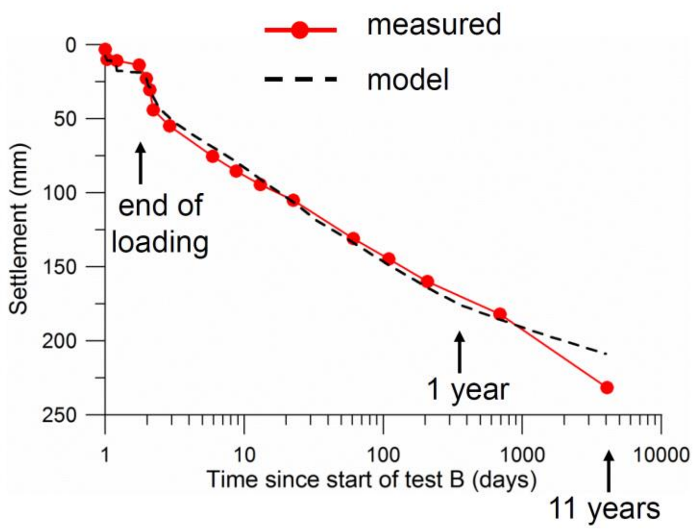

Figure 6. Settlement-time behaviour of Bothkennar rigid pad in Test B; field data after Lehane and Jardine (2003) and FEM predictions from Bodas Freitas et al. (2015).

Lehane and Jardine (2003) describe how Test C exhibited an initially stiff response to additional loading and ultimately manifested a 48% higher bearing capacity than Test A due to its long-term maintained vertical loading. Considering first the influence of consolidation, Lehane and Jardine (2003) compared the field gain in capacity with results from generic FE analyses by Zdravkovic et al. (2003) that employed a strain-rate-independent Modified Cam Clay (MCC) variant to assess how consolidation under load affected rigid footings. These analyses, which covered a range of initial OCRs and ratios of maintained loads to initial bearing capacities, employed input parameters that were considered well-suited to modelling soft clay stability problems.

However, the numerical modelling indicated significantly lower-than-measured capacity gains and Jardine et al. (2005) postulated that the disparity might be linked to two features of soft clay behaviour that had not been captured analytically: long-term creep straining and a potential re-alignment under load of the clay's anisotropy towards a pattern that better accommodated the stress regime generated by pad loading, as explored in Hollow Cylinder laboratory experiments by Zdravkovic and Jardine (2001).

Bodas Freitas et al. (2015) describe how a modified strain-rate-dependent elastic–viscoplastic (EVP) Critical State model was introduced into the FE code employed (ICFEP) to allow site-specific analyses of the pad tests, with clay parameters calibrated to Smith et al's (1992) laboratory experiments, which had included studies of the clay's time-dependent behaviour.

The new analyses provided the excellent hindcasts shown in Figures 5 and 6. Figure 7 shows the predicted evolution of the S_u profile under the pad centre-line as the clay consolidated and then crept under constant load; S_u gains are confined to the first 5m or ≈2B of clay, reflecting the spread of vertical stress with depth in combination with the initial YSR profile shown in Figure 4.

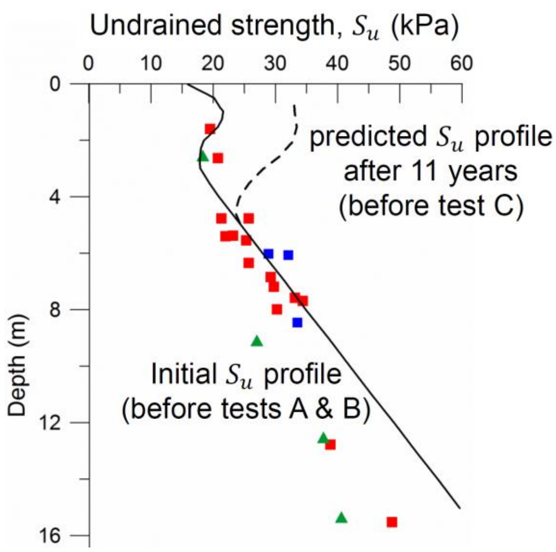

Figure 7. S_u under Bothkennar rigid pads. Continuous S_u profiles: FEM predictions by Bodas Freitas et al. (2015). Solid symbols show pre-construction CAU triaxial tests on Laval (red), Sherbrooke (blue) and Japanese piston (green) samples.

Zwanenburg and Jardine (2015) subsequently conducted larger scale instrumented rigid pad tests over peat deposits, near Markermeer in The Netherlands, that identified their initial vertical bearing capacity, and demonstrated how it improved under maintained load through consolidation and creep.

2.1.3 *Potential time-dependent capacity of spread foundations on stiff clays*

Stiff clays are also encountered at shallow depths across multiple offshore continental shelf areas, including much of the glacially loaded areas of the North and Baltic Seas, as well as the US East coast.

Raft foundations have been employed to support large gravity base structures (GBS) on relatively competent stiff clays and shallow foundations; they are also adopted routinely for smaller subsea facilities.

The high yield stress ratio (YSRs), or apparent OCRs, of stiff glacial clays were generated by more complex depositional processes than simple K_0 unloading; see Cotterill et al. (2012) or Ushev and Jardine (2022). Whether sustained loading leads to significant gains in short-term bearing capacity with such clays depends on how their undrained shear strengths grow with increasing effective stresses.

Clays, such as un-fissured low plasticity North Sea glacial tills, that behave as expected in classical Critical State models, develop relatively modest S_u gains over the range of pressures that are likely to be applied in practice. This is illustrated in Figure 8 by triaxial compression tests reported by Ushev and Jardine (2022) on Bolders Bank till samples from the Cowden PISA test site, which showed vertical oedometer yield stresses σ'_{vy} of 500 to 800 kPa.

Consolidation to mean effective stresses p'_0 higher than the undisturbed in-situ values, but below the till's oedometer yield σ'_{vy} pressures, led to a relatively flat relationship between S_u and p'_0, with S_u growing by less than 50% after imposing a more than five-fold increase in p'_0 and allowing extended (drained) periods for creep rates to stabilise to low values.

Staged preloading of shallow foundations installed over the broadly similar sandy, silty, stiff glacial clays, which extend over wide areas of the North and Baltic Seas, can be expected to deliver far less impressive relative bearing capacity gains than seen at Bothkennar.

However, the field bearing capacities available with more plastic, often fissured and extensively faulted, marine clays including the Tertiary London Clay and related units which extend from SE England to Belgium and Northern France, are generally lower than might be expected from their relatively high oedometer yield stresses. This results from their tendency to develop brittle strain localisations at early stages of shearing that truncate their undrained effective stress paths soon after the onset of dilative (pore pressure decreasing) behaviour. The resulting relatively low peak shear resistances are illustrated in Figures 8, 9 and 10 by adding triaxial experiments (from Gasparre 2005 and Hight et al. 2007) on London Clay samples taken at similar depths. Such clays' brittleness promotes progressive failure most readily when effective stresses reduce over time, as in excavation works; see Kovacevic et al. (2007).

The London clay samples had markedly higher oedometer yield stresses (2 MPa < σ'_{vy} < 3 MPa) than at Cowden, reflecting its greater ages and burial depths. However, under suitably stable loading conditions, the London Clay's micro-fabric promotes a more direct link between S_u and p'_0 that can lead to more significant improvements in bearing capacity through consolidation to higher effective stresses.

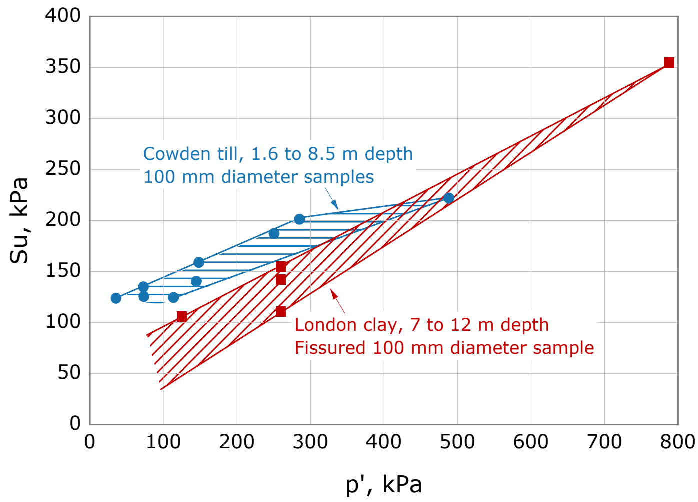

Figure 8. Relationships between isotropic consolidation pressure p' and triaxial compression undrained shear strength S_u for high YSR Cowden till and London Clay specimens from similar depths tested from similar pressures, which are all below their oedometer σ'_{vy} yield pressures.

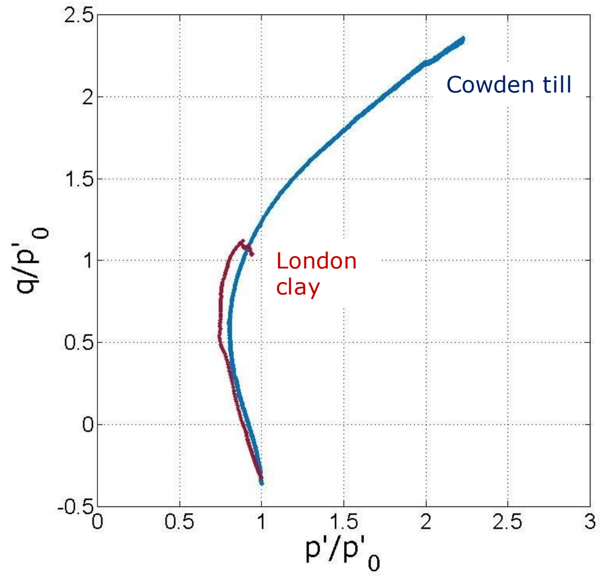

Figure 9. Deviator stress q, versus mean effective stress p' undrained effective stress paths, normalised by consolidation p'_0, from typical CAU compression tests on Cowden till (in blue) and London clay (in red) from ≈6m depth, after Jardine (2020).

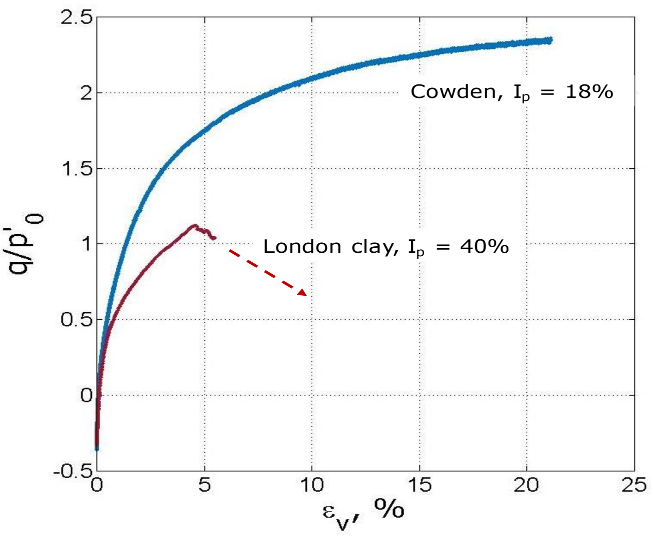

Figure 10. Normalised stress-strain curves from typical CAU triaxial tests on Cowden till and London clay from ≈6m depth; ε_v = vertical strain, I_p is plasticity index. After Jardine (2020).

Older Paleogene, Cretaceous and Jurassic high YSR plastic clay formations including the Baltic Femern and (North Sea) Gault, Kimmeridge, Lias and Oxford Clays have been encountered in many offshore projects. These respond in broadly similar ways to the London Clay, see Heilmann-Clausen (1984), Japsen and Bidstrup (1999), GEO (2011), Hosseini Kamal et al. (2014) or Brosse et al. (2017). Their brittle post-peak behaviour has many implications for offshore foundations including greater scope for taking benefits from pre-loading mats or rafts, despite the clays' high YSR values. As shown later, residual shear band formation also has an important influence on the axial capacity piles driven in such clays.

However, the stiff clays' typically low void ratios usually result in relatively low permeabilities, especially in the more plastic clays, and relatively long field consolidation times, unless the clays are parted by more permeable coarser laminae or open fissures.

While load-displacement behaviour is not the main theme of this paper, we note that extensive field monitoring has confirmed that locally instrumented triaxial tests on high quality samples, combined with fully non-linear numerical analysis, offers a representative means of predicting medium-term foundation load-displacement behaviour accurately for soft and stiff clay sites; see Jardine et al (1991), (2005). As with soft clays, stiff plastic clays are likely to creep significantly under load; Mesri and Vardhanabhuti (2006) showed that oedometer $c_{\alpha e} = \Delta e/\log t$ secondary consolidation coefficients correlate directly with compressibility C_c and often plasticity index I_p. Long-term creep movements can be expected at clay sites that are not captured by routine numerical modelling analyses employing rate-independent soil models.

2.2 *Shallow foundations on Chalk*

Chalk is encountered widely across northern Europe, under the North and Baltic seas (Mortimore 2013), parts of the eastern Mediterranean and Middle East and in other locations worldwide, including Austin, Texas. It is composed of mainly silt sized, biologically-bonded, $CaCO_3$ grains that are often hollow. Its UCS strengths typically fall between 1 and 20 MPa and correlate with dry density; Clayton et al. (1994).

Despite their Cretaceous age and considerable prior burial depths, low-to-medium density chalks retain high liquidity indices and can be reduced to very soft putty states by dynamic compaction applied at their natural water contents, indicating equivalent undrained shear strength sensitivities up to 100; see Lord et al. (2002), Jardine et al. (2018), Doughty et al. (2018) or Liu et al. (2023). As discussed later, this *micro*-fabric feature has profound effects on the behaviour of piles driven in chalk.

The chalk is often extensively fractured and jointed and this *macro*-fabric can dominate load-displacement behaviour with all types of foundations at chalk sites; Lord et al. (2002). The chalk's cementation, highly sensitive natural structure, brittleness, and fissuring tend to diminish progressively under high pressure consolidation; Leddra et al. (1993).

Figure 11 presents data from locally instrumented triaxial tests conducted from in-situ effective stress levels on high quality samples of intact low-to-medium chalk from the ALPACA piling JIP chalk test site at St Nicholas at Wade (SNW, Kent, UK); after Vinck et al. (2022). These show very high (typically over 4 GPa) initial vertical Young's moduli over nearly linear ranges of stress-strain response, before displaying marked brittleness after failing at relatively small axial strains (often less than 0.1%), confirming earlier findings by Jardine et al. (1984) (1985) from tests on stronger and denser (1.6 Mg/m^3 dry density) chalk from Northfleet (Kent, UK) whose stiffness maxima exceeded 5 GPa.

Experiments conducted by Liu et al. (2023) over a wide pressure range, identified the strongly curved peak shear strength envelope shown in Figure 12. Other tests demonstrated marked stiffness anisotropy under low pressures, with far lower horizontal than vertical stiffness (Vinck et al. 2022).

The SNW tests also showed considerable creep straining under modest stress levels, reflecting fissures closing and opening. Creep is also highly significant under high pressures that cause the chalk's sensitive micro-structure to gradually collapse. The latter features led to widespread, highly time-dependent, compaction settlements developing above the chalk reservoir rocks of the Norwegian Ekofisk offshore field as hydrocarbons were produced; Leddra et al. (1993).

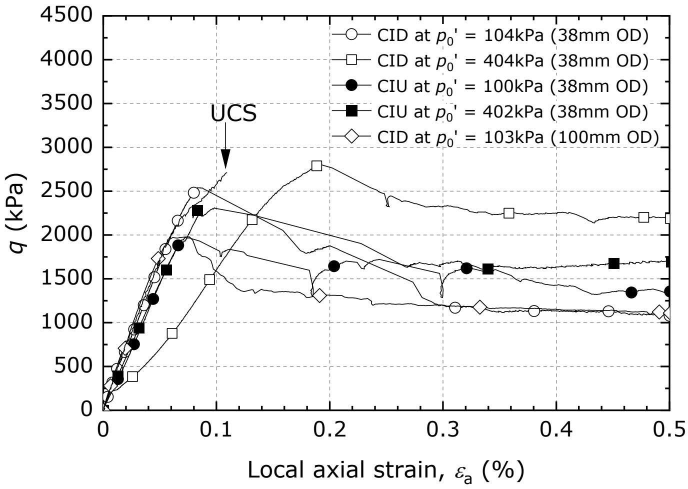

Figure 11. Example of stress-strain curves up to 0.5% axial strain from locally instrumented CIU and CID triaxial tests, after Vinck et al. (2022).

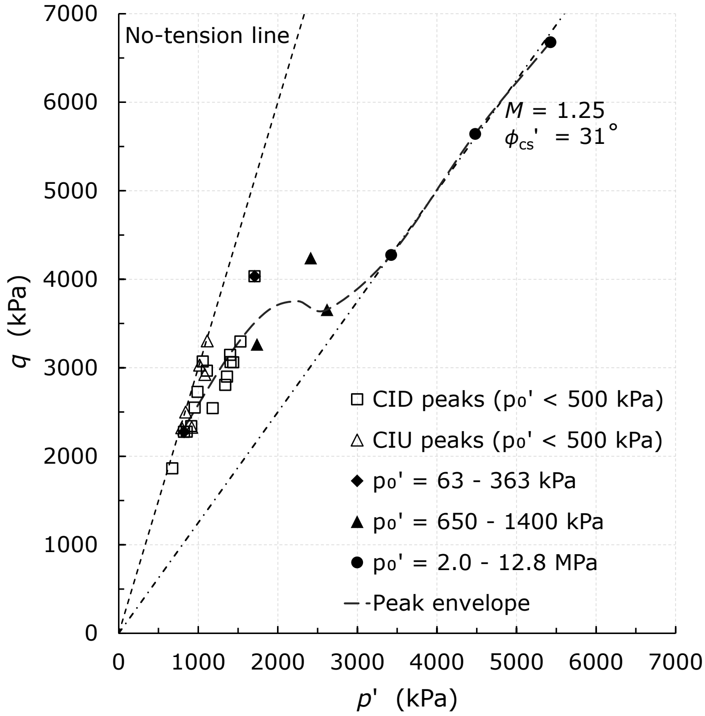

Figure 12. Curved failure envelope from high pressure tests on SNW chalk, after Liu et al. (2023).

As discussed in Part 2, driven pile capacities have been difficult to predict reliably in chalk. GBS foundation solutions have been chosen for some projects including the Fécamp windfarm offshore Le Havre, Normandy, France, where seventy-one, 7 MW, turbines rest on 31m diameter rafts, as shown in Figure 13.

Chalk's brittleness, sensitivity, pressure-dependency and variable systems of potentially open micro-to-macro fractures affect field testing. Recognising these features is vital to understanding how such foundations behave under load, over time. The following sections summarise relevant historical field investigations into how mat and raft foundations behave on chalk.

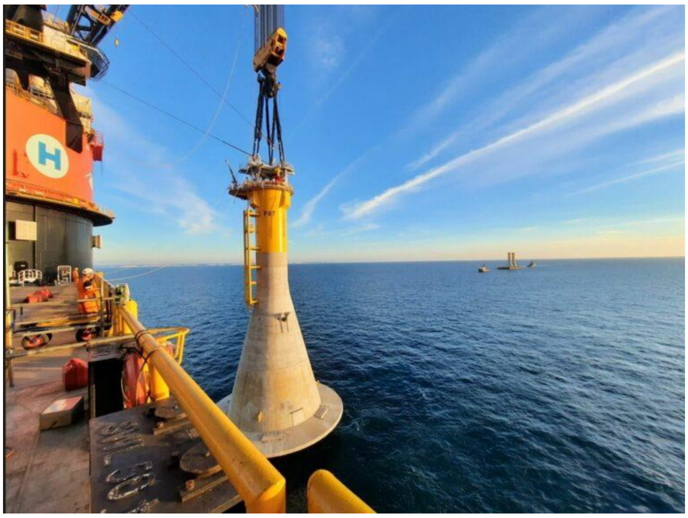

Figure 13. Installing GBS support structures on chalk for 71 (seven MW) wind turbines at Fécamp wind farm offshore Le Havre, France. Photograph from Heerema Marine Contractors.

2.2.1 *Instrumented loading tests at Mundford*

Ward et al. (1968) described intensive field investigations undertaken by the UK's Building Research Establishment (BRE) at a chalk site near Mundford, in Norfolk, England to assess the suitability of the local chalk for the potential construction of a very sensitive CERN large proton accelerator tunnel. Their seminal study confirmed that the chalk's monotonic field bearing behaviour depends critically on it its natural macro-fabric.

Ward et al. (1968) conducted 19 loading tests with an 864mm diameter (B) plate loading test system in three shafts bored to a maximum depth of 22.7m, in addition to the large-scale loading trial illustrated in Figure 14. The latter involved a raft-founded 18.3m diameter tank, under which they monitored the chalk's vertical straining with very high-resolution equipment. The chalk's systems of fractures led to essentially drained behaviour under loading.

Ward et al. (1968) divided the chalk into five grades. Their log of the chalk's structure is summarised in Figure 14, along with the subsequently developed CIRIA grades (see Lord et al. 2002) which were kindly assigned by Professor Rory Mortimore to aid the Author.

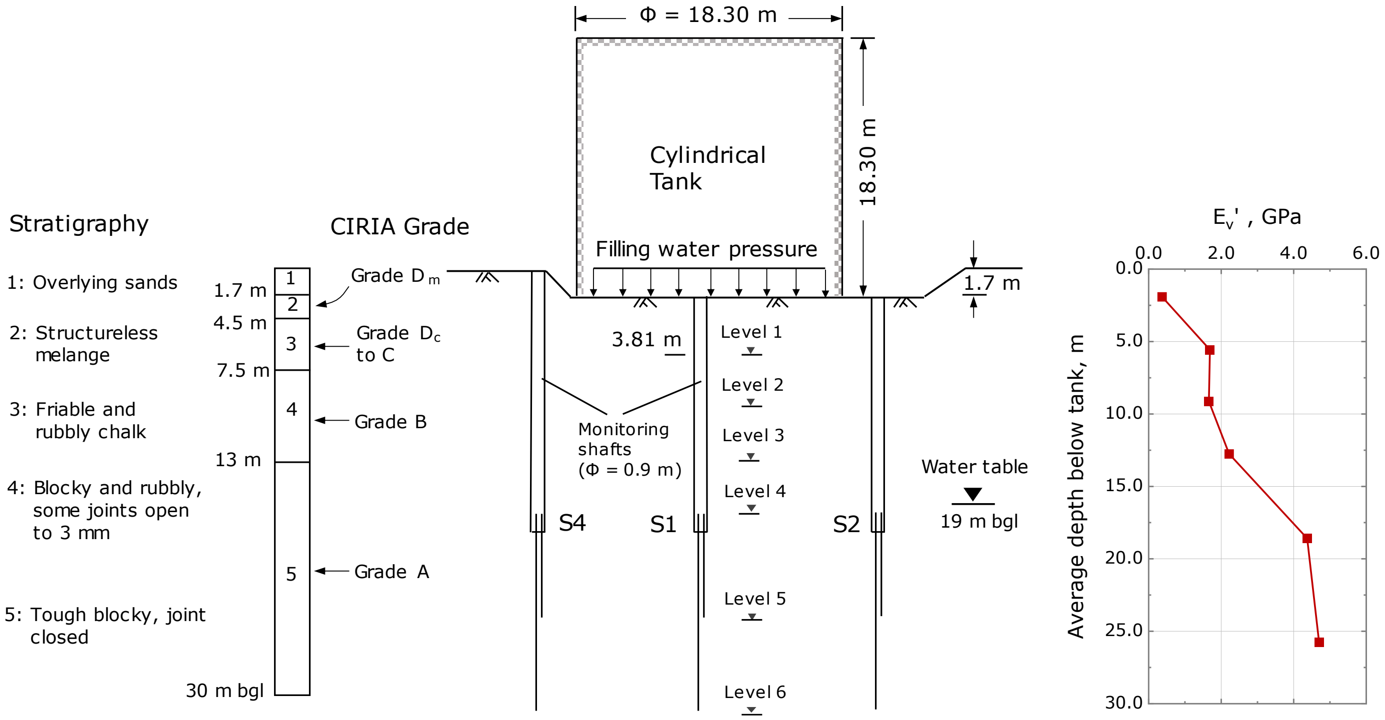

Figure 14. Mundford chalk and 18.3m diameter loading tests, modified from Ward et al. (1968).

The maximum vertical stiffnesses interpreted from the consistently linear initial loading stages of the plate loading tests through classical elastic solutions are also shown in Figure 14. The plate tests were limited to displacements less than 1mm (or 1.25 $*10^{-3}$ B) and developed bearing pressures as high as 1.5MPa and manifested a first form of yielding (also termed Y_1 by Jardine 1992a) after reaching the ends of their initially linear ranges but stopped far short of the B/10 test settlement limit at which plate failure is often defined.

The plate and tank tests indicated similar profiles of elastic vertical drained Young's moduli E_v' with depth, growing from 370 MPa in structureless Grade D_m chalk to over 4 GPa in the deepest (Grade A) structured chalk layer, whose joints were logged as being tightly closed.

Unconfined compression tests on intact (un-fissured) strain-gauged samples from a range of depths gave a far narrower 5.4 GPa $\leq E_v' \leq$ 6.8 GPa range of vertical stiffness. The ratio of mass (field) to laboratory stiffness rose from ≈0.3 in Grade B to C chalk to ≈0.7 in the deeper Grade A layers, reflecting the frequency of joints and fissures and the degree to which they were open or closed. Such behaviour, which is common in fractured rocks (see for example Hight and Higgins 1995) could not have been gauged reliably without undertaking the loading experiments.

The large tank applied a maximum bearing pressure of 183 kPa which, as shown in Figure 15, led to an overall average short-term displacement of just 1.2mm, or 6.5 $*10^{-5}$ *B*.

An extended, four-month duration, final loading stage led to the settlements recorded under the centreline shaft at the shallowest level (S1) increasing by 42%. No creep was recorded in the higher-grade chalk below Level 3, whose elastic straining recovered fully after unloading the tank.

It is reasonable to conclude that the creep settlements were primarily associated, under the 183 kPa load imposed, with partial fracture closure in the lower grade chalk.

While the intact chalk blocks experienced only modest average stress increments compared to their intact strength, intense local stress concentrations naturally develop around any asperities that bridge otherwise open gaps between the blocks. Time-dependent yielding of the asperities allows the gaps to close progressively over time, leading to improved unload-reload foundation stiffness.

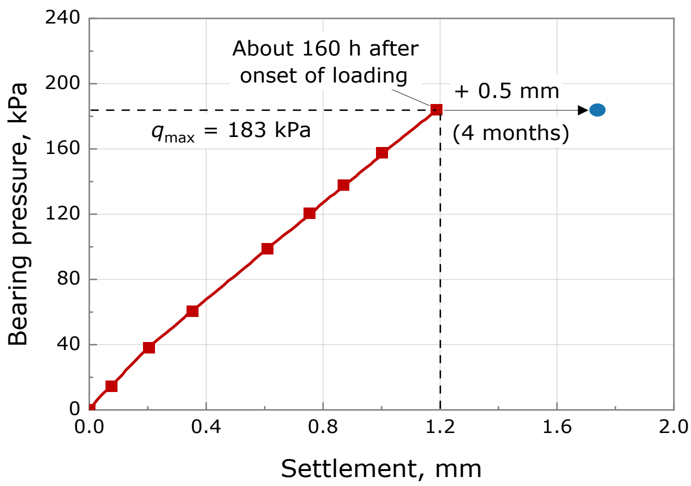

Figure 15. Load displacement behaviour at Mundford loading test, redrawn from Ward et al. (1968).

2.2.2 *Large plate loading tests at other chalk sites*

Matthews and Clayton (2004) report a suite of nine near-surface, more heavily loaded, plate tests at three weathered chalk sites located in the east of England. Their tests with a high capacity, 1.8m diameter, rigid steel plate loading system at North Ormsby (NO), Leatherhead (LE) and Needham Market (NM), concerned high, medium and low-density outcrops respectively.

Careful surveying of the chalk macro-fabric profiles with depth at each location distinguished 'structureless' and 'structured' chalk units, as well as the fissuring and presence of flint bands. Table 1 lists the sites' CIRIA grades, following Lord et al. (2002), as well as average laboratory measurements of density, UCS strength and maximum E'_v stiffness from triaxial tests equipped with high resolution axial strain sensors on intact samples. The laboratory UCS and E'_v values increased systematically with dry density. However, the lowest density site had the least fracturing and highest CIRIA grade.

Matthews and Clayton report three plate-loading tests at each location. Superficial material was removed before installing the plates at depths between 100 and 600mm on concrete blinding and plaster finished bases that reduced the 'bedding errors' that would otherwise lead to misleading plate settlements.

As shown by the representative examples plotted in Figure 16, the tests developed maximum settlements ranging from ≈12 to ≈95mm, with none approaching the 180mm (or D/10) displacement level required to define a conventional 'geotechnical' failure. As at Mundford, all showed linear initial portions up to the 1st 'yield' pressures listed along with the average E'_v maxima in Table 1. The plate tests' initial stiffness maxima represent only 2 to 11% of the laboratory maxima.

The yield stresses show similar trends. The yield pressures are interpreted as reflecting the open joints starting to close within the chalk mass at stages that correlate with the condition of the chalk's fractures and not with density or UCS. Yielding may also be related to local failure initiating around the plate perimeter, as noted analytically by Jardine et al. (1986).

Returning to the chalk's time-dependency, the dense North Ormsby site tests included one extended (40 day long) experiment where q_{mob} was maintained at 900 kPa, or ≈2/3 of the maximum applied. The settlement increased by around 40% over the 40 days, confirming that loading beyond the 1st yield pressure leads to significant creep, even at dense chalk sites.

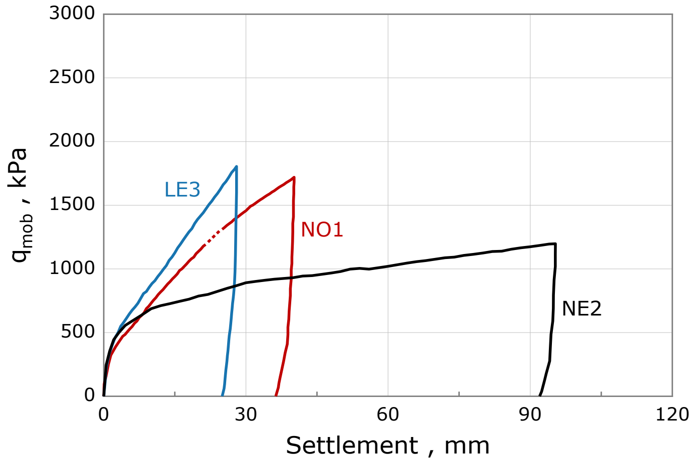

Figure 16. Summary of 1.8m plate load tests on weathered chalk at NO, LE and NM sites; Matthews and Clayton (2004).

Short term plate tests, when conducted on ductile, mean effective-pressure-independent, 'Tresca' geomaterials would be expected to develop (after a settlement ≈ D/10) failure loads q_{ult} = UCS x N_c/2, where $6.2 \leq N_c \leq 6.4$, depending on each pad test's embedment depth (which varied slightly from case-to-case).

However, the maximum bearing pressures applied (and plotted in Figure 16) represent q_{mob}/UCS ratios of just 0.14 to 1.44. While the plate tests only extended to reach 1.5% to 5% of their diameter *D*, extrapolation of their trend lines suggests that none was likely to have approached the limiting 3.2 ±0.1 q_{mob}/UCS ratio expected for a Tresca material.

Recalling that chalk shows principally drained behaviour under field loading (Lord et al. 2002) and noting the curved low-to-medium density SNW failure envelope illustrated in Figure 12, suggests that the disparity between the peak shear strengths implied by chalk element tests and the field plate q_{ult} values is still greater than indicated by the comparison made above based on *UCS* strengths. The chalk's fracturing and brittleness must be invoked to explain the anomalously soft field bearing pressure trends.

A numerical investigation by Pedone et al. (2023) of the ALPACA lateral loading tests on piles driven in un-weathered SNW chalk drew similar conclusions, as did Wen et al (2023a) from analyses of the ALPACA JIP's axial pile load tests.

Table 1. Summary of chalk conditions and 1.8m diameter plate test outcomes for three weathered chalk sites in East England; after Matthews and Clayton (2004).

Parameter	North Ormsby (NO)	Leatherhead (LE)	Needham Market (NM)
Average dry density, Mg/m^3	1.89, Dense	1.54, Medium	1.34, Low
CIRIA grades	C4/5 grading to B3	Dc grading to B3/4 and B3/2	B4/5 grading to B3
Average UCS, MPa	12	3	0.9
Average lab max E'_v, GPa	17	9.7	7.6
Average field max E'_v,MPa	365	573	842
Ratio of field/lab E'_v maxima	0.02	0.06	0.11
Average 1st yield stress, kPa	217	200	300

Combining site logging of fracture patterns with brittle, effective-stress-based, constitutive models calibrated to the Vinck et al. (2022) and Liu et al. (2023) laboratory tests allowed accurate numerical load-displacement modelling of the instrumented lateral pile tests described by Jardine et al. (2023a).

Allowing for the NO, LE and NM sites' more highly weathered profiles, and the differences between mass and single element chalk properties is central to representative numerical modelling of the 1.8m diameter plate loading tests.

2.3 *Shallow foundations on hard grained sands*

Hard grained, mainly quartz, sand deposits are also encountered widely in offshore and onshore development areas. Competent dense sands are common, for example in the southern North Sea and German Bight; Cathie et al. (2022). These offer scope for raft foundations as at the Thornton Bank windfarm, offshore Belgium, where the wind turbines illustrated in Figure 17 rest on dense sands and stiff clays.

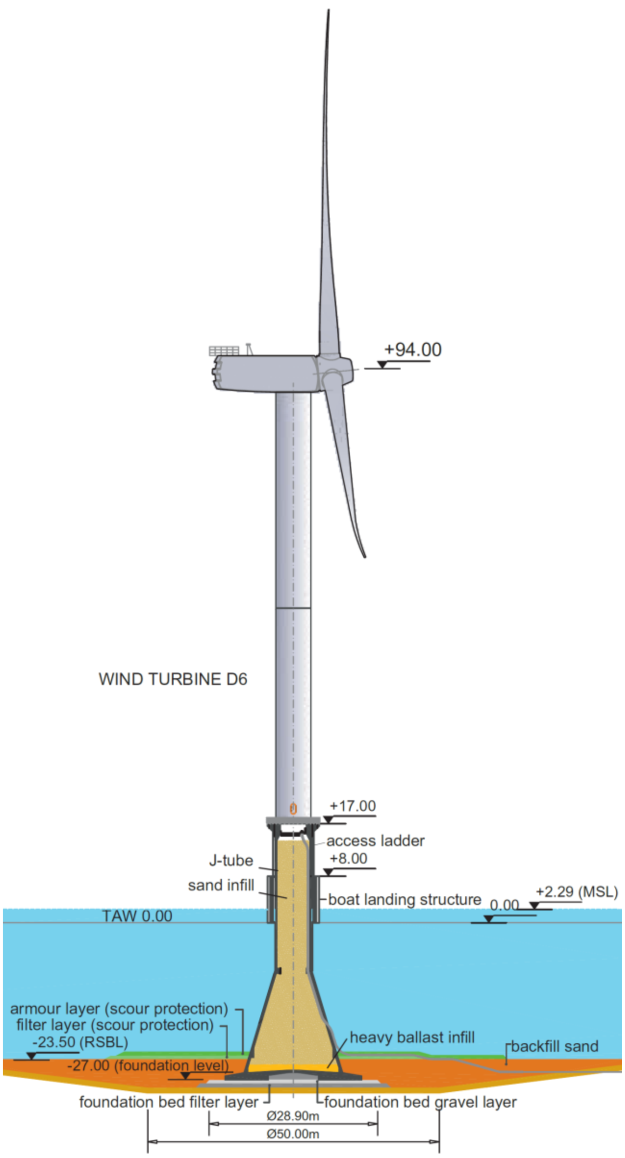

Figure 17. Thornton Bank Gravity Base offshore wind turbine foundations, after Piere et al. (2009).

However, only lightly loaded spread foundations are likely to be practically feasible when less favourable sand conditions prevail, as with the often loose (potentially micaceous) strata identified in some Taiwan Strait wind energy development areas: see for example Liao and Yu (2005) or Shonberg et al. (2023).

Long-term surface loading on sands involves substantially drained conditions, although episodes of significant cyclic loading by waves, wind or earthquakes can provoke partially drained or undrained responses, as can other types of extreme loading.

The evolution of drained shearing resistance as effective stresses rise under rigid shallow foundation loading is implicit in classical drained bearing capacity theory and needs no further consideration here.

Instead, we focus on the potentially significant impact of long-term creep straining and particle contact rearrangement that take place under long-term maintained loading, especially at unfavourable loose sand sites. While such movements have been traditionally neglected in foundation engineering, shallow foundation case histories show they can be highly significant; see Burland and Burridge (1984).

2.3.1 *Experiments at the Labenne dune sand site*

The French Laboratoires des Ponts et Chaussées (LPC) conducted in the 1980s an extensive long-term study of shallow foundation behaviour at several sites with supporting centrifuge testing as reported by, inter-alia, Amar et al. (1985), Amar et al. (1994) and Canépa and Garnier (2003).

Of interest here are the short and long-term tests on multiple small footings conducted on loose dune sand at their Labenne site near Biarritz in SW France, which was also employed by the Author's team for the first 'ICP' instrumented pile tests in sand. Lehane (1992) and Lehane et al. (1993) give details of the site profile, which included in-situ profiling with several tools, geological logging, index tests on piston samples and stress path triaxial testing on locally instrumented specimens at Imperial College.

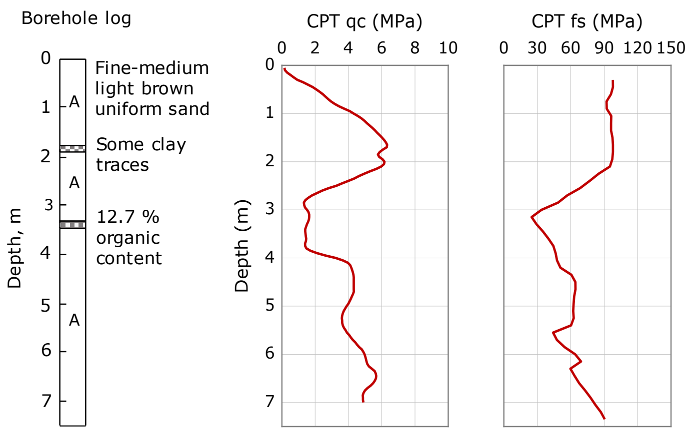

Figure 18. Labenne test site profile, water table at 2.9 m depth. Redrawn from Lehane et al. (1993).

The Labenne sands' strong variations in state with depth, as found commonly at offshore sites, are illustrated in Figure 18 by a CPT profile from the ICP pile test location. The LPC team employed a deadweight arrangement to apply vertical loading to several 0.71 by 0.71m width (B) square concrete pads which were installed at 0.7m depth on medium dense sand, whose average initial relative density I_D was assessed as ≈55%.

Several short-term tests indicated an average failure q_{ult} ≈900 kPa after displacements of 0.15B, as shown in Figure 19 along with the end points of long-duration maintained-load tests conducted on separate pads that imposed different initial loading levels. The settlement-time records presented in Figure 20 show stable long-term 'creep' settlement trends at low loading levels and steeper-than-linear settlement trends at loads greater than around half the 'collapse' load.

(1986)

Figure 19. Bearing pressure q-settlement behaviour of 0.71m pads at Labenne, showing a typical short-term test to failure and the end points of four long duration-maintained load tests.

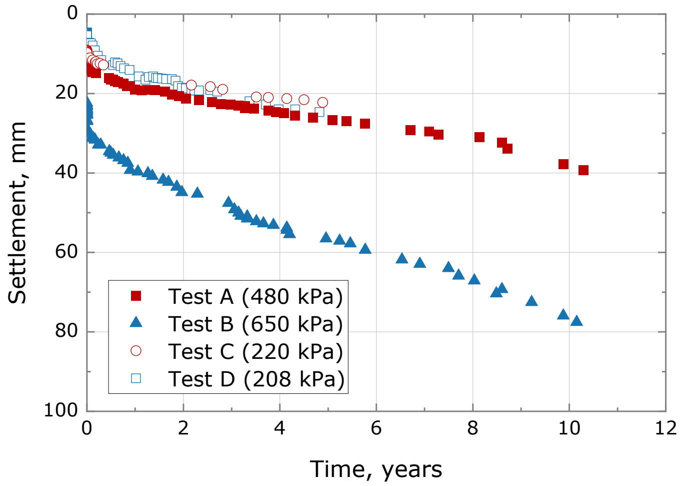

Figure 20. Settlement-time behaviour from four 10-year maintained load-tests by LPC on 0.71m square pads at Labenne.

It is interesting to explore the tests through simple analyses. Routine bearing capacity calculations show that the ≈900 kPa short term 'collapse' load is compatible with $ø' \approx 35.5^o$, which is close to the angle expected for axisymmetric conditions from Bolton's (1986) empirical expressions, given the sand's state (in-situ test stress levels and in-situ relative density) and the critical state *Pads installed at 0.7m depth* determined in triaxial compression tests.

An approximate estimate of how creep settlements recorded in Test B, under 2/3 of the short-term failure load, affected bearing capacity can be made by assuming that, as at Bothkennar, all significant creep straining takes place within a 2B depth range and that lateral creep straining was relatively minor. The resulting (≈4%) average volume strain within the failure zone implies an associated average increase in I_D that Bolton's expressions indicate would raise $ø'$ to ≈38° and so deliver a short-term bearing capacity gain (≈42%) approaching that proven at Bothkennar.

In addition to these $ø'$ gains through the sand's changing state, beneficial microfabric changes can be expected under stable loading levels. The rearrangement through stable creep of the highly redundant system of force chains should allow the sand mass to carry the imposed stress system more optimally. Gradual local flattening of the interparticle contacts could also boost peak $ø'$, although raising the loads significantly would probably generate additional creep settlements. However, these conjectures remain un-tested as no final loading-to-failure stage was incorporated into the Labenne field tests to examine the effects of prolonged pre-loading on bearing capacity.

Truly representative analyses of the tests would need to capture the sand's evolving state, as described for example by Taborda et al. (2020), and its time-dependency as observed in the laboratory (see for example Kuwano and Jardine 2002 or Di Benedetto et al. 2005) and modelled numerically by Di Benedetto (2015). Consideration of micro-fabric effects represents a further modelling challenge.

The Labenne footings were small and may have been affected by seasonal variations that would not apply offshore. However, long-term settlement growth is also considerable under far larger rafts that are less influenced by seasonal variations. Jardine et al. (2005) report on the settlement behaviour of a 100m by 50m, 3.5m thick, raft which supported two large nuclear power reactors founded on competent dense Cretaceous sand strata at a UK site.

The raft's scale and loading level is far larger than the offshore wind GBS shown in Figure 17, but comparable to, for example, the three 1970s Brent North Sea oil producing GBS platforms, whose foundations remain in place. Jardine et al. (2005) report that FE analyses employing fully non-linear elastic-plastic models based on field geophysical measurements and locally instrumented laboratory tests predicted the power station raft's deformed shape, as measured shortly after the end of construction, far better than any linear elastic analyses; see Figure 21a). As might be expected, the average long-term bearing pressure (around 330 kPa) represented a modest proportion of the predicted ultimate bearing capacity.

However, as shown in Figure 21b) settlements continued to grow over the (now decommissioned) reactors' working lives, following a far more stable pattern than the two most heavily loaded Labenne pads. Canépa (1998) reported that French nuclear power stations built on shallow rafts at competent sand sites follow similarly time-dependent settlement trends.

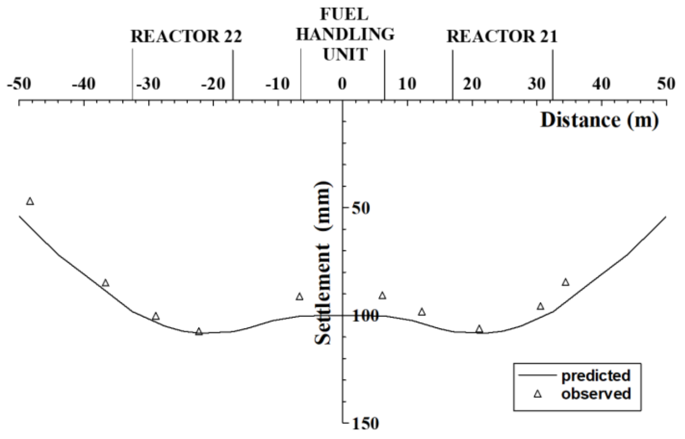

Figure 21a). Settlement-profiles recorded at project week 600 age under 100m by 50m nuclear power station raft on Cretaceous sand at a UK site, also showing predictions from fully non-linear FE analysis; after Jardine et al. (2005).

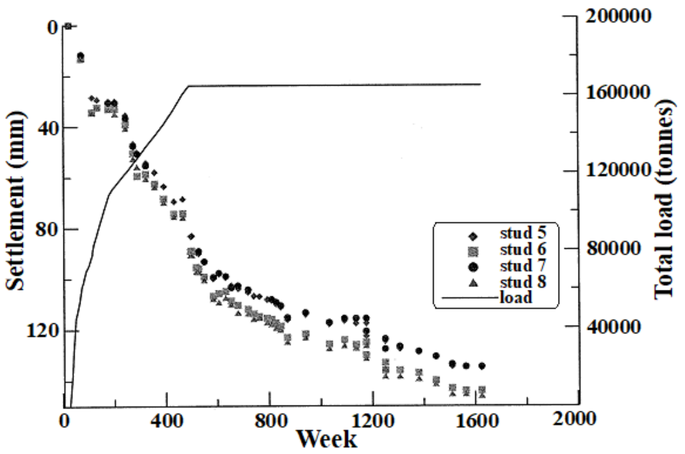

Figure 21b). Settlement-time-load trends over 31 years for 100m by 50m power station raft on Cretaceous sand; after Jardine et al. (2005).

The above field observations demonstrate that shallow foundations can be expected to experience significant creep settlements at sand sites. Their movements will often be augmented under offshore conditions by cyclic loading; see Burland and Burbridge (1984) or Andersen (2015).

While medium-term behaviour can be predicted well by current numerical methods combined with high-quality site characterisation, long-term analyses that capture sands' state and time dependent behaviour remain a challenge. Fully representative modelling could offer better predictions for long-term soil-structure interaction, settlement trends and any significant trend for the ability to sustain extreme loading events to improve with age. High quality long-duration, field observations provide the best means of checking the reliability of any such analyses.

2.4 *Part 1 summary*

The key points made regarding time-dependent shallow foundation bearing response in Part 1 are summarised below, considering the four time-dependent features identified in the introduction before returning to their practical implications.

Consolidation

Consolidation under loading maintained at 2/3 of bearing capacity led to significant relative gains in the ultimate loads that could be carried by sensitive and bio-cemented, low YSR, Bothkennar soft clay. Smaller relative gains are anticipated at high YSR sites, especially those involving clays that do not bifurcate when sheared towards failure and develop brittle local shear zones. However, consolidation is unlikely to contribute significantly to any bearing capacity gains over time at chalk or sand sites.

Micro-to-macro fabric

The open micro-structures and bio-cementing identified in Holocene low OCR marine clays and Cretaceous chalks, rendered them sensitive, anisotropic and brittle in shear. This affected their initial foundation bearing capacities and imparted highly non-linear field consolidation and creep characteristics.

Meso-to-macro-fabric can also be crucially important. The faults, joints, fractures, and fissures present in stiff clays and chalks affect their bearing capacities and have a dominant influence on the chalk's field stiffness and creep trends. Fractures and joints appear to close slowly as any bridging asperities yield slowly under highly concentrated local regimes. The tendency of stiff plastic clays to form brittle shear bands, which has many important implications, is often promoted by natural systems of fissures that develop in-situ through several geological processes.

Creep

Creep contributes significantly to long-term settlement and bearing capacity growth at low YSR soft clay sites. While a less pronounced impact might be expected at stiff, high YSR sites, rafts and pads founded on sands and chalks also manifest considerable long-term creep settlements under even relatively modest loads, which may lead to capacity gains due to void ratio and micro-fabric changes in sands.

Chemical processes

The only clear evidence identified of chemical processes affecting the vertical load carrying capacity shallow foundations relate to the initial (polysaccharide) organic bonding identified in the Bothkennar clay and the $CaCO_3$ cementing of chalks. These bonds may break under high field loading levels, and possibly re-form over time. Bonding may also be developed in sand strata through various natural processes.

Implications

Overall, the shallow foundation loading studies show how ageing progresses under loading. The processes described may: (i) enable optimized shallow foundation design, (ii) allow greater-than-anticipated loads to be borne safely at later stages of service life and (iii) affect the procedures and plant chosen for final decommissioning.

Shallow foundation bearing behaviour can differ from that assumed in classical limit analysis: it often involves local brittleness and is always time dependent. The extended field loading observations made at Bothkennar, North Ormsby, Mundford, Labenne and the nuclear power station sites all confirmed the importance of creep and indicated its potentially beneficial impact on short-term bearing capacity and load-dispalcement behaviour.

Field tests such as those reported valuable benchmarks against which analyses may be tested at a relatively low cost. Advanced numerical analyses employing constitutive models calibrated to locally instrumented stress-path triaxial tests, could match all aspects of the short and long-term Bothkennar field tests accurately. They also were also able to predict short-to-medium term field load-displacement behaviour well at a wide range of stiff clay and sand sites.

Further development is, however, necessary to enable reliable analyses of prolonged loading cases covering a wider range of geomaterials.

3 Part 2 – Time and fabric-dependent behaviour of driven piles

Part 2 considers the loading behaviour of driven steel driven piles, which support most existing large fixed offshore structures.

Marine piling began with modest 30-inch (762mm), or smaller, outside diameter (OD) piles; see for example Clarke et al (1985). Hammers and installation vessel sizes grew rapidly over the 1980s and 1990s. The 2.48m OD piles designed for the Borkum West 2 tripods shown in Figure 22, the first offshore wind farm (OWF) project in which the Author participated, were driven routinely in dense North Sea sands and stiff clays (Merritt et al. 2012).

Jacket piles with diameters greater than 3m are now commonly driven offshore and monopile diameters can exceed 10m; Cathie et al. (2022).

Figure 22. Installation of Borkum West 2 wind turbine tripods in 2011. German North Sea, photo by permission of Trianel.

The principal issues addressed below are how the time-dependent processes triggered by driving affect the micro-to-macro fabrics of clays, chalk and sand as well as their pile effective stress states and load-bearing capacity.

Before moving to these main topics, it is important to note that, as with shallow foundations, FE analyses that account for pile installation effects and apply reliable measurements from locally instrumented stress-path triaxial tests can deliver representative, site-specific, axial load-displacement predictions of offshore pile behaviour.

The fidelity of Class-A predictions made for the axial movements developed by full scale offshore foundations under service loading were confirmed by comparison with high resolution field measurements at the very stiff clay and dense sand North Sea Hutton TLP and Magnus jacket sites (Jardine and Potts 1988, 1993). Checks against onshore chalk pile test cases also show good agreement; Wen et al. (2023a, b). While piles driven in all three geomaterials show significant creep movements once loads exceed ≈1/3 of their shaft capacity, long-term maintained loading at lower levels had relatively little effect on the Hutton TLP pile groups' displacements over a seven-year service monitoring period (Stock et al. 1992).

Interesting field experiments by Karlsrud et al. (2014) showed that applying, over two-year durations, higher levels of sustained tension loading (up to

≈1/2 of the nominal capacities) to ≈500mm outside diameter (OD) driven piles had either a mildly beneficial, or a broadly neutral, effect on tension capacities at three clay sites. However, the NGI's parallel tests in silty Larvik sand showed 17% less tension shaft capacity than parallel tests on 'virgin' piles; still more marked effects were noted in gravelly Ryggkollen sand. It is not known whether sustained compression loading, which is more common for fixed platforms, has the opposite (positive) effect, or how maintained loading affects piles driven in chalk. However, the NGI's testing showed that caution needs to be applied when considering the ageing trends of tension anchor piles driven in sand.

3.1 *Piles driven in clays*

We concentrate first on the time-dependent behaviour of piles driven in clays. One-dimensional, cylindrical cavity expansion method (CEM) analyses by Butterfield and Bannerjee (1970) and Randolph et al. (1979) considered how rapid (undrained) pile driving imposes very large strains, total stress and pore pressure increases whose subsequent decay may be modelled in coupled analyses of the equalization process.

Two-dimensional (strain path method, SPM) analyses by Baligh (1985), Kavvadas (1982) and Whittle (1987) and FEM solutions (Sheil et al. 2014) have adopted more representative 2D pile geometries. The available solutions point to a wide range of predictions for dissipation times and trends for shaft capacity 'set-up'. The latter is defined here as the ratio Λ (t) of (total, base or shaft) capacity at times (t) after driving compared to the end of driving (EoD) values.

The theoretical predictions depend greatly on the geometrical idealisation made and constitutive model adopted, including its treatment of sensitivity/brittleness, anisotropy, strain-rate dependency, driving related cyclic loading and permeability variations with void ratio. Other physical features that might be modelled include residual shear band formation in clays containing susceptible minerals.

Objective evidence from high quality field experiments is essential to help test analyses and guide practical design. Reliable measurements of the pore pressures and cylindrical stress components developed at multiple levels on tubular piles can provide key insights, as can examination of how driving affects the properties of the ground around driven piles. Observations are also required of how pile capacities change with time after installation, ideally by either testing identical piles at a range of ages after driving but at least by measuring the piles installation resistance as well as its capacity at a suitable age after driving. High quality site investigations are also essential to field test interpretation.

The discussion that follows only considers cases that fulfil these criteria, drawing on subsets of the 'ICP-05' and 'Unified' clay test databases collated by Jardine et al (2005) and Lehane et al. (2017).

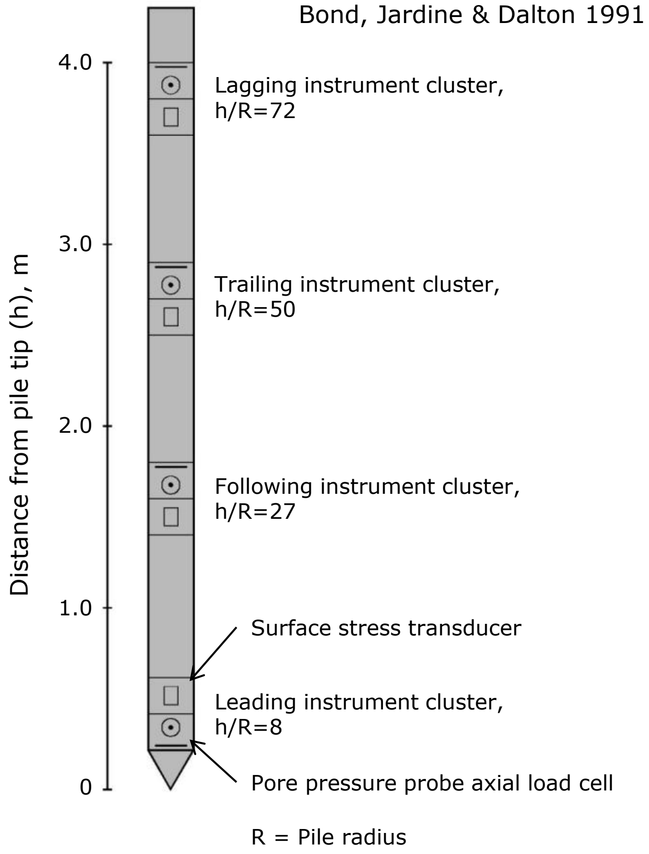

Figure 23. ICP instrumentation configuration (Jardine, 2020).

Figure 24. Locations of ICP sand and clay test sites; after Jardine (2020).

The Imperial College Pile (ICP; Bond et al. 1991), was developed to study shaft effective stresses during installation, equalisation and load testing. Bond and

Jardine (1991, 1995), Lehane and Jardine (1994a, b) and Jardine et al. (2005) summarised the key findings from Bond (1989), Lehane (1992) and Chow (1997) in which the ICP configurations shown in see Figure 23 provided local measurements of axial load, pore pressure, radial total and shear stresses on closed-ended 101.6mm diameter mild-steel piles. The latter were installed by fast cyclic jacking at the clay sites listed in Table 2 and identified in Figure 24. Also shown are the two ICP sand sites, which included LPC's shallow foundation test facility at Labenne.

The first ICP experiments were run in London Clay, at the UK, Building Research Establishment's (BRE) Canons Park test site, whose ground profile was investigated by Jardine (1985) as summarised below in Figure 25.

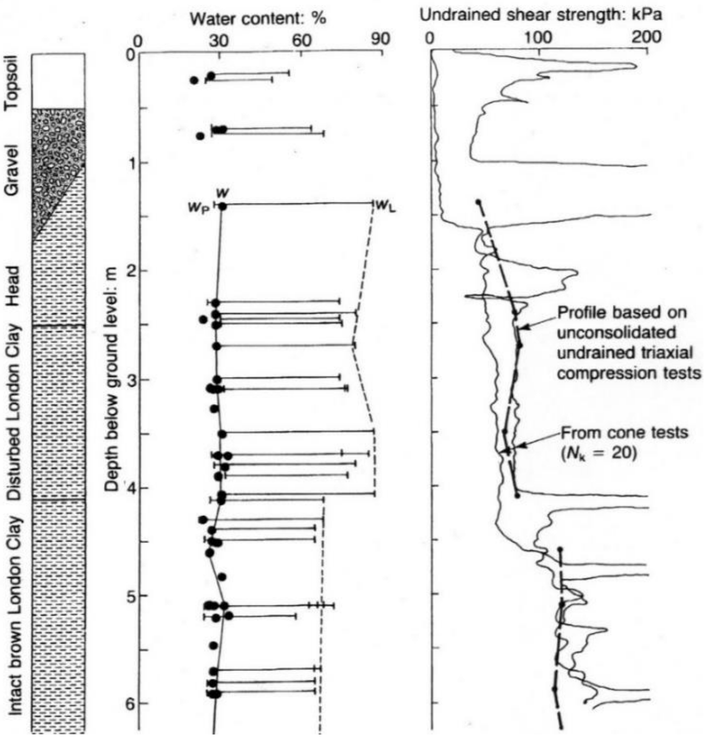

Figure 25. Geotechnical profile of London Clay at Canons Park, after Bond and Jardine (1991).

3.1.1 *Impact of installation displacement rate on shaft resistances and interface fabric in clay*

The ICP clay site programmes assessed the impact of pile installation displacement rates. Relatively fast-jacking, at 500mm/minute, led to long-term static axial shaft capacities around 50% greater at Canons Park than piles jacked at <100mm/minute.

Parallel tests with driven open and closed-ended steel tubular piles demonstrated axial capacities and load-displacement curves that were practically equivalent to those of fast jacked piles. A similarly strong jacking rate dependency was noted at Cowden; the Bothkennar and Pentre jacking resistances also varied with displacement rate.

Bond (1989) undertook intensive block sampling, micro-fabric and soil suction studies around steel Canons Park piles jacked and driven installed at various rates. The sampling, which took place ≈1 month after pile installation, proved that the influence of rate originated in the micro-fabric of the shear bands formed around the pile shafts.

While modest viscous rate effects were proven to apply at very slow jacking rates, the fabric induced by changed dramatically over the 100 to 500mm/minute range. Thin-section petrographic analyses showed that slow jacking generated one or more smooth continuous, polished, cylindrical principal displacement residual shear surfaces, on which the clay particles were aligned parallel to the shaft.

Driving and fast jacking led to multiple, less well-developed, matt shear surfaces on which the degrees of clay particle reorientation were lower. Interestingly, the excavations showed no clear sign of the steel piles having corroded significantly within a month of embedment below the water table.

The effective stress paths from local measurements made by the ICP surface stress transducers in load tests confirmed that shaft shearing resistance is governed by the Coulomb effective stress law given in Equation 1, which relates the local shaft shear stress τ_{rzf} at failure to the local radial effective stress σ'_{rf} with δ' being the angle of interface shearing resistance.

$$\tau_{rzf} = \sigma'_{rf} \tan \delta' \tag{1}$$

As illustrated in Figure 26, the fast-jacked piles' average peak δ'_{peak} was 13 ± 1°. However, the shear fabric was brittle; field τ_{rzf} and δ' values declined with displacement towards stable minima after initial shaft failure. Reloading tests, conducted after suitable re-consolidation pause periods, gave δ'_{ult} = 8 ± 1°, showing that the reductions in δ' were related to irreversible changes in the micro-fabric developed in the pile-soil interface shear zone. Slowly jacked piles manifested a similarly ductile response and average δ'_{peak} = δ'_{ult} = 8 ± 1°.

Pile shaft shearing conditions evidently promote marked clay particle reorientation. The ultimate angles developed along the pile shafts fall below those back-analysed from London clay landslides that have developed large slip movements: see Skempton (1986) or Kovacevic et al. (2007).

Ring shear tests that incorporate steel interfaces with 10μm CLA roughness and impose pre-conditioning 'pulses' of large-displacement fast shearing, as recommended and detailed by Ramsey et al. (1998) and Jardine at al. (2005), provide good models of pile shaft interface shearing behaviour in the field.

Table 2. Shaft t_{95} times and δ' angles from static tests on fast-jacked ICP piles at UK clay sites

Site and clay type	Time for 95% pore pressure decay, t_{95}	Mean δ'_{peak} & δ'_{ult}
Bothkennar Holocene low OCR, silty estuarine clay: 30% < I_p < 50%	20 days, for 1.2 to 6m embedded length	29º & 29º
Canons Park Eocene high OCR, marine London clay: 35% < I_p < 50%	2 days, for 2 to 6m embedded length	13º & 8º
Cowden Devensian high OCR, lodgement till: 18% < I_p < 23%	7 days, 2.4 to 6m embedded length	22º & 20º
Pentre Late Devensian low OCR, glacio-lacustrine clay: 10 to 15m: 10% < I_p < 23%	60 to 600 mins over 10-15m length	19º & 16º
Laminated glacio-lacustrine sand & clay-silt, 15 to 20m: 10% < I_p < 16%	5 to 45 mins over 15-20m length	23º & 19º

Such 'ICP-style' tests can predict field peak and ultimate angles δ′ accurately as well as the ultimate residual angles seen in the field ICP tests. They also provide a rational basis for defining the local softening rates needed for 'falling branch', brittle, *t-z* or FE analyses that capture the potentially progressive failure of long, relatively compressible, piles.

The four UK clays considered in Table 2 show a surprisingly wide δ' range. Even though Bothkennar and London clays have similar I_p values, their field and laboratory δ' angles fall at opposing ends of the full range. While London Clay is brittle, Bothkennar shows no post-peak reduction from its mean peak φ' = 29º.

Also interesting are the angles shown by low I_p, mainly silt-sized Pentre soils, which varied from being massive silty clays, to being regularly laminated with fine sand or appearing as 'marbled', probably due to prior mass movements.

Soils containing less than 20% of active clay sized particles are not expected to develop residual shear surfaces; Skempton (1986). However, oriented shear micro-fabrics were proven to develop in a large proportion of the Pentre sediment sequence.

Chow (1997)'s thin-section analyses of Pentre samples, taken from ICP pile shafts, identified highly oriented shear surfaces, as shown in Figure 27. Thin section analyses of samples taken around piles tested in London Clay showed similar features (Bond and Jardine 1995), as did samples from ring shear interface tests on both clays.

The Pentre 'clay' composition ranged from being up to 85% quartz-silt in some layers, which can give δ' > 30º in 'ICP' style ring shear tests (Ho et al. 2011) to comprising 75% aggregated assemblies of Illite-mica, chlorite and plagioclase feldspar clay minerals. Chow (1997) showed that the aggregates could be broken down in 'ICP' style ring-shear tests to give lower residual strengths.

The mixed Pentre soils showed variable behaviour with δ' angles as low as 14º in some tests. The ring shear δ'_{peak} = 24.5º and δ'_{ult} = 19º averages marginally exceeded those from the ICP surface stress transducers and pore pressure sensors tests.

The Bothkennar tests showed far higher δ' angles but much greater sensitivity, with notably low installation resistances that declined markedly with *h/R* towards 'remoulded' values that reflected the clay's open-structure and high liquidity indices.

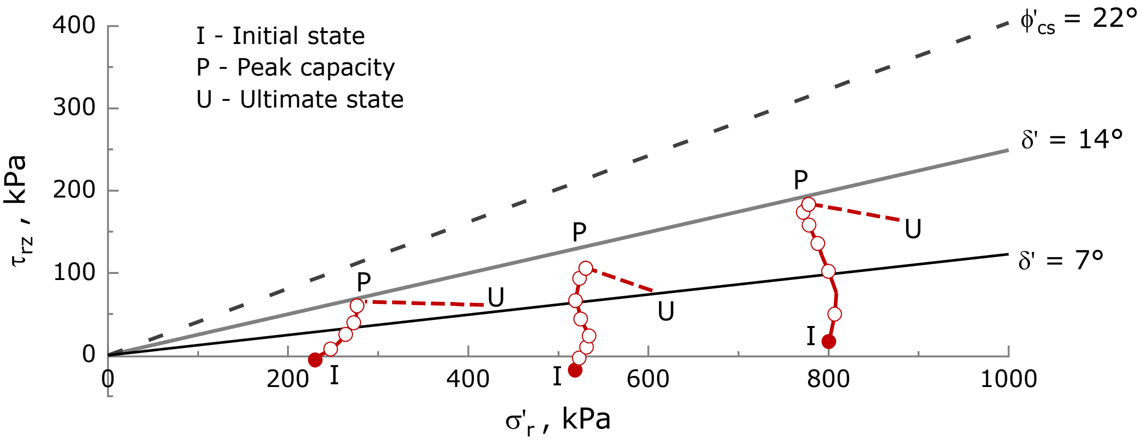

Figure 26. Effective stress paths followed in ICP tests in London clay on fast jacked piles, progressing from initial (I) to peak (P) and ultimate (U) conditions; redrawn from Bond and Jardine (1995). See Figure 23 for the leading (right trace), trailing (middle) and following (left trace) instrument positions.

Figure 27. Thin section specimen, ≈10mm wide, showing well-developed (vertical) principal displacement shears, from ICP pile shaft shear zone in silty Pentre clay, after Chow (1997).

3.1.2 *Fast jacked ICP piles' pore pressure equalisation and set-up trends*

The ICP experiments summarised in Table 2 also recorded how the pore-pressures generated by pile installation dissipated at the four clay sites and tracked the linked variations in local shaft effective radial stresses. Later static tests identified their impact on axial capacity.

Figure 28 illustrates how shaft pore pressures, which had negative values immediately after installation at Canons Park, rose at the Leading instrument position (400mm above the tip) to reach the highest maxima (≈400 kPa) seen in all ICP tests and then decayed to near hydrostatic values over two days. The negative pressures sensed at the Following and Trailing sensors higher on the shaft rose more slowly and hardly exceeded their pre-installation values.

The installation shaft radial effective stresses σ'_r generally far exceeded the undisturbed 'free-field' values associated with the in-situ σ'_{v0} and $\sigma'_{h0} = K_0\, \sigma'_{v0}$ stresses. Bond and Jardine (1991) found little further overall change in average shaft radial effective stresses σ'_r during equalisation. The final $K_c = \sigma'_{rc} / \sigma'_{v0}$ ratios remained high near the tip but reduced systematically with relative height (h/R) towards the undisturbed, far-field, K_0 stresses.

The times taken by ICP tests to reach 95% equalisation after installation varied from 20 days in the sensitive, high compressibility, low permeability, sensitive Bothkennar clay, to just an hour in the far higher permeability and less compressible laminated Pentre strata. The ICP installation process takes several hours. Extended pauses are required to add and seal pile extensions, re-thread and re-set instrument cables and reposition the jacking assembly. This allowed far more substantial drainage than would apply around efficiently driven industrial piles.

The ICP static loading tests at clay sites, which were conducted after high degrees of pore-pressure equalisation, led to the results in Table 3. The axial-load cells confirmed that base resistance offers relatively minor axial capacity contributions that vary directly with CPT q_t and show no systematic setup.

The final ICP jacking shaft forces were reduced by 20% (based on separate rate tests by Pellew 2002) when calculating setup to allow for jacking being ≈10^3 faster than monotonic testing to failure. The Pentre piles, whose installation was substantially drained, gave notably lower Λ ratios than at Bothkennar; the two stiff clay cases showed modest, $1.15 \geq \Lambda \geq 1.2$ setups. Also shown are factors from the LDP experiments summarised by Gibbs et al. (1993) on three open 762mm OD steel tubular piles driven at the low YSR (NC) Pentre and Tilbrook high YSR (OC) clay sites, which are discussed further below.

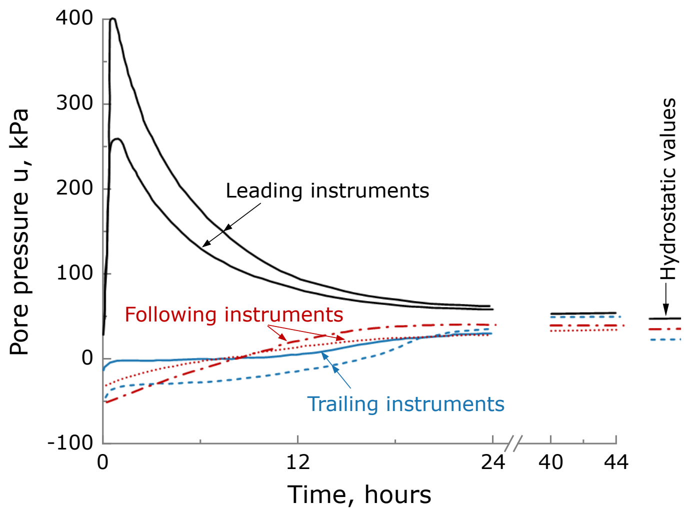

Figure 28. Pore pressure dissipation around ICP installed in London Clay at Canons Park, after Bond and Jardine (1991); see Figure 23 for instrument positions.

3.1.3 *Effective stress shaft capacity design methods derived from ICP closed-ended pile tests*

New effective stress approaches evolved for designing piles driven at clay sites as results emerged from the ICP tests described above, and other studies reported in the literature. The key points were:

- The Coulomb Equation (1) applies satisfactorily and representative field δ' angles can be predicted accurately by suitable 'ICP-style' ring shear tests.
- On average, the static shaft failure σ'_{rf} values are around 20% lower than the 'consolidated' equilibrium values σ'_{rc} applying prior to loading.

- The local σ'_{rc} values applying on pile shafts rise with σ'_{v0} and yield stress ratio (YSR) and decline with clay sensitivity S_t. And, very importantly, σ'_{rc} falls sharply with relative pile tip depth, *h/R*.

Heerema (1980) had inferred from earlier pile driving experience in hard North Sea clays that local shaft resistances decay markedly with *h* during driving, which he termed 'friction fatigue'. Fully coupled strain-path method (SPM) analyses by Whittle (1987) with the anisotropic and potentially sensitive advanced MIT-E3 clay model indicated that the *h/R* dependency is principally due the geometry of clay 'flow' around the advancing tip, rather than 'fatigue', although the cyclic loading implicit in pile driving adds to this. Whittle's SPM analyses also captured the tendency for shaft resistances to fall with S_t.

Despite the powerful insights SPM analyses provide, they could not capture all the processes at work sufficiently well to deliver accurate Class-A predictions for ICP clay tests. A more direct approach was required to develop robust design guidance.

Lehane et al. (1994) proposed simple empirical expressions for σ'_{rf} and σ'_{rc} that captured the key field observations within an effective stress framework that was informed by the SPM analyses. Their expressions offered a new practical design approach for closed-ended piles. Chow (1997) confirmed that the formulae gave broadly satisfactory predictions for the final capacities of the ICP tests she undertook at Pentre, before drawing on outcomes from the LDP tests to address how to consider open-ended offshore piles.

3.1.4 *LDP, NGI and BRE tests on piles driven in clay*

The Joint Industry LDP tests, extensive programmes by NGI (Karlsrud et al. 1993, 2014), and further experiments at Canons Park by Wardle et al. (1992), Pellew (2002) and Pellew and Jardine (2018) offered the driven pile cases summarized in Table 4. The piles' geometries, the ground conditions established from high-quality site investigations, key references and measured or calculated t_{95} values are also listed.

The LDP laboratory characterisation included interface tests with 'Bishop' ring shear apparatus at City University, London. These tests, which preceded the 'ICP-05 procedures', did not employ fast pre-shearing stages or, it seems, interfaces prepared to ≈10μm 'pile-shaft' roughness. Tests on remoulded Pentre samples against probably relatively smooth (R_{CLA} < 1 μm) interfaces showed $19^o \leq \delta'_{peak} \leq 26^o$ and $11^o \leq \delta'_{ult} \leq 16^o$, while Chow's (1997) Imperial College 'ICP-style' tests gave averages of $\delta'_{peak} = 24.5^o$ and $\delta'_{ult} = 19^o$ over the 5 to 20m depth range, including the laminated section of strata.

As listed in Table 2, the local ICP stress sensors indicated average $\delta'_{peak} = 19^o$ and $\delta'_{ult} = 16^o$ in the Pentre clays. While other researchers have adopted the LDP's 4 ±1° lower ultimate angle, the 19° and δ'_{ult} = 16° angles are taken here as the most representative to apply to the Pentre LDP test.

Similar uncertainties apply to the interface shear tests conducted for the Tilbrook piles. These are most important for the Oxford Clay unit which contributed ≈60% of shaft capacity. Narayana (2010) conducted later 'ICP-style' tests on Oxford Clay samples with a typical median I_p = 33%, finding $\delta'_{peak} = 12.5^o$, 14% greater than that indicated by the LDP laboratory tests, which also showed an improbably low $\delta'_{ult} = 16^o$ for the sandy Lowestoft till. 'ICP-style' tests on Cowden till, which has a similar I_p range and slightly lower triaxial φ', suggest 19° as being more representative for the Tilbrook LDP piles.

Table 4 summarises how the Pentre NC pile drove with full coring and equalised rapidly, with t_{95} between 3 and 12 hours in most layers, although 100 days were required for full dissipation in one relatively thin plastic clay sub-layer. The NC pile was tested after 44 days. Very low EoD driving resistances applied at Pentre, which fell below the remoulded shear strengths indicated by the strata's liquidity indices. Such resistances may lead to pile runs in comparably sensitive, lean, strata - such as those noted at some Taiwan Strait OWF sites.

The Tilbrook piles developed plugging over 43% of their drive lengths which extended their t_{95} dissipation times as listed in Table 4, based on the Author's interpretation of the pile piezometer data. The Lowestoft till and Oxford clay layers did not reach t_{95} before the OC test was conducted, 130 days after driving, although full equalisation was probably reached before the later test on the second (TP) pile.

Randolph (1993) undertook stress-wave matching of the LPD piles' dynamic driving strain and acceleration data to quantify equivalent static soil resistances to driving (SRD). He confirmed that local (inner plus outer) τ_{rzf} values decline sharply with relative pile tip depth, *h*, until the end of driving (EoD).

Despite multiple failures, the LDP piles' axial strain gauges identified the field shaft load-transfer profiles and the base resistances during later static testing. Table 3 indicates the key results for shaft set-up taken from these data. The Tilbrook LDP piles' $1.26 \leq \Lambda \leq 1.41$ set-up factors, which are defined relative to the total (inner plus outer) EoD shaft driving resistances, were comparable to, but slightly greater than, the 1.15 and 1.24 Λ ratios shown by closed-ended ICP piles in high YSR clays at Canons Park and Cowden over shorter times: see Table 2.

While the open Pentre LDP OC pile's $\Lambda = 2.39$ was less than that manifested by the Bothkennar ICP test, it exceeded the $0.95 \leq \Lambda \leq 1.25$ Pentre ICP piles' range. Drainage during installation is considered the primary reason for the lower Λ values interpreted for Pentre, although additional ageing processes (involving creep, fabric or chemical reactions) may have boosted the Pentre LDP pile's aged capacity.

Table 3. Summary of shaft setup Λ factors. End of installation values from final jack stroke load of ICP tests and stress-wave matches for LDP piles; 'representative' *YSR* and S_t values are defined at 2/3 penetration length L_p in each stratum.

Site, piles and set-up times allowed before testing	L_p/D	Representative *YSR*	Representative S_t	Shaft set-up Λ
Bothkennar ICP piles, within one week	47	1.55	7	3.6
Canons Park ICP piles, within one week	39	30	1	1.15
Cowden ICP piles, within one week	45	9.2	1	1.2
Pentre ICP piles within one week: Clay section Laminated clay-silt section	 49 49	 1.75 1.55	 6 8	 1.25 0.94
Pentre LDP Pile NC, after 44 days	52.5	1.24	3.6	2.39
Tilbrook LDP Pile OC, after 130 days **Tilbrook** LDP Pile TP, after 670 days	39.4 39.4	12.5 in Lowestoft till, 18.5 in Oxford clay	1 in both	1.26 1.41

3.1.5 *Development of ICP-05 clay effective stress design method*

Chow (1997) concluded from analysis of the LDP tests that it was only necessary to substitute the effective radius R^* (as defined below) in place of R in Lehane's (1992) expression for K_c to cover open and closed-ended piles, in tension and compression, at both sites. Chow (1997) also modified the sensitivity term employed in shaft resistance predictions and provided CPT q_t linked expressions to calculate base resistances. Equations 1 to 4 could then be employed to predict shaft resistance:

$$\sigma'_{rf} = 0.8\,\sigma'_{rc} \tag{2}$$

$$\sigma'_{rc} = K_c\,\sigma'_{vo} \tag{3}$$

$$K_c = [2.2 + 0.016YSR - 0.87\Delta I_{vy}]YSR^{0.42}(h/R^*)^{-0.2} \tag{4}$$

Where $R^* = [R^2_{outer} - R^2_{inner}]^{0.5} = D^*/2$ for open piles, $R_{outer} = D$ for closed piles and h/R^* is limited to ≥ 8.

Chow (1997) assembled a database to test her approach, facing multiple challenges regarding incomplete details for piles, tests and site characterisation datasets. Few case histories included 'ICP-style' interface shear tests. Nevertheless, Chow identified 55 clay cases from 16 sites for which it was feasible to assess input parameters with reasonable confidence. Statistical analysis showed encouraging agreement between calculated and measured capacities.

Jardine and Chow (1996) set out how the extended method could be applied in practice and demonstrated its performance against Chow's (1997) pile test database. They emphasised that the approach calls for different site investigation testing and interpretation to existing total stress 'alpha' design methods and can only be applied when the necessary input parameters have been derived by high quality sampling, CPT profiling and laboratory testing. Ring shear tests that apply the Ramsey et al. (1998) procedures, with interfaces of suitable roughness made with appropriate steels, are essential.

Jardine and Chow (1996) discuss how to assess *YSR*. CPTu profiles often offer the best approach at low OCR clay sites but are more difficult to interpret with high *YSR* cases, where standard oedometer tests can also give misleading results. *YSR* is better assessed from high-pressure oedometer tests and/or reference to reliable geological knowledge of prior burial depths. High quality undrained strength data can be applied to estimate *YSR* through 'SHANSEP' S_u/σ'_{vo} = f(*YSR*) relationships for clays that manifest stable critical states, but not for brittle (often plastic) clays that bifurcate in triaxial shear tests. As discussed in Part 1, the residual fabric shear bands that form in plastic clays eliminate any systematic relationship between S_u/σ'_{vo} and *YSR*.

Jardine and Chow (1996) recommended that sensitivity, expressed as $\Delta I_{vy} = \log S_t$ should be derived from either: (i) paired oedometer tests on reconstituted and intact clay samples, or (ii) the ratio of peak to remoulded S_u values, where the latter could be estimated from the clays' natural liquidity index I_L.

Jardine et al. (2005) updated the 1996 'MTD' design booklet, bringing in further high-quality load tests and addressing a range of additional factors, including the application of reliability-based methods.

Wave matching and other back-analyses of driving records have shown encouraging agreement with predictions for multiple cases where the recommended site investigation, design and parameter selection procedures have been followed. Overy (2007), Argiolas and Jardine (2017), Hampson et al. (2017) and others have reported examples of the successful use of the ICP-05 clay and sand procedures in major North Sea projects, including nine of Shell (UK)'s oil platforms and the 102 jacket structures installed for the East Anglia OffshoreOne windfarm; Rattley et al. (2017), Scottish Power Renewables (2019).

However, Jardine et al (2005) warned that the approach greatly over-predicted the capacity of piles driven in sensitive low OCR, low I_p clay at the Norwegian Lierstranda site, with similarly low capacities being proven at Sandpoint, Idaho (Fellenius et al. 2004). While such clays appear rare in the UK North Sea, the cautious Reduction Factor (RF) scheme based on normalised CPT resistances shown in Figure

29 may be helpful in less familiar soil types when no representative local pile test data is available.

Local offshore static and/or dynamic field testing can be more cost-effective than applying cautious reduction factors, as Shonberg et al. (2023) report from intensively instrumented large diameter pile tests conducted in low YSR, low I_p clays, silts and loose (potentially micaceous) sands at a Taiwan Strait site.

3.1.6 *'Unified' CPT-based design method*

Recognising the difficulties of applying effective stress, or undrained shear strength, based procedures in cases where the key design parameters were not, or could not, be measured satisfactorily, Lehane et al. (2020) set out a 'Unified' CPT-based procedure. They developed design equations that minimised the average difference between calculated capacities Q_c and those measured (Q_m) in tests drawn mainly from Lehane et al. (2017) 'Unified database', whose entries included the LDP cases and passed scrutiny by a panel that included the Author. The CPT-based, total stress, Equation 5 gave the best overall fit for shaft resistance in compression and tension, where q_t is corrected cone tip resistance subject to a minimum *h/D** of 1 along with other equations for base resistances; Lehane et al. (2020).

$$\tau_{rzf} = 0.07Fst\; q_t\; (h/R^*)^{-0.25} \tag{5}$$

As with the ICP-05, low OCR, low I_p, sensitive clays need special treatment. The factor *Fst*, taken as 1 for the Zone 2, 3 and 4 clays defined in Figure 29, is 0.5 ± 0.2 for Zone 1 clays and clay-silts. Lehane et al. (2023) note that Equation 5 may be less representative in clays with δ' angles that vary far from the mid-range of the possible $10^o \leq \delta'_{peak} \leq 40^o$ spectrum identified by Jardine et al. (2005). Such cases include the London and Bothkennar clays, whose peak angles are 13^o and 29^o respectively.

Clay design approaches are implicitly intended to predict axial shaft capacities after full, or at least 80%, pore pressure equalisation. However, no systematic study, involving a range of clay types and pile scales, was available of the capacities developed at later stages until Karlsrud et al. (2014) reported NGI's 'Time effects on pile capacity' JIP.

3.1.7 *NGI's study of time-dependent axial capacity in clay*

The most efficient way to monitor shaft capacity development over time is to drive multiple identical piles and test them individually, in tension, at different ages. This allows a clearer isolation of base resistance and avoids conflating the effects of ageing with those of prior load testing; Jardine et al. (2006). Karlsrud et al. (2014) described applying this approach at Cowden in the UK; at the Onsoy and Stjordal Norwegian sites; and at Femern in Denmark.

Table 4 summarises aspects of the tension tests on five open-ended, around 500mm diameter, steel piles that were left undisturbed at each site until first-time tension loading tests were conducted to failure between ≈1 month and ≈2 years after driving.

Table 4. Summary of considered piles driven at clay sites.

Site, pile code, outside diameter, and clay type	Principal references	Depths: of casing; to pile tip; and to top of clay core	t_{95} values and sources
Pentre LDP Pile NC, 762mm, low OCR, 10% < I_p <30% clay & clay-silt, UK	Lambson et al. (1993), Gibbs et al. (1993), Randolph (1993), Chow (1997)	15m casing; open tip at 55m; core rose above casing	3 to 12 hours, LDP field measurements
Tilbrook LDP Piles OC & TP 762mm, high OCR, 15 < I_p <30% Lowestoft till to 18.6m over high OCR, 25% < I_p < 40% Oxford clay, UK	Lambson et al. (1993) Gibbs et al. (1993), Randolph (1993), Chow (1997), Narayana (2010)	OC - no casing; open tip at 30m TP - 1.6m pit; open tip at 30.5; core top 13m below ground	Extrapolated as ≈300 days from ≈87% and ≈67% dissipation after 130 days in Lowestoft till and Oxford Clay respectively
Cowden NGI piles C1 to C6, 457mm, high OCR 18% < I_p < 23% clay till, UK	Karlsrud et al. (2014), Lehane & Jardine (1994), Zdravkovic et al. (2020), Ushev and Jardine (2023)	1m casing; open tip at 10m; core to 1.5m below casing	Interpolated as ≈17 days from ICP and 2m OD PISA piles' dissipation data
Femern NGI piles, F1 to F6, 508mm, high OCR, 70% < I_p < 150% clay, Denmark	Karlsrud et al. (2014), Japsen and Bidstrup (1999), GEO (2011), Yang (2023)	No casing; open tip at 25m; core drilled out continuously	Extrapolated as ≈4 years from ≈85% dissipation recorded after 670 days
Onsoy NGI piles, O1 to O6, 508mm, low OCR, 22% < I_p < 40% clay, Norway	Karlsrud et al. (1993), Ridgway and Jardine (2007), Karlsrud et al. (2014)	1.4m casing; open tip at 19.1m; core top 2m below casing	Extrapolated as ≈8 days from 219mm OD closed-end pile dissipation data
Stjordal NGI piles S1 to S6, 508mm, 7% < I_p < 15% low OCR, silty clay, Norway	Karlsrud et al. (2014), Yang (2023)	1m casing; open tip at 23.6m; core top 9m below casing	No dissipation data, 80-day t_{95} estimate made by NGI
Canons Park BRE Pile D, 168mm, high OCR, 35% < I_p < 50% London clay, UK	Wardle et al. (1992), Pellew and Jardine (2008)	2.25m casing; 6.38m to closed tip	Extrapolated as ≈5 days from Bond and Jardine (1991) ICP dissipation data

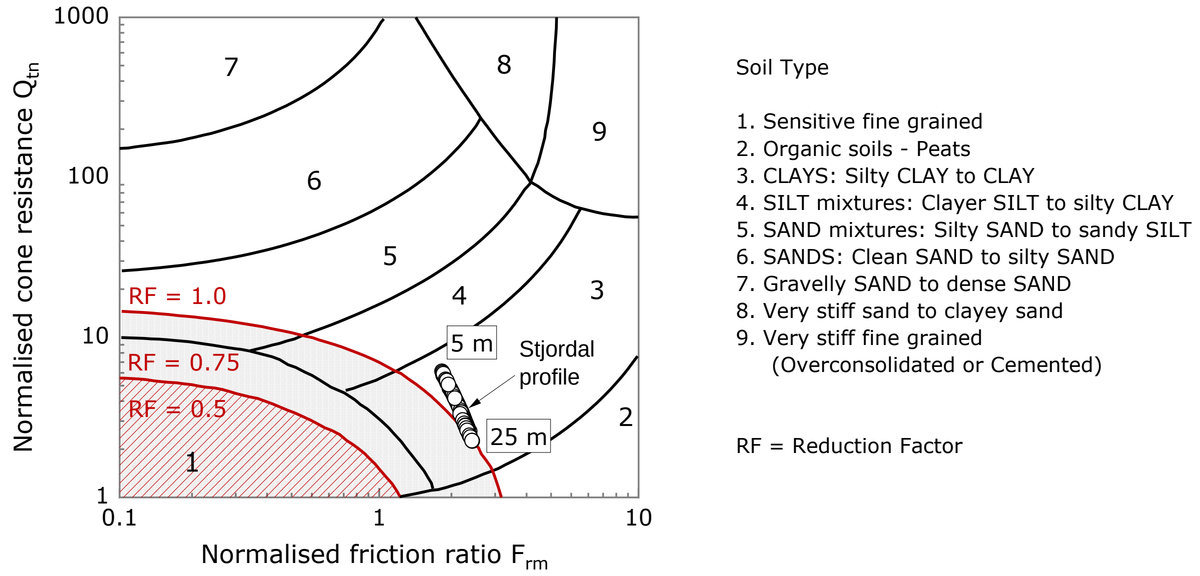

Figure 29. Cautious reduction factors RF) proposed for ICP-05 predictions based on normalised Q_{tn} and F_{rm} CPT resistances defined by Robertson (2009). F_{rm} - Q_{tn} trend with depth for NGI's low *YSR*, low I_p Stjordal silty-clay courtesy of Carotuneto (2023).

Pile installation induced pore-pressure generation and dissipation was only monitored at Fermen. Table 4 gives the Author's estimates for the t_{95} times applying to the NGI's mainly coring Cowden and Onsoy piles, based on dissipation monitoring on closed-ended piles (of diameter D) driven earlier in the same clays and, following Carter et al. (1979), employing Equation 6 to gauge t_{95} times through their $D^* = 2R^*$ values. This leads, for example, to t_{95} estimates of ≈17 days for Cowden and ≈8 days for Onsoy. The same procedure can be applied to make direct estimates for pore-pressure equalisation times applying over the lower sections of open-ended pile shafts from piezocone dissipation tests.

$$t_{95}/[t_{95}]^{CPT} = [D^*/D]^2 \qquad (6)$$

As with the Oxford clay at Tilbrook, dissipation was orders of magnitude slower in the low permeability, heavily pre-loaded and plastic Femern clay, where t_{95} ≈4 years. This may reflect partial plugging, although the Femern pile cores were drilled out at several stages during driving.

The proportionally faster dissipation seen at Canons Park reflects the London Clay's partially open shallow fissures and the presence of sand laminae at greater depths (Jardine 1985, Bond 1989). Lower clay-sized fractions (23 to 26%) were noted at Stjordal than at Onsoy (44 to 66%), which might suggest that the Stjordal piles would equalise more rapidly than similar piles at Onsoy. However, the Stjordal piles plugged partially during driving and had a mean final filling ratio (FFR) of 0.60. Karlsrud et al. (2014) estimate that this plugging extended the Femern piles' t_{95} durations to 80 days.

The impact of serial loading tests to failure on single piles was also investigated by Karlsrud et al. (2014) who found that, as with the brittle London Clay tested at Canons Park, the Femern piles lost capacity markedly with each test repetition, following a brittle pattern that probably resulted from clay shear zone particle re-alignment and consequent reductions in interface shear resistance. Their tests at Cowden and Onsoy on medium I_p clays showed more ductile trends that scattered around the corresponding 1st time capacities. However, the piles driven in very silty, low I_p, Stjordal clay gained shaft capacity after each failure, as noted by Karlsrud and Haugen (1985) from tension tests in low I_p Haga clay.

Karlsrud et al. (2014) did not record end of driving (EoD) shaft resistances at their clay sites, so their piles' absolute set-up cannot be tracked. However, shaft capacity evolution can be considered non-dimensionally by comparing measurements made at different times with shaft capacity method predictions.

Karlsrud et al. (2014) employed an 'alpha-based' total stress procedure for normalisation, which relied on defining representative S_u profiles for the clays. As noted in Part 1, such profiles are often hard to gauge as S_u is affected by sampling disturbance, anisotropy and testing rates. Karlsrud et al. (2014)'s alpha capacity calculations also neglected the potentially important influence on capacity of h/R^* or 'friction fatigue'. The Unified CPT-based approach circumvents both difficulties and Lehane at al. (2020) list shaft capacities predicted for the four NGI and two LDP sites. Only the Stjordal F_{tn}-F_{rn} trace came near to Zone 1 in Figure 29, so no Fst = 0.5 correction was required.

Figure 30 shows how the measured-to-Unified calculation method shaft capacity ratios varied with time. Most tests were conducted at ages exceeding the piles' t_{95} values listed in Table 4. The exceptions were the LDP EoD resistances, all the Femern tests and the Tilbrook OC case.

The trace shown for the low YSR Pentre NC LDP pile starts from its relatively low EoD capacity and attempts to indicate the steep gains it probably achieved through rapid dissipation of its driving excess pore pressures. Far slower changes applied to the Tilbrook piles driven in the high YSR and insensitive Lowestoft till and Oxford Clay strata encountered.

Overall, the field capacities exceeded the predicted values within a few weeks of driving at Onsoy, Femern and Onsoy, while the Pentre LDP pile was only gradually approaching its expected value after 44 days. The Stjordal and Tilbrook piles took a year, or more, to achieve their Unified shaft capacities. However, the capacities grew significantly with age, with this trend continuing at times exceeding t_{95}.

It is instructive to consider also the trends for shaft capacities normalised by effective stress ICP-05 predictions. Karlsrud et al. (2014) did not measure the input parameters as required by Jardine et al. (2005). Table 5 notes the sources of the δ', *YSR* and S_t parameters applied by the Author for the six clay sites, as well as a pile driven in London Clay by the BRE at Canons Park.

Samples from Femern, Onsoy and Stjordal were acquired for 'ICP-style' testing by colleagues at Imperial College (Ridgway and Jardine 2007) and Zhejiang University (ZJU) China with the kind assistance of Professor Zhongxuan Yang and Mr Huang who undertook the testing as part of his studies at ZJU. Other tests were undertaken at Imperial College on Cowden till, Oxford Clay and Pentre clay-silt. As no Lowestoft till samples could be obtained, their interface shear angles were estimated from tests run at Imperial College on the closely comparable Cowden till.

The YSR profiles of the stiff plastic London, Femern and Oxford clays were based on reliable geological evidence; the Author is grateful to Dr Kenny Sorensen at Aarhus University for his assistance with the Femern case. Much of this information was not available to the NGI, or Unified method, teams for their earlier ICP-05 predictions for these sites. Their assessments may therefore vary significantly from the best-estimate assessments made for this paper.

Figure 31 plots the equivalent spreads of measured to ICP-05 calculated shaft capacity Q_s ratios against log-time. The ICP-05 gives broadly satisfactory predictions of the capacities measured at t > t_{95} for five of the six clay cases. However, ICP-05 is clearly non-conservative for the low I_p, low YSR, Stjordal silty clay, even 2 years after driving. Karlsrud et al. (2014) report $\varphi' = 34.2^o$ for Stjordal clay-silt.

Ridgway and Jardine suggested, following Karlsrud et al. (1993), that arching mechanisms may develop around piles driven in low YSR, lean and sensitive clays with such high φ' values and angular silt grains which, they argued, could promote circumferential arching and reduce the σ'_{rc} stresses acting on pile shafts. They also speculated that high silt content and inactive minerals may promote partial drainage during driving.

Ridgway and Jardine (2007) discussed ICP-05's over-estimation of shaft capacity at Lierstranda, another low YSR, very low I_p Norwegian silty clay site. This analysis, combined with other field evidence discussed earlier and the very low capacities reported by Flaate (1968) for Norwegian timber piles driven in similar clays and led to the cautious scheme of RF factors illustrated in Figure 29.

It is encouraging that the Taiwan Strait tests reported by Shonberg et al. (2023) indicate that such reduction factors may not be required in all low *Ip*, low YSR, silty clay strata.

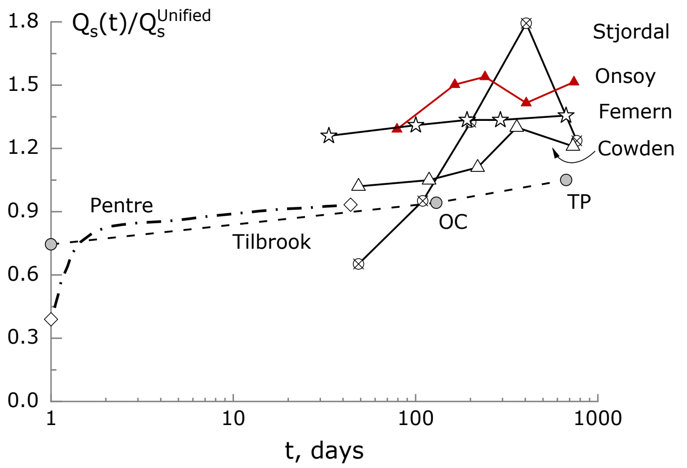

Figure 30. Shaft Q_s capacity-time trends for six clay sites expressed as multiples of Q_s values predicted by the Unified (Lehane et al. 2022) CPT-based method.

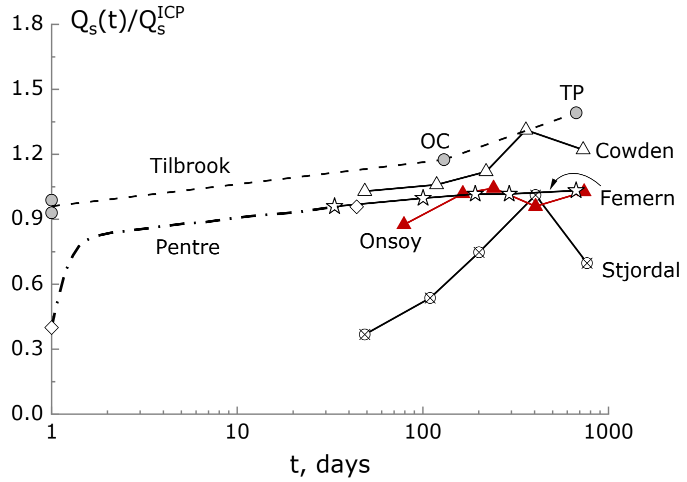

Figure 31. Shaft Q_s capacity-time trends for six clay sites expressed as multiples of Q_s values predicted by ICP-05 (Jardine et al. 2005) method; parameter sources as listed in Table 5.

Table 5. Parameter sources for ICP-05 shaft capacity calculations applied to normalise clay shaft capacities shown in Figure 31.

Case	Strata ages and source for *YSR* profiles	Ring shear δ' test source	Sensitivity St and source
Canons Park BRE Pile D	Approx. 45m years with 1.6 MPa pre-load, *YSR* reduced in disturbed clay near ground surface	Imperial College	1 Bond (1988)
Pentre LDP Pile NC	Less than 18k years; NGI CPT profile	Imperial College, LDP	From ΔI_{vy}, Chow (1997)
Tilbrook LDP Piles OC & TP	In till ≈450k: *YSR* from LDP S_u profile. In Oxford Clay ≈160m, YSR from 4 MPa geological pre-load	Imperial College, LDP	1 Chow (1997)
Cowden NGI C1 to C6	Approx. 20k; *YSR* from S_u and high-pressure oedometer tests, noting under-drained pore water pressures; after Zdravkovic et al. (2020)	Imperial College	1 Ushev & Jardine (2022)
Femern NGI F1 to F5	Approx. 55m years; *YSR* from 3.5 MPa geological preload, reduced near disturbed surface	Zhejiang University	1 NGI
Onsoy NGI O1 to O6	Less than 11k; *YSR* profile from NGI CPT profile, noting slightly artesian pore-pressures	Imperial College	6 to 25, NGI
Stjordal NGI S1 to S6	Less than <10k; *YSR* from NGI CPT profile. ICP RF correction made from 20 to 25m, after Figure 29	Zhejiang University	6 to 9 From S_u & I_L

3.1.8 *Summary for setup due to pore-pressure equalisation*

In relatively uniform clay profiles, the end-of-installation pore pressures are usually highest, and dissipate most rapidly, over the lower shaft lengths (see Figures 28 and 32) that often contribute a large proportion of the overall axial shaft capacity. It was proposed earlier that consolidation times could be estimated around the lower sections of piles from piezocone dissipation recorded at the same levels by applying Equation 6. The (longer) equilibrium times required for piles that plug can be estimated by accounting for their final filling ratios (FFRs) when calculating D*.

Pile and piezocone dissipation observations made at Cowden allow this approach to be tested. Robertson et al. (1992) report average t_{50} = 33 minutes from multiple (u_2 position) dissipation tests run at Cowden with 10cm^2 cones. Applying Teh and Houlsby's (1991) theoretical solutions allows the t_{95} times to be estimated as ≈1150 minutes.

Table 6. Piezocone predictions of dissipation for Cowden piles.

Case	Prediction for t_{95} from Eq. 6, days	Field measured t_{95} over lower shaft length, days
ICP 102mm OD closed-ended piles, Lehane and Jardine (1994a)	6.4	≈7
PISA 2m OD open-ended pile; see Figure 32, after PISA (2015)	114	≈100

Table 6 shows encouraging agreement between t_{95} predictions made from Equation 6 and field dissipation observations made around displacement piles of two types, covering a twenty-fold range of diameters. Scaling up further in this way suggests that fully coring 3.5m OD offshore piles would take up almost a year to equalise in the Bolders Bank till at Cowden, more than 4 years in the Oxford Clay encountered at Tilbrook and potentially 20 years in the Paleogene Femern clay.

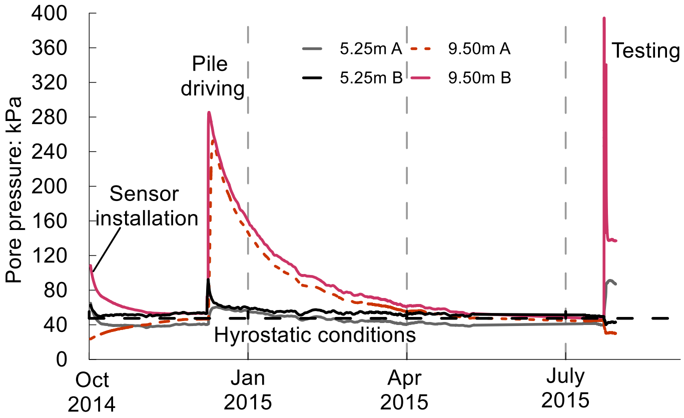

Figure 32. Pore pressure dissipation at 5.25 and 9.6m depths close to shaft of 2m OD, 10m L_p, open pile driven in Cowden till, extending to start of lateral load testing (PISA 2015).

The field cases considered above indicate that only modest setup develops due to pore pressure equalisation in high *YSR* clays, which accords with the assumptions implicit in the resistance-to-driving relationships proposed by Semple and Gemeinhardt (1981). However, high YSR clays, especially those with high I_p are often relatively impermeable, unless fissured or parted by permeable silt or sand laminae. Piles (with 500mm and 762mm diameters) driven in high YSR Femern and Oxford clays (at Tilbrook) also developed partial plugging which led to slow drainage and greatly extended dissipation times.

The low *YSR* clay cases listed in Table 4 showed far more marked setup as pore pressures equalised after driving, although with greatly varying t_{95} durations. While only 3-12 hours were required in the Pentre clay-silts found over most of the 762mm OD LDP pile's shaft length, ≈100 days were required in a single relatively thin plastic clay layer. A comparable 6-month t_{95} period was recorded with piezometers around a similar open 762mm OD pile driven in under-consolidated high I_p clays at the WD58A platform in the Gulf of Mexico; Bogard and Matlock (1998). Even fully coring 3.5m OD offshore piles (with similar D/t_w ratios) might require a decade to reach hydraulic equilibrium.

Consolidation driven setup appears unlikely to advance sufficiently rapidly around large diameter piles driven in slow-draining low YSR clays to deliver the ‘equalized’ axial capacities predicted by routine design methods until ages that extend multiple years into their service lives.

3.1.9 *Set-up processes other than consolidation*

Chow et al. (1998) postulated three further processes that might contribute to pile shaft set-up, independently of pore pressure equalisation:

- Physio-chemical reactions involving the shaft material and surrounding soil.
- Creep related relaxation of arching systems developed around pile shafts.
- Modified dilatancy within the shaft shear zone.

The following paragraphs consider how these processes might contribute to piles driven in clay.

3.1.10 *Pile steel corrosion in the ground*

Ohsaki (1982) reported how 126, L-shaped, 15m long, steel piles driven in clays, silts, sands and gravels corroded at ten sites involving relatively shallow water table depths. Piles were extracted after 2, 5 or 10 years of embedment and over 7,500 micrometer steel thickness measurements were made after all corroded products had been removed by machine wire-brushing.

The relatively modest and scattered steel loss rates may have been slowed initially by the piles retaining their mill-scale varnish, which also reduces axial capacity (Ove Arup & Partners 1986).

Ohsaki (1982) considered the possible impacts on corrosion rates of multiple potential influential factors statistically, reporting that time was the most important factor, with rates falling significantly as passive corrosion products coated the steel. He also noted that: (i) oxygen access above the water table accelerated corrosion; (ii) rates appeared ≈20% higher in clays than sands; and (iii) losses were marginally greater with low pH groundwater.

The Author’s summary of the overall mean trends (± 1 standard deviation) for steel loss, in mm, on each exposed surface is shown on Figure 33 with a tentative trend curve that reflects Bond and Jardine’s (1991) observation that little corrosion was evident around Canons Park steel piles after a single month of embedment in London Clay.

Pellew (2002) and Pellew and Jardine (2008) examined in more detail how such processes might contribute to the longer-term ageing behaviour of piles in London clay. They note that steel corrosion produces, in most cases, hydrous Iron (II) oxides and Iron (III) oxide-hydroxide compounds with molecular masses between 1.6 and 6.6 times those of their incorporated Fe atoms.

The reactions, which draw in water, oxygen and other molecules from the surrounding ground, can be catalysed by metallic elements (including Calcium, Ca). Sulphate Reducing Bacteria (SRB) may enable anaerobic reactions in sulphate-bearing soils that generate black Iron Sulphide (FeS) products which are 60% heavier than their incorporated iron.

The corrosion products, which are largely insoluble in water, also have specific gravities of 2.4 to 4.75, lower than that (≈7.85) of the parent steel, so their crystallised volumes are 2.6 to 17 times those of the lost steel. The products produce annuli around piles driven in clays that swell out radially over time.

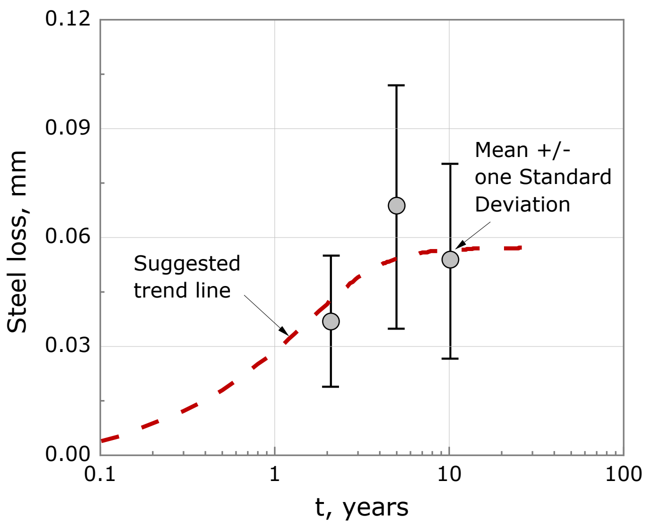

Figure 33. Long-term steel loss rates from 126 piles driven at 10 Japanese sites, after Ohsaki (1982).

Considering piles installed 17 years earlier by BRE at Canons Park, Pellew and Jardine (2008) first confirmed that steel displacement piles developed marked additional set-up over a 14-year rest period, while bored-and-cast in-situ concrete piles did not. They then explored the ageing behaviour of ‘BRE Pile D’ a 168mm OD, closed-ended, pile driven in 1982; see Table 4. A similar jacked pile, equipped with a base load cell identified a tip capacity of 55 kN; Wardle et al. (1992).

Pile D had experienced multiple compression tests over its first 3.1 years after driving. The total (shaft plus tip) resistance trends identified by BRE over 1130 days are shown in Figure 34. Three initial tests, conducted the day after driving, showed a brittle shaft response, as expected from the ICP tests discussed above. The initial ratios of measured-to-calculated (peak) shaft capacities were 0.54 and 0.92 for the Unified and ICP-05 methods respectively, supporting the earlier conclusion that the CPT-based method may be non-conservative in low δ' clays.

Some shaft setup, perhaps 15% based on Table 6, might be expected over the 5 day t_{95} time projected for Pile D, but this could not explain the ≈40% gain observed 108 days after driving. Pile D continued to show modest brittleness in all subsequent tests before recovering and growing to new maxima over extended inter-test pauses. Gerwyn Price and the Author relocated Pile D in 1999 in a hut completely overgrown by vegetation. Later tests by Pellew (2002) identified the large capacity gain, and renewed brittleness, shown as 6200 day age tests in Figure 34.

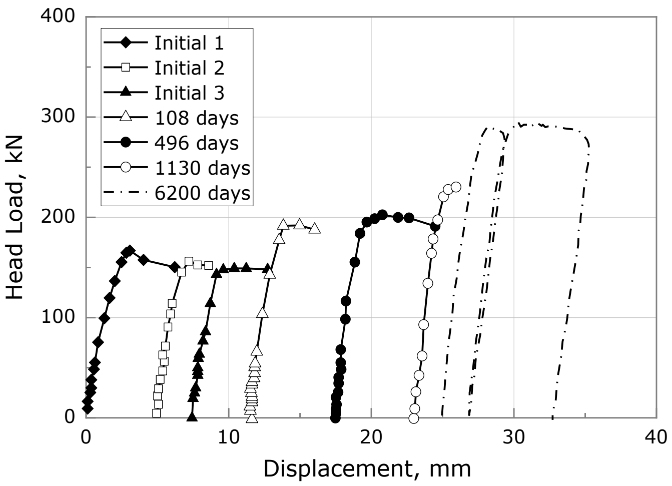

Figure 34. Compression tests on BRE Canons Park Pile D, redrawn from Pellew (2002).

Pellew (2002) excavated a fully supported pit around Pile D and other jacked and bored piles and took undisturbed block samples down to 4.5 m depth for intensive index, suction, micro-fabric, chemical and biological testing. As shown in Figure 35, a layer of a black corrosion product, ≈0.5mm thick, had developed as a new and separate layer between Pile D's shaft and the surrounding clay.

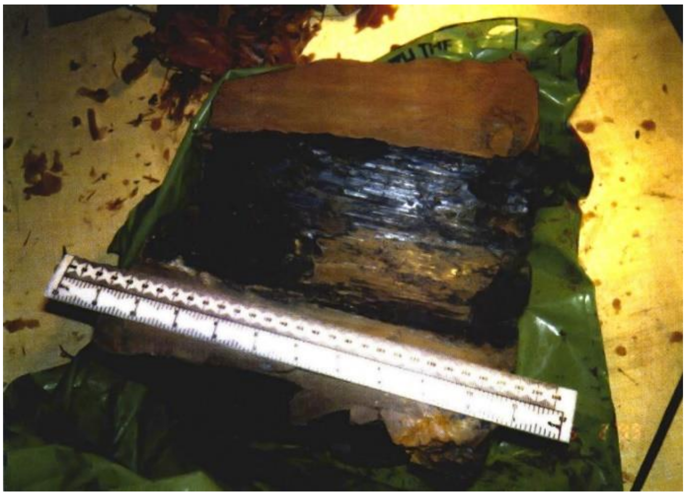

Figure 35. Black FeS corrosion product formed on BRE Pile D at Canons Park, from Pellew (2002).

The 'black material' was striated with an imprint of the fully residual shear surfaces formed by its multiple prior slow tests to failure. SEM and chemical analysis showed the corrosion product consisted primarily of FeS, although with a significant organic content and microbial populations of Sulphate Reducing Bacteria (SRB) as well as alloy trace elements.

The clay contained within an ≈150mm thick annulus around the pile also had its plastic limits w_p raised by up to 5% and its Liquidity Indices I_L reduced by ≈0.08 through the ageing processes, while Torvane and laboratory water content tests showed no consistent variation with radial distance from the shaft. However, laboratory suctions, measured as recommended by Chandler et al. (1992), showed high maxima at the pile surface and a systematic decay with radial distance (r/R) from the shaft.

The suctions retained by isotropic elastic clays after 'perfect' sampling are theoretically equal to the mean effective stress p' they sustained in-situ before sampling and are expressed in this way in Figure 36.

Bond and Jardine (1991) had made similar measurements on block samples taken 1 month after installation at the same (≈3.3m) depth around 102mm diameter closed-ended piles driven and jacked to the same ≈6m tip depth. While they saw little evidence of corrosion, they identified that installation and pore-pressure dissipation had generated marked radial changes in the in-situ mean effective stresses p' of the surrounding clay.

Figure 36 contrasts the radial profiles found from the two studies; ICP-05 σ'_{rc} predictions are also noted which are ≈10% higher around Pile D at the same depth because of its larger diameter and therefore lower local h/R value While $\sigma'_{rc}/p' \approx 1$ close to the shaft (at $r/R = 1$) one month after driving this ratio rose to ≈ 2.7 over 17-years, which compares with the pile's long-term Λ ≈2. The pile's multiple prior tests are likely to have reduced the brittle London Clay δ' angles: higher Λ values could be expected from parallel tests on equivalent 'virgin' piles.

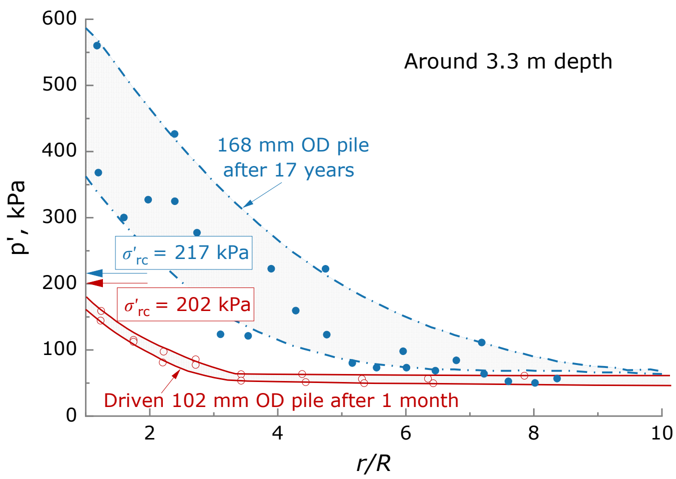

Figure 36. Distributions of p′ around piles at Canons Park measured 1 month and 17 years after driving in London Clay; after Bond and Jardine (1991) and Pellew (2002). Author's (medium term) ICP σ'_{rc} predictions are also shown for both cases.

Pellew (2022) summarised the shaft-groundwater-clay chemical reactions as shown in Figure 37 and concluded from mass balance and density considerations that the black corrosion product generated by SRB facilitated reactions had expanded ≈0.5mm radially outwards into the surrounding clay mass. The observed corrosion product growth can be compared with the mean steel loss of ≈0.09mm expected from Figure 33, with a 50% standard deviation, raised to ≈0.11mm to allow for the ≈20% greater-than-average rates found in clays.

As noted earlier, Ohsaki's piles had retained their mill scale, which may have slowed corrosion initially. Applying the published specific gravities of solid FeS particles and steels suggests a minimum annular FeS thickness of ≈0.3mm, marginally lower than the measured 0.5mm. However, Pile D's corrosion coating included organic and other molecules that might account for any slight (0.2mm) apparent shortfall.

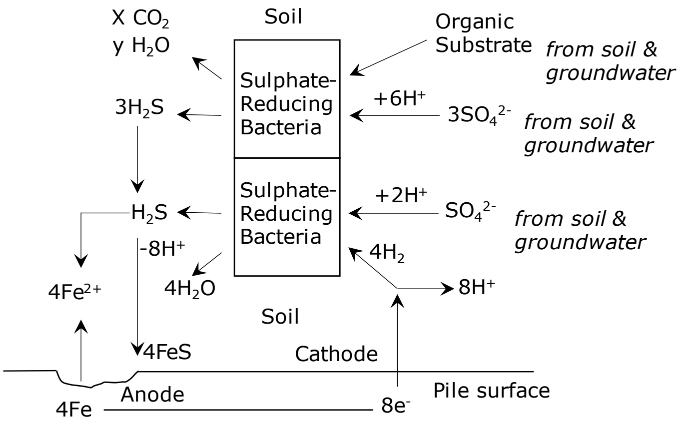

Figure 37. Sulphate Reducing Bacteria corrosion reactions around Canons Park Pile D. Re-drawn from Pellew (2002).

After accounting for the estimated 0.11mm of lost steel, a radially outward movement Δr = 0.39mm of the clay surrounding the pile would have caused an ≈0.5% cylindrical cavity strain (ε_C) and provoked, in turn, an increase in the 'consolidated' shaft radial effective stresses, σ'_{rc}.

Site-specific geo-metallurgical analyses can predict how corrosion rates may vary with geochemistry, pore fluid pressures, temperature, salinity and dissolved oxygen levels. The potential corrosion product thicknesses Δr they predict should be independent, for any fixed set of ground conditions, of pile scale. However, the cavity strains $\varepsilon_C = 2\Delta r/D$ generated around pile shafts vary inversely with pile diameter, D.

As shown later in relation to a comparable sand case, the impact of the corrosion growth may be quantified through representative, drained, non-linear elastic-plastic cylindrical cavity expansion analysis. Analyses conducted to predict the σ'_{rc} gains need to capture faithfully the: (i) initial soil stress fields, (ii) non-linear relationships between tangent G and invariant shear strain ε_s and mean effective stress p', (iv) corresponding Poisson's ratios (or bulk moduli K' functions) and (v) geomaterials' yielding behaviour.

Alternatively, undrained self-boring pressuremeter (SBP) can also provide direct, albeit approximate, experimental indications of the potential ground response. Tests conducted in undisturbed London Clay at Canons Park included an expansion test at the 3.25m mean depth of the suction sampling; Jardine (1985). As shown in Figure 38, this test developed a radial stress increase $\Delta\sigma_r \approx$ 250 kPa after applying a 0.6% cavity strain, which could raise the pile shaft σ'_{rc} by a factor of 2.2, and so approach the level required to explain the growth of shaft capacity and in-situ p'. However, the undrained test probably generated large stress changes than applied under long-term drained field conditions.

The SBP test's unload-reload stages indicate that the radial loading response is non-linear and shows sharply reduced stiffness when the radial pressure and cavity strain exceed their previous maximum values. It is possible that the σ'_{rc} stresses developed around Pile D built to final values approaching the London Clay's local cylindrical cavity expansion limits.

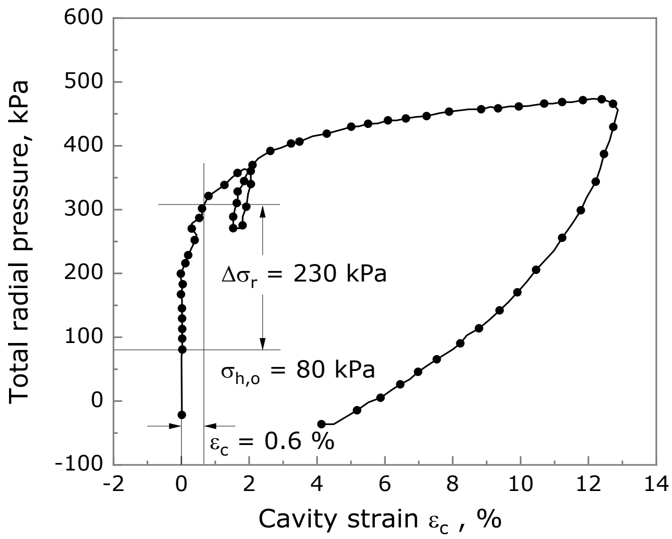

Figure 38. Estimate of $\Delta\sigma_r$ caused by corrosion product growth around BRE Canons Park Pile D from SBP test at 3.25m depth.

Noting that Pile D showed renewed brittleness after its extended pause periods, Pellew (2002) postulated that the chemical changes might have affected the residual shear surfaces formed by successive testing. Any crystallisation of corrosion products over the pile shaft shear surfaces, or alteration of their surface chemistry, might raise their δ' angles, with the ≈21° angles associated with first time shearing in the nearby de-structured London Clay providing an upper limit. The brittle load-displacement curve developed in Pile D's 6200 day tests (see Figure 34) suggests marginal increases in operational δ' had developed over the pile's extended ageing period.

Overall, the Pile D investigations prove that slow corrosion reactions generate capacity gains and indicate how they can be gauged by combining physical chemistry, representative steel loss rates and representative geotechnical calculations.

3.1.11 *Postulated arching and enhanced dilatancy ageing mechanisms*

Corrosion is not the only potential additional long-term set-up mechanism. Karlsrud et al. (1993) and Ridgeway and Jardine (2007) postulated that arching may develop around piles during driving in high φ', sensitive, low YSR, low I_p clays which might explain their low shaft capacities and tendency to show higher capacities when re-tested serially, either monotonically or cyclically. Creep that occurs after the extreme stresses and strains imposed by driving could weaken any arching system and allow shaft capacities to build over time. Cycling or monotonic testing might also promote relaxation of any arching.

The steady improvements of shaft capacities seen at Stjordal, and possibly Onsoy, by open-ended piles with high D/t_w (≈80.6) ratios and around solid timber piles driven in similar clays (Flaate 1968) are compatible with such a mechanism applying after driving in high φ', low I_p and potentially sensitive, yet inactive, clays. However, further direct field evidence is needed to confirm the hypothesised mechanism.

North Sea driving records suggest that significant setup takes place at high YSR, low I_p sandy glacial clay sites over time scales that are unlikely, considering the earlier discussion on clay t_{95} times, to have allowed significant gains through consolidation.

Durning et al. (1978) and Battacharya et al. (2009) report early age re-strike data from six North Sea platform sites involving high YSR, low permeability clays, where notably higher blow counts were required to achieve effective re-driving after operational pauses of 2 to 300 hours. 'Calibrated wave equation' approaches led to the short-term set-up trends in Figure 39 for the 'clay only' Heather site with the largest (1.54m OD, 63.5mm t_w) piles. The mean Λ trend rose to 1.18 ±0.1 within 100 hours, which is too early to be explained by corrosion. Consolidation seems improbable too, as its impact is limited with high YSR clays. Many months may have been required to achieve equalisation at such sites and only slight dissipation could be expected over 100 hours; see Figure 32.

As reviewed later in connection with piles driven in sands, calibration chamber experiments and advanced numerical analyses demonstrate that arching develops during drained displacement pile installation in high φ' soils. Sensitive low YSR soils with angular particles are more likely to be affected by arching and creep processes than lower φ' geomaterials. The closed-ended piles driven in the plastic London clay considered in Figure 36 showed no sign of arching applying in their interpreted p' profiles.

Enhanced interface shear dilatancy has also been also shown, in credible field measurements, to contribute to driven pile set-up in sands. While such 'dilatancy-related' gains may also apply after extended ageing in clays, the Author is not aware of any experimental confirmation, or otherwise, that this mechanism applies in the field to piles driven in clays.

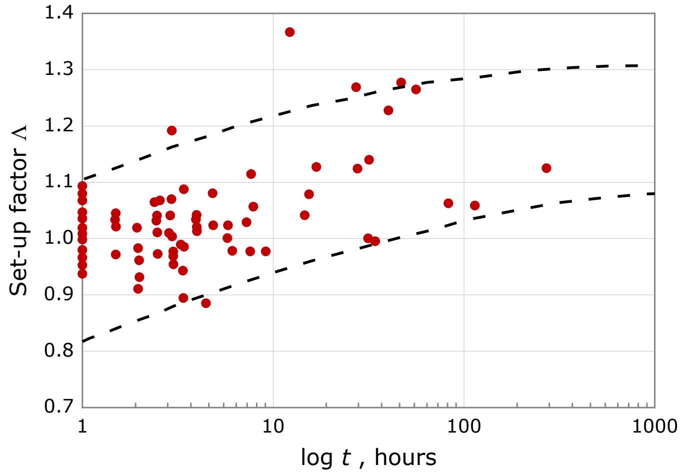

Figure 39. Short-term setup inferred from driving behaviour in very stiff-to-hard glacial high YSR sandy clays with 5% ≤ I_p ≤ 25% at the Heather field; re-drawn from Durning et al. (1978).

3.2 *Piles driven in chalk*

Northern European offshore developments frequently encounter chalk. As noted in Section 2.2, chalk can manifest in states ranging from competent limestone through to high porosity, lightly-cemented, sensitive carbonate silts with liquidity indices close to unity. Both extremes present challenges when designing piles, rather than rafts, to support offshore structures.

Driving refusals can occur in high density chalks and piles can fall freely under self-weight in lower density strata (Carotenuto et al. 2018, Jardine et al. 2018) and little information existed until recently to guide axial design. While current CIRIA C574 (Lord et al. 2002) guidance advises site-specific pile tests wherever possible, it also gives remarkably low default ultimate shaft resistances of 120kPa for open-ended steel piles driven in high density chalk and 20kPa in all lower densities, reducing to 10kPa for slender piles that 'whip' under percussive driving.

The urgent need to design cost-effective piled foundations for multiple chalk OWF sites led to both industrial and academic research. Studies undertaken up to 2017 include the Windsupport JIP (Ciavaglia et al. 2017) and the Innovate-UK programme involving Imperial College, Iberdrola and GCG, London. Buckley et al. (2018a, b) and Jardine et al. (2018) describe the Innovate-UK research programme. Its main aim was to support large-scale dynamic, static and cyclic offshore pile testing at the glacial till over low-to-medium density chalk Wikinger OWF site in the Baltic Sea. Its programme included static and cyclic tests on several 139mm steep open-ended piles driven at St Nicholas-at-Wade (sited in NE Kent, UK).

The offshore experiments on nine 1.37m diameter steel piles driven in ≈40m water depths, required the innovative, entirely remotely operated seabed equipment illustrated in Figures 40 and 41 and described by Barbosa et al. (2015). Conducting the Wikinger programme ahead of production piling enabled considerable reductions in the Wikinger OWF project risks, along with greatly reduced foundation costs and embedded CO_2 emissions; Barbosa et al. (2017).

The Wikinger dynamic tests confirmed very low End of Driving shaft resistances. Dynamic and static tests conducted after 78 to 108-days of ageing also indicated high chalk setup factors Λ that exceeded those associated with low YSR clays. The field shaft capacities were far higher than expected by the CIRIA guidelines; see Figure 42. This allowed shorter-than-anticipated chalk penetration lengths (L_p) for the 2.7m and 3.76m OD production piles driven to support the 70 Wikinger offshore wind turbine (OWT) jacket structures depicted in Figure 43 and their offshore sub-station (OSS) platform.

Signal matching analyses of the production piles' driving and re-strike records led to the setup Λ – log time trends in Figure 44, where piles with an average $L_p/D \approx 6.8$ length in chalk developed a mean $\Lambda \approx 4$ within one week of driving.

Figure 40. Placing pile guide frame at a Wikinger pile test location, after Barbosa et al. (2015).

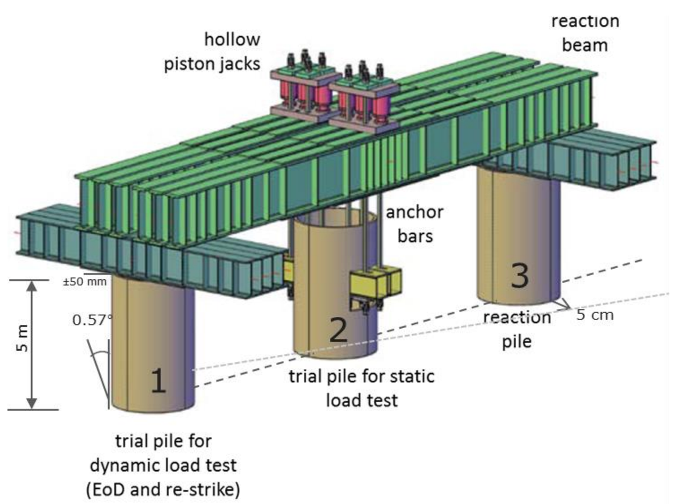

Figure 41. Schematic of Wikinger static testing arrangements; after Jardine (2020).

The SNW tests also confirmed very low End of Driving shaft resistances, with the chalk de-structuring to soft putty in annuli formed around the pile shafts.

High long-term Λ factors were confirmed by tension tests on the 139mm OD open steel piles driven at SNW, while axial cyclic loading tests provided further valuable insights; Buckley et al. (2018b).

Additional laboratory testing by Doughty et al. (2018) investigated how the putty chalk's stiffness and shearing resistances could increase over time through consolidation and carbonate re-bonding.

Taken together, the investigations provided fresh insights into installation behaviour including the basic mechanisms of axial resistance under monotonic and cyclic loading and the marked effects on axial capacity of age after driving in chalk, Buckley et al. (2020) and Jardine (2020).

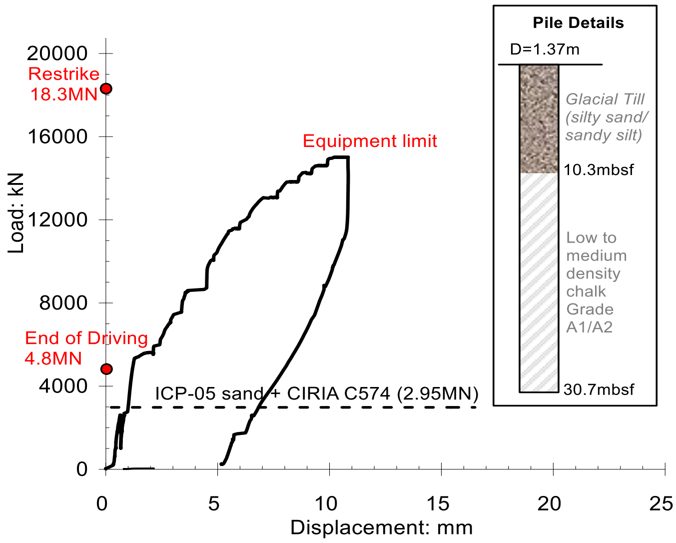

Figure 42. Dynamic EoD and 78-day age re-strike and static tension shaft resistances for 1.37m OD, 30.7m long, 40mm wall thickness Wikinger piles at WK43-2 location. Dashed-line indicates prediction from CIRIA in chalk, in combination with ICP-05 sand method for till; after Buckley et al. (2020b).

Figure 43. Three OWT jacket structures in transit to Wikinger; photograph courtesy of Scottish Power Renewables.

The research described above led Jardine et al. (2018) and Buckley et al. (2020a) to propose tentative 'Chalk ICP-18' approaches for predicting axial chalk resistance to driving (CRD) and long-term axial resistance. They aimed to match the available field evidence through a similar framework to the ICP-05 CPT-based method for sands.

However, their scope was limited by: (i) the Wikinger site investigations not including complete CPT profiles in the chalk, (ii) the lack of any strain gauges in test piles to separate the glacial till and chalk contributions to capacity and (iii) the offshore tension loading systems' inability to reach the (unexpectedly high) loads required to fully fail piles at the two chalk-dominated locations (see Figure 42).

Also, no compression test had been conducted, and the un-instrumented piles driven at SNW had been positioned entirely above the water table. Jardine et al. (2018) therefore emphasised that more field experiments were required to develop and deliver a fully supported CPT-based design method.

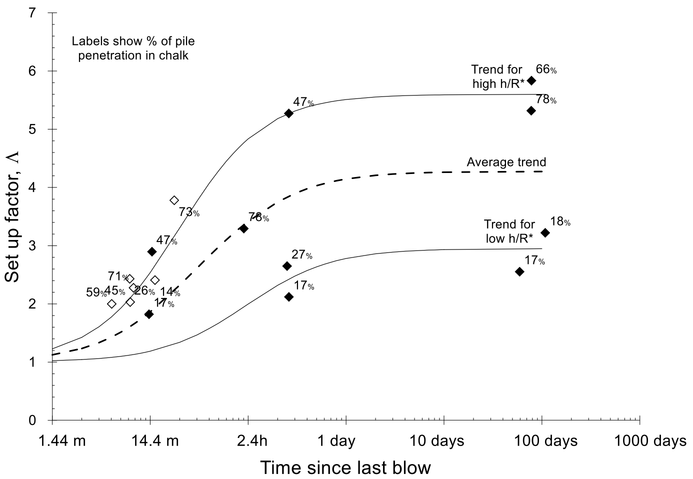

Figure 44. Setup Λ trends from re-strikes on 2.70 and 3.76m OD piles at Wikinger with average trend for piles with embedment in chalk to diameter ratio L_p/D = 6.8; after Buckley et al. (2020).

The ALPACA and ALPACA Plus JIPs described by Jardine et al. (2023a, b) aimed to test the key design method conjectures against new field evidence. Dynamic and monotonic axial tests were conducted on 27 piles with outside diameters ranging from 139mm to 1.8m and embedded lengths from 3.08 to 18m. Figure 45 illustrates the ALPACA LD pile layout; Buckley et al. (2023) present further details of the test arrangements and control systems.

Most steel piles were equipped with diametrically opposed strings of Fibre Bragg Grating (FBG) fibre-optical axial strain gauges. The piles were driven with some shafts positioned entirely above the water table, others that were fully submerged, while most spanned both conditions. Piles were fabricated from standard steels, concrete and stainless steels, with a range of wall thicknesses and end conditions. Testing was undertaken at various ages up to 409 days after driving.

Figure 45. ALPACA LD piling operations at St Nicholas at Wade; November 2017.

Buckley et al. (2018a), Vinck et al. (2022) and Liu et al. (2022) describe the SNW site's characterisation through extensive CPTu and geophysical profiling as well as intensive laboratory testing. Figure 46 summarises the multiple CPTu soundings made in the test area where the water table lies at ≈5.5 to 6m depth. Weathered chalk was removed by prior quarrying to leave CIRIA grade B2 (Lord et al. 2002) structured, very weak-to-weak, low-to-medium density white structured chalk with closed-to-slightly open stained joints and beds of 250 mm average thickness, along with mainly vertically oriented micro-fissures spaced at 10 to 25mm apart.

Figures 11 and 12 gave examples of the 50 monotonic locally instrumented (drained and undrained) triaxial tests conducted on Geobore-S wireline rotary boreholes and block samples, while Liu et al. (2023) explored the behaviour of the putty chalk. Over 40 cyclic laboratory tests were conducted to support the cyclic field pile testing analysis.

Vinck et al. (2023) report how normal effective stress levels, interface material, ageing, corrosion, and testing procedure affect chalk's interface shearing resistances. Mild steel corrosion raised ultimate δ'_{ult} angles to ≈4° above the de-structured chalk's critical state $\phi'_{cs} \approx 31°$.

Air can flow through open fissures above the water table in chalk, so Vinck (2021) examined how oxygen and salinity affect surface corrosion mass loss rates for steels in contact with chalk under idealised laboratory conditions. The reaction rates developed over periods up to 67 days, expressed in µm steel loss per year, were (i) ten times slower in isolated anoxic tests than when exposed to air, (ii) three or more times faster with saline than fresh groundwater and (iii) comparable between various oxidisable construction steels, but ninety times slower with stainless steel. Vinck's results indicate a greater sensitivity to potential site conditions than Ohsaki's (1982) tests, although none of the latter's sites involved chalk.

The ALPACA and ALPACA Plus studies included additional programmes of axial cyclic, as well as monotonic and cyclic lateral tests on other instrumented piles. Jardine et al. (2023a) summarise the integrated research streams and cite several journal papers that provide details of the ALPACA programme's individual components.

The following paragraphs focus principally on the piles' axial capacity behaviour. Wen et al. (2023a, b) analyse the piles' load-displacement behaviour and propose both beam column (t-z, Q-z) and advanced non-linear FE analysis predictive approaches that make use of high-quality core logging, CPT profiling and stress-path laboratory testing. The most relevant overall findings regarding axial capacity are:

1. As anticipated in Chalk ICP-18, the local shaft resistances mobilised during driving, and after ageing are proportional to local CPT resistance q_t and decline steeply with relative pile tip depth, *h/R*, showing far steeper reductions than at clay or sand sites.
2. Chalk ICP-18 offered generally good predictions for Chalk's Resistance to Driving.
3. Monotonic tests conducted at various ages on piles of different types, scales and geometries gave an extraordinarily wide range (11 to 205 kPa) of average axial shaft resistances, τ_{rzf}.
4. Surprisingly, the overall (internal and external) long-term shaft resistances were around twice as high under compression loading than in tension. It is essential to allow for this feature, which was not anticipated in Chalk ICP-18, when assessing setup trends by comparing tensile static tests on aged piles with compressive dynamic EoD resistances.
5. Setup was notably slower and less marked below the water table than above it, leading to Chalk ICP-18 over-predicting long-term resistances for submerged piles, especially those driven with high *L/D* ratios and tested in tension.
6. Setup and reconsolidation were enhanced above the water table due to: (i) air flow through the chalk's open fractures accelerating corrosion and (ii) pore water suctions, whose near hydrostatic profile reached 55 kPa near ground surface.
7. While the stainless and mild steels prepared with the same 10 µm CLA roughness showed similar driving resistances, corrosion led to the mild steel piles developing (at 127 ±2 day ages) ≈70 ±10% higher shaft capacities.

Detailed information was gained on how local shaft resistance varies over time. Figure 47 provides an example by comparing the compressive (signal matched) EoD τ_{rzf} profile of the 1.8m OD, 18m long, ALPACA Plus TP1 pile with that determined in tension from its 24 FBG strain gauges when tested to failure 371 days later.

Figure 48 provides a summary of how piles driven principally below the water table developed their setup over time. High *L/D* piles showed slower and less marked gains than the low *L/D* piles (TP1, R1 and R2) whose trends fall (in most cases) relatively close to the average trend for Wikinger piles (with mean L_p/D = 6.8) shown in Figure 44.

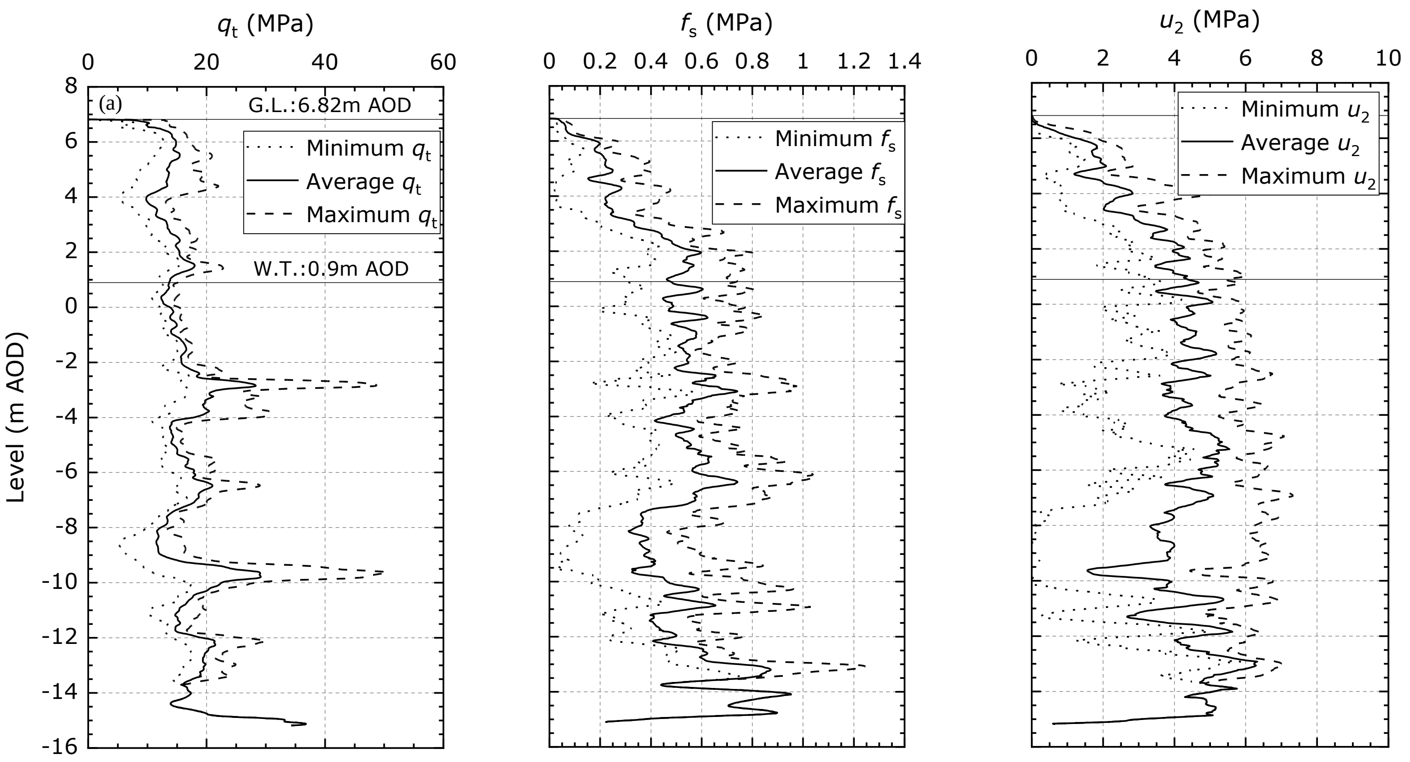

Figure 46. Summary CPTu profiles in the ALPACA test area at SNW; after Vinck et al. (2022).

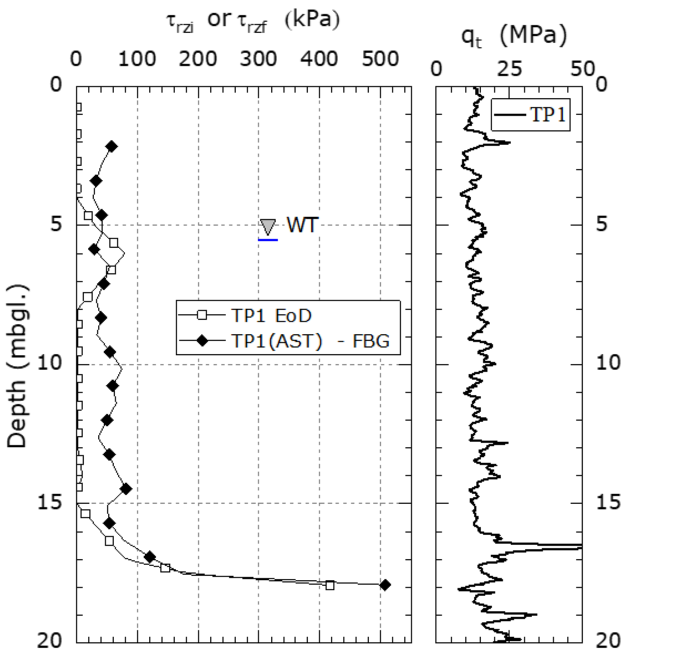

Figure 47. Compressive EoD and aged tension static shaft shear stress distributions for ALPACA Plus (1.8m OD, 18m long) TP 1 pile, also showing local CPT profile; after Jardine et al. (2023b).

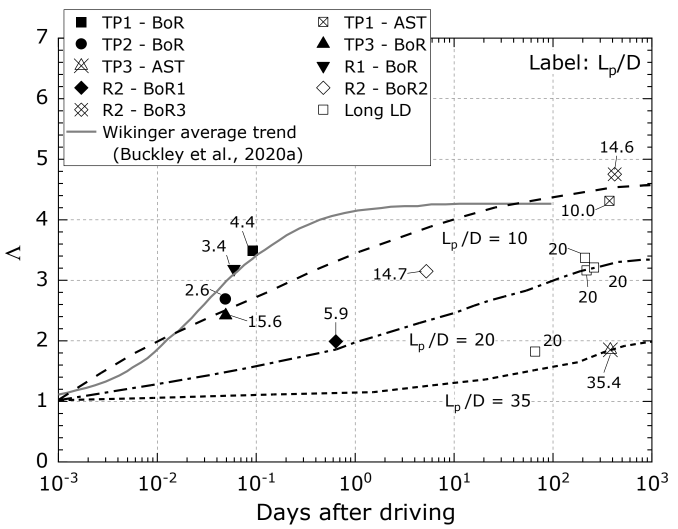

Figure 48. Set up factor Λ – time trends from compressive EoD and beginning of restrike (BoR) and static tension (AST) tests for ALPACA and ALPACA Plus piles, after Jardine et al. (2023b).

Returning to driving resistance, Equations 7 and 8 from Chalk ICP-18 gave total EoD shaft capacity predictions Q_s that fortuitously led to a mean calculated-to-measured (Q_c/Q_m) ratio of 1.00 (and CoV = 0.38) for the new dataset. The expressions captured very well the tendency for τ_{rzi} to reduce sharply with h/R^* during driving and were therefore retained in the recalibrated 'ALPACA-SNW' approach. The only significant revision was the adoption of Equation 9 to achieve a more conservative fit to the available dynamic base resistance data in place of Chalk ICP-18's tentatively suggested $q_b/q_t \approx 0.6$. Any 'internal' shaft resistance developed by open-ended piles under compression loading was assumed to be built into this end bearing expression.

$$\tau_{rzi} = \sigma'_{ri} \tan \delta'_{ult} \tag{7}$$

$$\sigma'_{ri} = 0.031 q_t \left(\frac{h}{R^*}\right)^{-0.481\left(\frac{D}{t_w}\right)^{0.145}} \quad (h/R^* \geq 6) \tag{8}$$

$$\frac{q_b}{q_t} = (D/t_w)^{-0.175} \tag{9}$$

The recalibrated approach next applied Equation 10 to assess long-term shaft resistance:

$$\tau_{rzf} = f_L[\sigma'_{rc} + \Delta\sigma'_{rd}] \tan \delta' \tag{10}$$

With loading factors f_L taken as 2/3 and 4/3 in tension and compression respectively. The $\Delta\sigma'_{rd}$ interface dilation term was modified to recognise that the B2 grade SNW chalk mass's maximum elastic shear stiffness is only 1/4 of that expected from seismic CPT testing. As discussed in Section 1.2, lower and higher multiples apply in poorer and better grade chalks respectively and the stiffnesses substituted into Equation 11 should reflect the site-specific fracture profiles. The associated radial (dilative) displacement with failure below-the-water was interpreted as $\Delta r \approx 3\mu$m.

$$\Delta\sigma'_{rd} = 4G_{ope}\Delta r/D \tag{11}$$

$$\sigma'_{rc}/q_t = f_{\text{tip}} \times 0.025 \times (h/R)^{-0.8} \text{ for } h/R \geq 0.5 \tag{12}$$

Equation 12 was developed from careful analysis of the FBG strain gauge data (taking $\delta' = 32^o$) to give the best fitting σ'_{rc}/q_t expression for oxidisable (mild) steels under fully submerged conditions. An equivalent expression was developed for cases above the water table that predicts higher σ'_{rc} stresses for given q_t values.

Statistical evaluation was made for all tests made at ages ≥120 days, after eliminating the stainless-steel piles and three very high L_p/D (and unusually flexible) open-ended piles driven through cased holes.

It is convenient to consider here the tests' measured-to-calculated capacity Q_m/Q_c parameters. The fitting for Equation 12 was constrained to give an average Q_m/Q_c of unity; the resulting CoV was 0.16. The subset of 'offshore-like' open-ended steel piles driven with shafts principally below the water table indicated slightly less ideal $Q_m/Q_c = 0.93$ and $CoV = 0.26$ outcomes. In comparison, applying CIRIA 574 gave a highly conservative $Q_c/Q_m = 2.7$.

Setup factors may be predicted by dividing the calculated SRD resistances into the long-term compressive capacities, which leads to Λ values for t ≥ 120 days that decline with L_p/D.

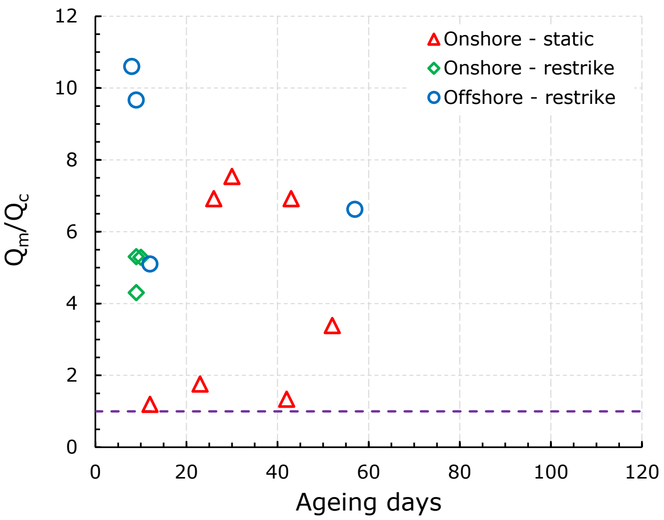

Figure 49. Independent checking of CIRIA 574 Q_m/Q_c shaft capacity ratios against time: 14 tests at UK, French and German sites on 0.61 to 1.5m OD steel piles driven in low-to-medium density chalk.

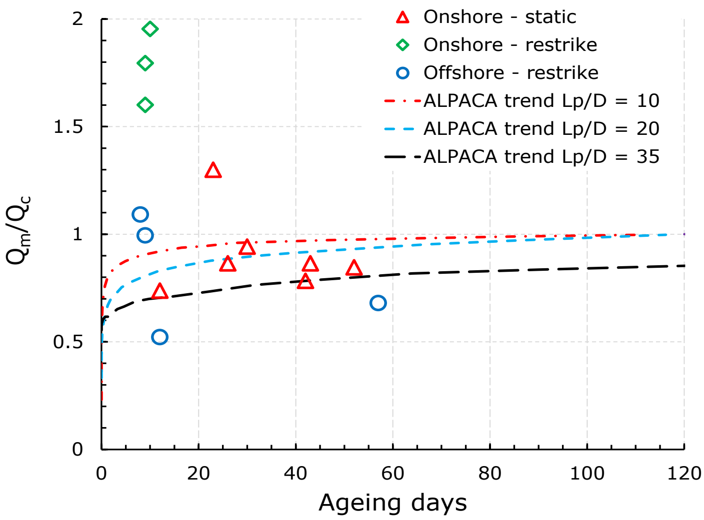

Figure 50. Independent checking of ALPACA-SNW Q_m/Q_c shaft capacity ratios against time: 14 tests at UK, French and German sites on 0.61 to 1.5m OD steel piles driven in low-to-medium density chalk.

It is always important to check empirical relationships with independent experiments. Vinck (2021) and Vinck et al. (2023) describe how liaison with industrial groups led to a second and separate dataset of fourteen, 0.61 to 1.5m diameter, 'fully submerged' steel piles driven at low-to-medium density chalk sites in France, Germany and the UK. Dynamic EoD data was available for all cases, static 'aged' capacity measurements for seven, and dynamic restrikes for the remaining half, whose results were inevitably less certain. The 'aged' measurements were made, on average, 24 days after driving, which is typical of industrial practice (Jardine et al. 2005) but falls short of the proposed 120-day target design age.

The independent test sites' ground investigations enabled dynamic analyses of the EoD resistances and any restrike tests as well as unambiguous CIRIA 574 and ALPACA-SNW capacity calculations. The CIRIA outcomes plotted as Q_m/Q_c against time in Figure 49 indicate a highly conservative mean of 5.4, while the ALPACA-SNW predictions in Figure 50 show a slightly conservative mean Q_m/Q_c = 1.07 and far less scatter.

The offshore restrikes appear broadly compatible with the static tests in Figure 50. However, three onshore restrikes appear as outlying high Q_m/Q_c points. Discounting these three outlying re-strikes reduces the scatter greatly and leads to the new method's mean Q_m/Q_c (for tests with a 28-day average age) falling to 0.88, below the desired value of unity.

However, the early age Q_m/Q_c – time predictions (developed from the SNW trends in Figure 48) plotted in Figure 50 suggest that that the remaining group of 11 piles were on track to deliver mean Q_m/Q_c closer to unity at the 120-day target age, as well as a still higher (and more conservative) Q_m/Q_c for CIRIA 574.

3.2.1 *Chalk setup processes below the water table*

The ageing mechanisms discussed in Section 2.1 for piles driven in clays are equally relevant to low-to-medium density chalks. Considering consolidation first, the SNW CPTu profiles in Figure 46 show CPTu shoulder (u_2) excess pressures of 6 MPa and higher. Still larger pressures are recorded at the u_1 face position (Buckley et al. 2020a). Far lower pressures may be expected higher on the shaft (see Figures 28 and 32) in response to the total stresses imposed at the tips reducing steeply with increasing h/R and partial dissipation occurring as piles continue to penetrate.

The high CPTu tip pressures reflect the collapse of the chalk's sensitive structure beneath and around the cone. Lord et al. (2002) found that a similar collapse generates soft putty annuli around open pile shafts. MuirWood et al. (2015) and Buckley et al. (2020a), report radial thickness of putty comparable to their piles' wall thicknesses t_w. A second annular region of damage is found around open-ended piles within which the chalk undergoes additional brittle fracturing that greatly reduces its operational stiffness; Pedone et al. (2023).

Figure 51 illustrates these two zones with a photograph taken in a shallow pit excavated, around 420 days after pile driving, around the lightly corroded shaft of R2, a 1.22m OD pile with a 24.6mm t_w. The fractured chalk extended out radially by 10t_w beyond the first, ≈25mm thick, annulus of de-structured, formerly putty, chalk which had reconsolidated and rebonded at this depth, several metres above the water table. Corrosion was evident on the pile shaft and at the putty-to-pile contact in a pit excavated around the 508mm diameter ALPACA LD piles ≈360 days after driving. Unfortunately, it was not possible to measure the thickness of corrosion product formed above the water table in either case.

Figure 51. Putty and fracture zones of driving damage around Pile R2 after completing axial testing, also showing annulus of corroded steel at putty-to-pile shaft contact.

Multiple CPTu dissipation tests conducted at SNW with 15cm^2 cones showed $t_{95} \leq 80$s, reflecting the chalk's open fractures (Vinck et al. 2022). Applying Equation 6 to the low *L/D*, (1.22 and 1.8m OD) ALPACA Plus R1 and TP1 indicates $\approx$1 and 2 hour t_{95} dissipation times respectively for their lower shaft sections. Relating these to Figure 46 trends suggests that consolidation provided 60 ±20% of these piles' (415 and 373 day) long-term setups. Considerably less 'consolidation' setup is indicated for the high *L/D* piles, probably reflecting their average EoD excess pore pressures being relatively low.

Returning to the Wikinger piles and assuming their field radial consolidation coefficients were similar to those at SNW suggests t_{95} durations of ≈3 and ≈6 hours for the lower shaft sections of the 2.7 and 3.76m OD production piles. Their mean set-up trend, in Figure 44, suggests that consolidation could account for ≈85% of their average 10-day setup.

Additional processes are required to account for the remaining additional long-term setup interpreted from tests at both sites. As discussed in Section 2.1, relaxation of circumferential arching around pile shafts through creep potentially adds to (probably) medium-term setup. While any role of enhanced interface dilation remains to be demonstrated, side-by-side ALPACA tests on mild and stainless-steel piles prove conclusively that corrosion at the shaft-to-chalk interface (see Figure 51) adds significantly to long-term setup.

The potential for a similar corrosion-and-cavity expansion mechanism to that set out in Section 2.1 to apply to chalk can be examined most clearly by considering R2, the only pile on which the τ_{rzf} values were measured at three ages. Signal matches show its average EoD shaft resistance τ_{rzf} as 24.2 kPa, while a limited restrike after 5.2 days (which is considered unlikely to have affected long-term capacity greatly) indicated 76.2 kPa. A final group of restrikes applied after 421 days led to large sets and showed a clear maximum mean τ_{rzf} = 117.4 kPa.

The ALPACA-SNW calculation procedures set out earlier employ, for simplicity, the δ' angle measured against fresh interfaces at all ages. However, Vinck (2021) showed that δ' rises by ≈4º as interface corrode, which could account for ≈30% of the 5.2-to-421 day capacity gain. If the dilative $\Delta\sigma'_{rd}$ component remains unchanged, then Equation 10 indicates a $\Delta\sigma'_{rc}$ increase ≈ 36 kPa is required to explain the remaining 70% of the long-term set up.

Recent SEM studies by Dr Livia Cupertino Malheiros at Imperial College examined the chalk's structure and corrosion near the steel-to-pile interface. As illustrated in Figure 52, pile driving fractured a large proportion of the previously intact chalk coccoliths, as also noted previously by Bialowas (2017). Backscattered SEM analysis indicated almost pure $CaCO_3$; corrosion products appear unable to penetrate the (low void) ratio de-structured chalk and concentrated in distinct annuli, as shown in Figure 51, although soluble salts migrated out radially and stained the first 2mm of 'putty' chalk.

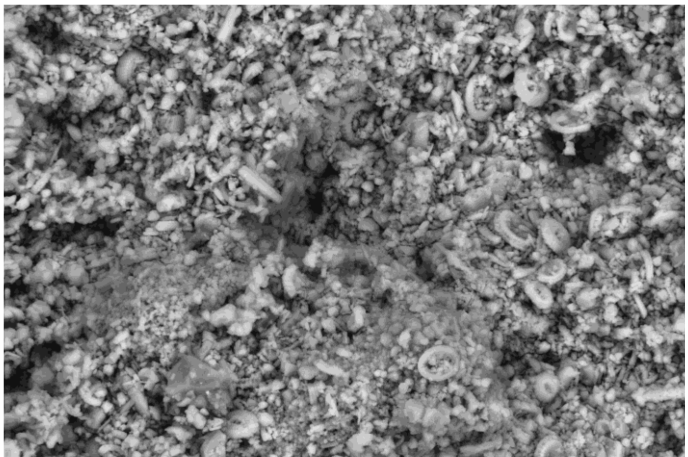

Figure 52. SEM image of shattered coccoliths in de-structured chalk annulus around ALPACA LD pile; note 10µm scale on bottom right corner.

Less corrosion and lower product thicknesses Δr can be expected below the water table than appear in Figure 51 to have developed at shallow depth around Pile R2. First order illustrative estimates have been made of the Δr required to generate an average 36 kPa $\Delta\sigma'_{rc}$ over Pile R2's 18m length. Pedone et al. (2023) obtained good 3D FEM matches for lateral loading tests on ALPACA piles by treating the de-structured 'former putty' chalk above the water table as a strongly non-linear material with G_o = 1 GPa, while taking G_o = 0.5 GPa in the outer chalk mass and reducing G_o tenfold in the broader annulus of chalk fractured by driving.

A simple, three-region, elastic treatment that applies these shear moduli (with a 50% reduction to allow for non-linearity in the putty) predicts Δr ≈0.1mm. If the putty had remained uncemented and followed its K_o virgin compression line, with C_c ≈0.1, as noted in oedometer tests by Liu et al. (2023a), then the estimated increase in σ'_{rc} would have caused a further Δr component ≈150 μm across the de-structured annulus, giving a total of ≈0.25mm. However, chalk putty is known to re-bond with age under even completely undrained conditions (Doughty et al. 2018), so the Author's best estimate falls between these limits.

The 0.1 to 0.25mm estimates for the thickness of low-density iron hydroxides formed by corrosion are broadly compatible with the several times smaller (≈ 30μm) steel loss trend expected from Figure 33. As shown earlier the thicknesses of the corrosion product annuli are several times greater than the steel loss.

Offshore piles driven in cold, high pressure, saline water might corrode at different rates. Site-specific predictions could be made by combining reliable corrosion analyses with representative (radially non-homogenous) drained cavity expansion analyses of the full pile shafts. However, Figure 50 does not signal any major difference between onshore and offshore trends. The Wikinger field tests, which are not included, also indicated encouragingly high setup factors. While Δr should be independent, for any fixed set of ground conditions, of pile OD, the cavity strains $\varepsilon_c = 2\Delta r/D$ developed around the pile shafts vary inversely with D and the putty thicknesses grow with wall thickness t_w. Any long-term σ'_{rc} gains due to corrosion will fall with increasing t_w and diameter D.

In summary, extensive field testing has been vital to establishing how the open micro-structures of low-to-medium density chalk lead to very low driving resistances, an extreme sensitivity to relative pile tip depth h/R and higher degrees of post-installation setup Λ than even sensitive low YSR clays, probably due to the chalk's anomalously low driving resistance and its relatively high field stiffness.

Consolidation appears to be the main cause of the marked short-term setup seen around low L_p/D piles, with the associated t_{95} dissipation times predicted from CPTu dissipation tests increasing, as for clays, with $[D^*]^2$. While relaxation of circumferential arching linked to creep probably also contributes to longer term setup, corrosion was proven explicitly to contribute significantly to long-term setup. Its relative impact at SNW was greatest with small diameter, high L_p/D, piles driven above the water table, but it also contributed to the setup of the larger diameter, mostly submerged, ALPACA Plus test piles.

The new ALPACA-SNW CPT-based calculation approach developed from the field research recognises the field trend for shaft capacities to be markedly higher in compression than in tension and anticipates that open steel piles work most effectively when driven to low chalk penetration L_p/D ratios.

The proposed method is able to capture, with an encouragingly low CoV, the wide range of resistances to driving and static testing shown after ageing by SNW piles with differing L/D, D/t_w ratios, both above and below the water table. It also offers encouragingly satisfactory predictions for an independent dataset of 14 submerged, near-offshore scale (0.61m ≤ D ≤ 1.8m), open-ended steel piles driven and tested in low-to-medium density northern European chalks.

3.3 *Piles driven in sand*

Recognition that conventional 'Main Text' API/ISO procedures offer poor predictive reliability for offshore piles driven at sand sites (Tang et al. 1990) led to extensive research into, and discussion on, how to develop better design methods. These included testing campaigns with ICP piles by Lehane (1992), Lehane et al. (1993) and Chow (1997) at the loose-to-medium dense Labenne and Dunkirk dense sand sites identified in Figure 24, whose ground profiles are illustrated in Figures 18 and 53. The short-term experiments at Labenne and Dunkirk showed modest setup, (with average Λ = 1.05 ± 0.03) over the up to 15-hour pauses imposed between installation and compression load testing. Overall, these campaigns proved five key findings:

- End bearing q_b and local shaft resistances τ_{rzf} are proportional to local CPT resistance q_t.
- Local τ_{rzf} and σ'_{rf} shaft stresses decline with relative pile tip position h/R at rates that exceed those found with clays.
- Local shaft failure obeyed the Coulomb law, as in Equations 1 and 10.
- The field δ' angles are critical state values that are (i) independent of relative density, (ii) decrease with d_{50} and (iii) can be predicted accurately by laboratory interface shear tests.
- Shaft capacity is ≈ 20% lower in tension than compression for closed ended piles.

Lehane et al. (1993) proposed that shaft failure conditions could be expressed by Equation 13:

$$\tau_{rzf} = [\, f_L\, \sigma'_{rc} + \Delta\sigma'_{rd}]\tan\delta' \tag{13}$$

Where σ'_{rc} depends on q_c, σ'_{v0} and h/R, f_L is unity in compression and 0.8 in tension. Their expression for σ'_{rf} includes a dilation component that varies inversely with D and directly with shear stiffness G, as in Equation 11, with $\Delta\sigma'_{rd} = 2\,G\Delta r/R$.

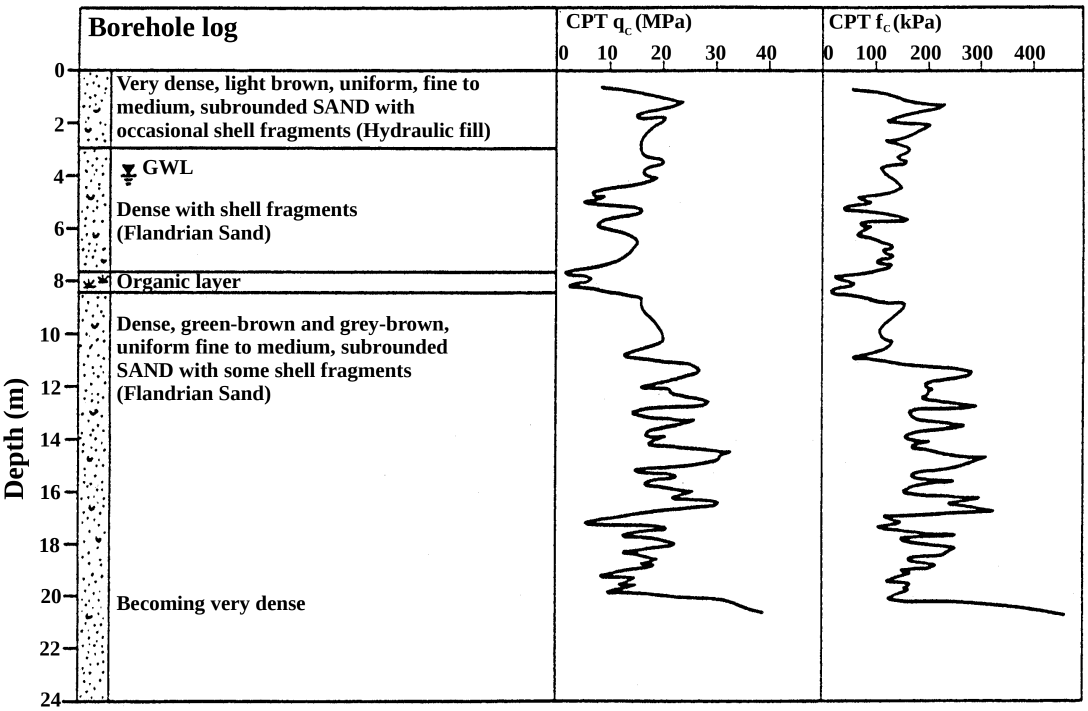

Figure 53. Ground conditions at Dunkirk, after Chow (1997).

Chow (1997) undertook further analysis of tests conducted nearby at Dunkirk with strain gauged open-ended piles driven by the French CLAROM group. Detailed interpretation of these tests allowed Chow to extend the ICP approach to cover open driven piles by proposing Equation 14 to predict σ'_{rc} (again with a lower h/R^* limit of 8).

Chow also proposed that the shear modulus G employed to evaluate $\Delta\sigma'_{rd}$ = $2\ G\Delta r/R$ (from Eq. 11), could be evaluated by estimating G from CPT q_t profiles, following Baldi et al. (1989), taking Δr as twice the pile shaft R_{CLA} (centre-line-average roughness) and a default Δr = 20μm. The dilative $\Delta\sigma'_{rd}$ term typically has a relatively minor effect for most industrial scale piles when tested at modest ages. A further reduction factor of 0.9 was introduced into Equation 13 for tension loading cases involving open ended piles and CPT-linked expressions were proposed for end bearing capacities that varied strongly with pile diameter D.

Chow (1997) tested the updated approach successfully against a mostly independent dataset collated from publications and industrial files. The resulting Jardine and Chow (1996) design guidance was applied by Shell UK and others to design piles for multiple offshore structures; see Overy (2007).

$$\sigma'_{rc} = 0.029 q_t [\sigma'_{v0}/P_a]^{0.13} (h/R^*)^{-0.38} \qquad (14)$$

The method was extended, with input from colleagues from Shell and Imperial College, as ICP-05 sand, which became (in an unfortunately incorrectly 'simplified' version) one of the four 'CPT-based' methods listed in the API (2014) commentary and related ISO documents. Ho et al. (2011) have since shown that that the δ' values of sands shearing against steel interfaces with the 10μm roughness of industrial piles range between 26° and 30° and show a weaker dependence on d_{50} than originally thought. Experience gained over decades of use has identified that ICP-05's expression for G is not applicable under all possible offshore conditions; Masters et al. (2017).

Also included in the API (2014) commentary was the UWA-05 method, proposed by Lehane et al. (2005), which employed an alternative 'effective base area' approach to cover open-ended piles and tested this against an updated pile test database.

The relative reliability of alternative CPT-based methods was re-assessed by Yang et al. (2016) against a further extended field test database which confirmed ICP-05 and UWA-05 as giving the best statistical fits. Noting that the spread of alternative approaches was found undesirable by pile designers, Lehane et al. (2017) undertook a collaborative data-centred study project, in which the Author participated. The team assembled a 'Unified database' of carefully quality-assured field test information. A calibration exercise followed that delivered a new 'Unified' design method that gave the best-fit to the agreed database. In this method σ'_{rc} is calculated as:

$$\sigma'_{rc} = \frac{q_c}{44} A_{re}^{0.3} \left[Max[1, (h/D)]\right]^{-0.4} \qquad (15)$$

where A_{re} is the effective area ratio of an open-ended pile, defined by Lehane et al. (2020) as *"the ratio of the displacement induced to that of a fully plugged pile"*, which depends on the final filling ratio (FFR) or the plug length ratio (PLR) as:

$$A_{re} = 1 - FFR \cdot (D_i/D)^2 \approx 1 - PLR \cdot (D_i/D)^2 \quad (16)$$

where D_i is the inner pile diameter. An approximate expression is recommended to estimate PLR in the absence of direct measurements. Shaft failure conditions are predicted by Equations 17 and 18, where factor f_L is unity in compression and 0.75 in tension.

$$\Delta\sigma'_{rd} = \left(\frac{q_c}{10}\right)\left(\frac{q_c}{\sigma'_v}\right)^{-0.33}\left(\frac{d_{CPT}}{D}\right) \quad (17)$$

$$\tau_{rzf} = f_L\,(\sigma'_{rc} + \Delta\sigma'_{rd})\tan\delta' \quad (18)$$

However, the Chow (1997), Lehane et al (2005), Yang et al. (2016) and Unified databases contained only one case with D > 0.81m. Apart from this Trans Tokyo Bay Highway (Shioi et al. 1992, Cathie et al. 2023) case, no other data existed, until recently, to test design method predictions against tests on offshore-scale piles.

3.3.1 *Recent research into pile ageing in sand*

One reason why predictions and measurements can vary greatly at sand sites is that driven pile shaft capacities vary significantly over time, as identified by by Tavenas and Audy (1972), Skov and Denver (1988), Bullock et al. (2005) and others.

The Author first encountered ageing in sand through re-testing open-ended steel piles that had been driven five years earlier at Dunkirk. The piles' remarkable tension capacity growth was documented by Chow et al. (1998) who considered the potential causes of the long-term setup.

As with clays and chalks, corrosion and sand grain bonding might lead to gains in Δr, σ'_{rf}, δ' and τ_{rzf} around mild steel piles. Chow (1997) undertook extended laboratory shear tests on Dunkirk sand against stainless steel interfaces with the typical R_{CLA} = 10 μm roughness of industrial steel piles. While their δ' angles did not change over 63 days under σ'_v = 300 kPa, the samples showed significant creep. The associated grain reorientation and flattening also led to 60% more dilation on shearing to failure than in short-term tests. Equations 11 and 18 predict that equivalent gains in Δr would boost σ'_{rf} and τ_{rzf}, especially around small diameter piles, whatever their shaft material.

Jardine et al. (2006) explored ageing behaviour further through staged tension tests on four 'virgin' 457mm OD, 19m long piles driven at Dunkirk, whose capacities primarily developed below the water table, supplemented by a 324mm OD, 21m long, neighbouring pile driven five years earlier. Karlsrud et al. (2014) reported two similar programmes in two sand deposits, including the relatively loose silty fluvial Larvik site at which CPTu tests indicated 1 MPa ≤ q_c ≤ 6 MPa in most layers. Six 508mm OD, 21.5m long, test piles were primarily submerged below the water table. Although the NGI's parallel tests at Ryggkollen showed similar capacity trends, full CPT probing was unfeasible in the gravelly sands. Comparable ageing tension tests were also undertaken by University College Dublin (Gavin et al. 2013) on 340 mm OD, 21m long open-ended steel piles that were driven entirely above the water table in dense sand derived from weathered limestone at Blessington, Ireland.

Instrumented driving data existed for Larvik and Dunkirk piles that, after averaging, allowed assessment of their end of driving resistances. One pile was also tested at Blessington within a day of driving.

Rimoy et al. (2015) and Gavin et al. (2015) brought the tests together in Figure 54, normalising their tension capacities by ICP-05 predictions and assuming zero setup over the first day. Given the considerable differences between the sites' conditions, the trends were remarkably similar, with EoD shaft resistances falling ≈30% below the predicted 'medium-term' capacities, which were typically achieved within 10 days. Shaft capacities continued to rise and after around 200 days reached values ≈2.5 times those predicted and then stabilised.

Re-tests showed that tension testing to failure damaged aged shaft capacity markedly and irrevocably disrupted setup.

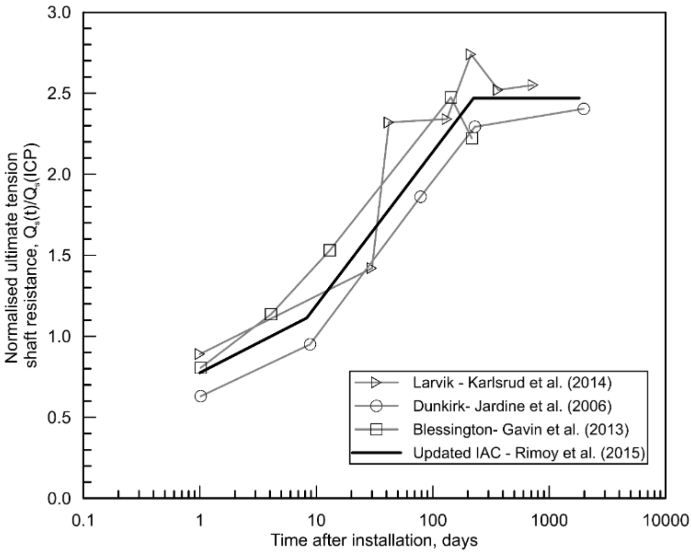

Figure 54. Variation of shaft tension capacity with age for 340 to 508mm OD steel piles driven at three sand sites, normalised by ICP-05 predictions, with intact ageing characteristic (IAC) defined by Jardine et al (2006). Capacities assumed constant over 1st day after driving, after Rimoy et al. (2015).

The key question was whether the trends illustrated in Figure 54 apply to large offshore piles. Jardine et al. (2015) reported encouraging early-age data from re-strikes conducted on 2.13m OD, 38.5m penetration, piles driven in dense sand at the Borkum Riffgrund German North Sea OWF substation jacket structure illustrated in Figure 55.

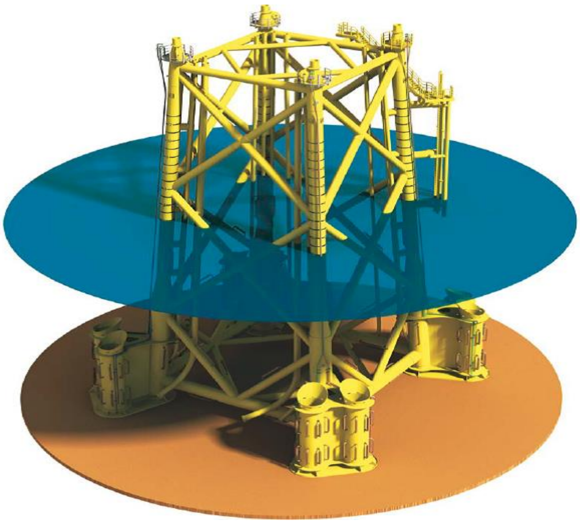

Figure 55. Borkum Riffgrund North Sea offshore substation jacket structure; Jardine et al. (2015).

Joint research projects in which the Author and his colleagues addressed whether the long-term ageing mechanisms vary systematically with diameter *D*, wall thickness t_w, length *L* (or their relative ratios) included: (i) experimental studies with Grenoble 3S-R into the micro-fabrics generated by pile installation (Yang et al. 2010), (ii) a field study with Grenoble 3S-R, NGI and UCD on driven micro-piles (Carroll et al. 2020), (iii) the 'PAGE' JIP database study of dynamic tests on full-scale, offshore pile with Cathie Group and GCG, London (Cathie et al. 2022) and (iv) experimental and numerical analysis studies with Grenoble 3S-R, Zhejiang University, University of Sydney and others into the stress regime applying around model displacement piles; see for example Yang et al. (2010), Jardine et al. (2013a, b), Yang et al. (2014), Zhang et al. (2014), Rimoy et al. (2015), Ciantia et al. (2019) or Jardine (2020).

We consider first the calibration chamber experiments conducted with the Grenoble 3S-R group, where 36mm OD, 1m long, stainless steel mini-ICP piles were jacked into pressurised, medium-dense to dense, Fontainebleau sand. These piles, which had the same local stress measurement capabilities as the field ICP shown in Figure 23, developed their full ICP-05 capacities by the end of their cyclically jacked installation. Despite varying many test factors, the piles showed no significant capacity growth over extended, fully pressurised, ageing periods.

Later sections consider the sand stress measurements made in these experiments and the degree to which they can be matched by numerical analysis. However, we focus first on the densification, grain breakage and other fabric features identified beneath and around model and field test piles.

3.3.2 *Studies of pile shaft shear zone fabric*

Yang et al (2010) describe the crushed sand annuli that developed around the mini-ICP shafts, whose thicknesses varied with d_{50} grain size. Their widths at given depths, grew from $\approx 2.4d_{50}$ just above the pile tip, as the tip advanced to greater depth, *h*, and grain crushing continued actively in the interface shear zone and reached maximum $\approx 10d_{50}$ widths after *h* exceeded 1m. Multiple 'Talysurf' shaft roughness measurements proved that interface shearing abraded 'high-spots' off the pile shafts, producing steel fragments that mixed in the sand and rendered its fine fraction susceptible to magnetic attraction.

Crusts of crushed sand were also found around the piles driven at Blessington (Gavin et al. 2013) and the 762mm OD open EURIPIDES test pile (Kolk et al. 2005). The oxic and anoxic corrosion reactions noted at clay and chalk sites appear equally active in sands; the EURIPIDES 'crusts' were cemented with iron hydroxides after extended ageing below the water table.

Rimoy et al. (2015) argued that because the annular thicknesses of the crushed sand annuli depended principally on d_{50} and *h* they represented a greater proportion of the mini-ICP piles' outside diameters than would apply to larger open-ended piles. Pile driving, pile tip geometry and the localised volume straining within the densifying shear zones might contribute to significantly different ageing behaviours between small model and larger diameter field piles.

Carroll et al. (2020) report on the interface fabric and steel roughnesses applying around mild steel micro-piles after driving and ageing in a corroding environment. Figure 56 shows the shafts of a 50mm mild steel pile (whose shaft capacity trends are discussed later) after a year of embedment at Dunkirk.

Figure 56. Open-ended mild steel 50mm OD micro-pile retrieved 2 years after driving above the water table, note ≈1mm thick adhered sand grain zone bonded with corrosion product.

The 2m OD open-ended steel piles driven at Dunkirk for the PISA programme (McAdam et al. 2020) at locations around 30m north of the micro-pile tests, offered another opportunity to examine the sand fabric. Figure 57 presents an example SEM image from Dr Livia Cupertino-Malheiros' study of samples taken above the water table from the crushed sand annuli 'crusts' that adhered to their shafts. The image, whose width is around 1.5 times the natural sand's d_{50}

≈0.26mm size, shows abundant crushed fine particles that are largely absent in the parent sand. Shaft abrasion sorts the grains, as in the classical particulate mechanics 'Brazil nut problem' (see for example van der Linden et al 2023) with fines migrating towards the shaft. Back-scattered analysis of 'bright-points' 17 to 19 in Figure 57 confirms iron (Fe) while the other particles are primarily silica with $CaCO_3$ fragments.

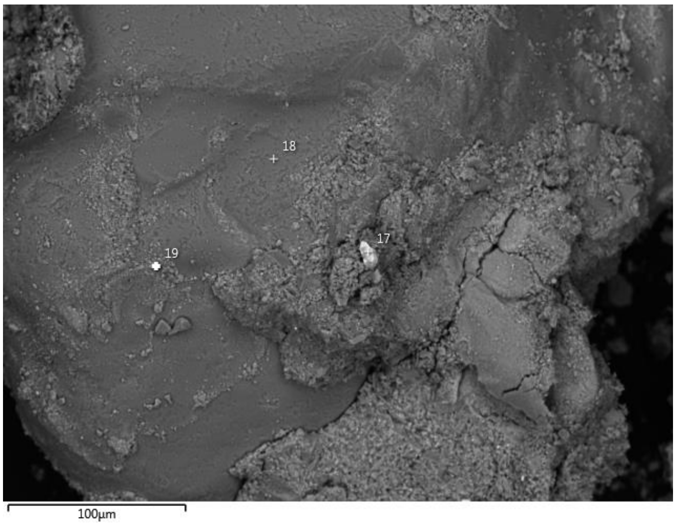

Figure 57. SEM image of partially crushed sand sampled from shaft of 2m OD PISA pile driven at Dunkirk. Bright spots 17 to 18 are iron rich. Note lower left 100µm scale.

Figure 58 offers a schematic illustration of the sand fabric around a 1mm length of steel shaft which integrates the above observations, considering a relatively early stage of the in-situ process. Corrosion products gradual fill the surrounding void spaces and bond with sand grains, rather than immediately forming isolated annuli and expanding out cylindrically, as interpreted earlier for finer grained clays and chalk.

The black colour of the exposed steel shown in Figure 56 suggests that conditions gradually become anoxic as corrosion progressed and its products restricted the supply of air to the shaft, leaving its surface reduced (and black) rather than 'rusty' and oxidised.

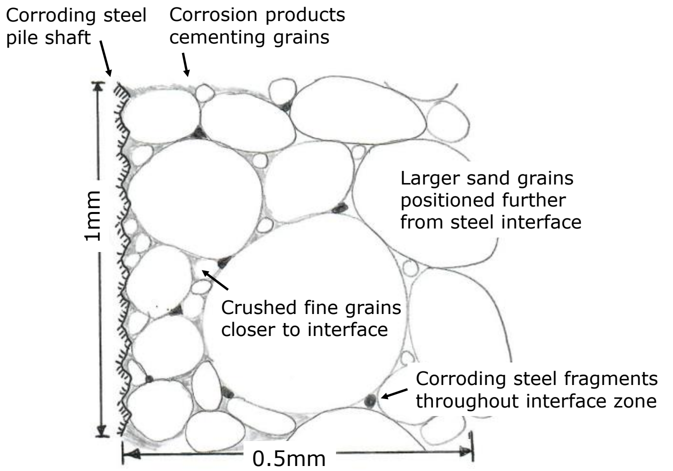

Figure 58. Schematic view of sand fabric close to shaft of ageing pile driven in sand.

3.3.3 *Micro-pile experiments*

One relatively inexpensive way of investigating scale effects is to drive and test micro-piles. Such field experiments provide an opportunity to check the potential role of corrosion and test to the extreme the predictions from Equation 11 (or 18) regarding the interface dilation components of shaft resistance.

Carroll et al. (2020) returned to the Larvik, Dunkirk and Blessington sites considered in Figure 54 and drove over fifty, around 2m embedded length, 50 to 60mm OD (with $6 \leq D/t_w \leq 25$) open mild (MS), stainless (SS) or galvanised (GS) steel piles which they tested in tension over the following 2 years. As expected, the micro-piles developed greater degrees of plugging, with 0.4 ± 0.2 plug length ratios (PLRs), far lower than recorded in larger piles driven at the same sites. While it was not feasible to monitor EoD driving resistances dynamically, loading tests were conducted at all sites between 2 hours and two days after driving. Marginal setup may have occurred over these intervals, as seen in the ICP sand site campaigns.

Figure 59 presents the micro-piles' test outcomes as Q_s^m/Q_s^{ICP} - ratios of the measured shaft capacities to those predicted by ICP-05 - along with the mean trend of the larger piles' from Figure 54. Part a) considers the loose silty Larvik sand cases, where MS piles gave $Q_s^m/Q_s^{ICP} = 0.23$ one day after driving.

SS piles with the same dimensions, and air-abraded to the same initial roughness, showed similar Q_s^m/Q_s^{ICP} ratios when tested 21 and 314 days after driving. The parallel tests on aged MS piles showed setup Λ (up to 2.09) and $Q_s^m/Q_s^{ICP} = 0.48$ after 313 days, while still later tests scattered around the same mean values over a further 380 days.

Carroll et al. (2020) report that the MS Larvik piles corroded readily as they aged in-situ in relatively low pH groundwater. Despite Equations 11 and 18 predicting that any linked growth in Δr would affect the small diameter micro-piles particularly markedly, their short long-term Q_s^m/Q_s^{ICP} ratios were far smaller than shown by the 508mm MS piles, as were their Λ values.

Over 80% of the ICP-05's prediction for the Larvik micro-piles' shaft capacities originates in the $\Delta\sigma'_{rd}$ interface dilation term; the Unified method anticipates a similar breakdown. While the true field split between the average $\Delta\sigma'_{rd}$ and σ'_{rc} contributions is unknown, the primary reason for the shaft capacities can only reside in ICP-05 greatly overpredicting the dilation component. Assuming that the ICP-05 σ'_{rc} predictions are representative, leads to an average EoD $\Delta\sigma'_{rd}/(\sigma'_{rc})^{ICP}$ ratio ≈0.28, rather than the predicted 4.6 ratio. It also indicates that the $(\sigma'_{rf} - \sigma'_{rc}{}^{ICP})/(\sigma'_{rc})^{ICP}$ rises over time through growth in $\Delta\sigma'_{rd}$ and/or σ'_{rc} to reach an upper limit of ≈1.7 over 10 months. Overall, the Larvik piles' long-term average field $\sigma'_{rf}/\sigma'_{rc}{}^{ICP}$ ratios could not exceed 2.7.

Figure 59b) considers the 51mm OD Dunkirk micro-piles in the same way. In this dense sand, the MS micro-piles' gave Q_s^m/Q_s^{ICP} = 1.71 within 2 hours of driving. The Unified predictions, which account more explicitly for the piles' partial plugging, led to $Q_s^m/Q_s^{\mathrm{Unified}}$ = 1.14. The MS piles' tension capacities rose gradually to reach stable Q_s^m/Q_s^{ICP} maxima ≈2.46 after around 6 months, similar to those of the 457mm OD piles, while showing significantly less setup.

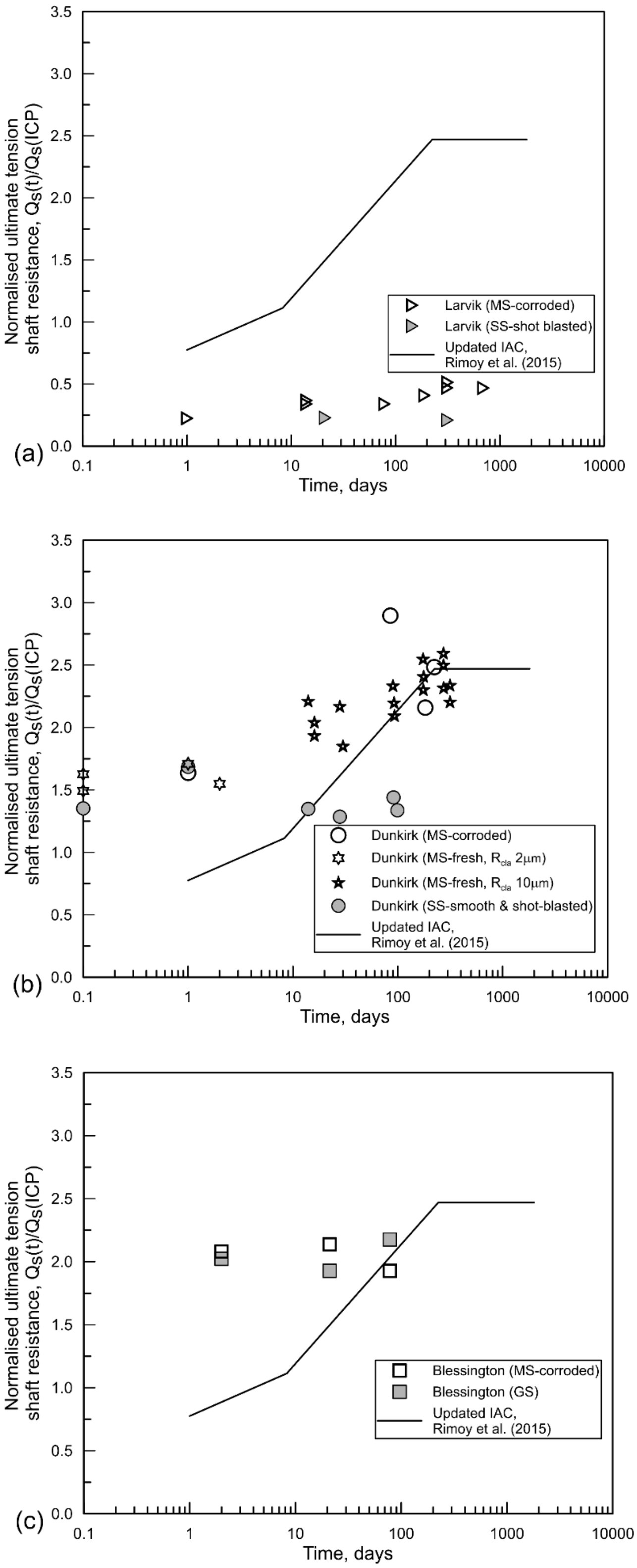

Figure 59. Normalised tension capacity trends for Galvanised (GS), Mild (MS) and Stainless (SS) steel micro-piles driven at Larvik (a), Dunkirk (b) and Blessington (c), compared with mean Figure 54 ageing (IAC) trend; after Carroll et al (2020).

The matching stainless steel (SS) piles gave similar 2-hour age capacities to the MS piles and no further change over the following months. Around 32% of the Dunkirk micro-piles' Q_s^{ICP} capacity estimate was related to the $\Delta\sigma'_{rd}$ term. Setting aside again any changes in δ', indicates an average $\sigma'_{rf}/(\sigma'_{rc})^{ICP}$ ratio ≈2.5 shortly after driving which grew towards a stable upper limit of ≈3.6 over the following six months.

The 60mm OD micro-piles initially proved difficult to drive in the dense Blessington sand. Changing to a greatly oversized hammer led to the MS and GS steel piles penetrating with large sets of around 60mm per blow. Low blow counts can boost subsequent static test capacity, see for example White and Lehane (2004), or Lim and Lehane (2014).

Part c) of Figure 59 presents the Blessington micro-piles' subsequent load test outcomes. The MS and GS micro-piles achieved similar Q_s^m/Q_s^{ICP} = 2.05 (and $Q_s^m/Q_s^{Unified}$ = 1.43) ratios within their first day. However, the tension capacities remained unchanged over the next four months for both pile types. In this case $\Delta\sigma'_{rd}$ contributed ≈26% of the Q_s^{ICP} prediction and the field $\sigma'_{rf}/(\sigma'_{rc})^{ICP}$ ratio was ≈2.8 within a day of driving. The Blessington MS micro-piles' static capacities followed stable flat-lines after this, despite active in-situ corrosion reactions.

The micro-piles' shaft capacities appear to be constrained at all ages by limiting radial effective stress conditions. It is proposed that these limits are controlled by the non-linear cylindrical cavity expansion mechanism applying around the pile shafts, which is controlled by the sand properties and post-driving effective stress fields. These limits apply from installation onwards and cap any gains that might develop in response to corrosion product growth or enhanced dilation. The field σ'_{rf} values, especially those applying to small diameter piles, may consequently fall far below those predicted from the linear elastic Equation 11.

Setting aside any parallel changes in δ' indicates that the average $\sigma'_{rf}/(\sigma'_{rc})^{ICP}$ ratios were limited to maxima of 3.2 ±0.4 at all three sites. Perhaps coincidentally, a similar ratio was inferred in Figure 38 from the suction measurements made around Canons Park Pile D after 17 years of ageing in London Clay. Applying $\sigma'_{rf}/(\sigma'_{rc})^{ICP} \leq 3.2$ while keeping δ' unchanged leads to $Q_s(t)/Q_s^{ICP}$ limits of 0.58, 2.18 and 2.37 for the Larvik, Dunkirk and Blessington piles respectively, which fall with ± 20% of the average maxima achieved in field tests at each site. This potential limit is explored further through numerical analysis in a later section.

The contrasting ageing behaviours of MS and SS piles at Larvik and Dunkirk proves that corrosion contributed greatly to in-situ ageing around steel piles whose end of driving $\sigma'_{rf}/(\sigma'_{rc})^{ICP}$ conditions did not approach the 3.2 ±0.4 limit, as they had at Blessington.

The crusts developed around mild steel piles through grain crushing and corrosion reactions (see Figures 56, 57 and 58) can also be expected to gradually push the shaft failure towards a soil-soil rather than interface shearing mechanism, so engaging critical state φ' rather than the sand-steel δ' angle. Any switch from critical state δ' to φ' might boost resistance by a modest ≈10% for typical silica sands and so reduce the $\sigma'_{rf}/(\sigma'_{rc})^{ICP}$ upper limit to ≈3. More significantly, the displaced mechanism would enhance the dilation associated with shaft loading to failure.

The absolute reliability of any 'dilation' measurements made in constant normal load or stiffness direct shear tests is limited by their marked stress non-uniformity; see Potts et al. (1987), or Shibuya (1997). However, direct and ring shear interface tests can identify key aspects of how dilation varies with interface roughness. Direct shear tests by Lings and Dietz (2005) showed a marked increase in dilative normal displacements once centre-line average (CLA) interface roughness R_{CLA} exceeded $d_{50}/10$, after which the surfaces become 'fully rough', and a shear banding mechanism developed within the sand mass. Lings and Dietz (2005) report that, under moderate pressures, their normal dilative displacements (equivalent to Δr adjacent to pile shafts) increased from magnitudes ≈$2R_{CLA}$ for partially rough interfaces to values comparable to the grain size, with a mean displacement of 1.75 ± 0.4 d_{50} that fell with increasing d_{50}.

Considering the $0.15 < d_{50} < 0.3$ ranges typical of North Sea sands, including those encountered at Dunkirk, only modest increases in R_{CLA} from the typical 10μm of industrial piles up to 15-30μm could be sufficient to achieve fully rough conditions and so boost dilative Δr displacements to the 0.2 to 0.6mm range.

The precepts of critical state soil mechanics (see for example Bolton 1986) indicate that dilative displacements should vary with the local levels of stationary (σ'_{rc}) radial effective stresses. However, the crushed sand annuli formed around the pile shafts are densely packed (see Yang et al. 2010 and Figures 56 to 58) and the local dilative $\Delta\sigma'_{rd}$ responses seen field tests on (unaged) ICP piles appear relatively insensitive to σ'_{rc} level; Lehane et al. (1993), Chow (1997). Any corrosion product growth that displaced the sand grains radially outwards, through a cavity expansion mechanism comparable to that identified for clays and chalk, would add to the overall radial displacement.

It is, however, important to re-emphasise that concrete driven piles also setup in sand; see Tavenas and Audy (1972), Axelsson (2000) or Rimoy et al. (2015). Steel corrosion cannot be the only ageing process at work in promoting enhanced dilation.

3.3.4 *Full-scale offshore pile setup*

Moving to the opposite end of the scale spectrum, the PAGE JIP explored the shaft capacities of large open steel piles driven at fully submerged offshore sand sites. Recognising the lack of static tests, Cathie et al. (2022) focused on collating from the offshore industry twenty-five, previously unpublished, pairs of dynamic tests on 1.37 to 3.35m (2.77m average) OD open-ended steel piles, with $8 \leq L/D \leq 53$ and 18 to 67 D/t_w ratios driven with known (large) offshore hydraulic hammers such as that depicted in Figure 60.

All piles were driven at well-characterised sites with mean relative densities ranging from 76 to 100%. The sand layers provided at least 75% of the shaft capacity at all but one of the test sites, for which a slightly lower proportion was accepted.

Figure 60. Typical offshore pile driving arrangements. Photograph courtesy of Mr P van Esch, Heerema.

The PAGE JIP also identified supplementary dynamic and static 'ageing' tests on 0.45 to 2.0m OD piles, driven mainly at onshore and nearshore sites, adding these to the Dunkirk and Larvik cases summarised in Figure 54.

Shaft capacity predictions were made for (i) all offshore cases with the ICP-05 and Unified CPT-based sand methods and (ii) all supplementary 'case studies' for which CPT profiles were available.

High-quality signals were available for all offshore cases from pile-mounted dynamic strain gauge and accelerometer sensors, along with corresponding Beginning of Restrike (BoR) measurements made at ages up to 374 days after driving. The PAGE team undertook careful quality-assured signal matching for all cases, including fully independent analyses by different teams employing either CAPWAP or IMPACT signal matching codes and different soil dynamic models.

Calibrated wave equation (WEAP) analyses were also undertaken for the subset of cases where BoR sets fell below the recognised minimum acceptable (3mm) set per blow. Independent EoD and BoR analyses were made for all of the supplementary test cases where reliable dynamic signal data was available, including the EURIPIDES and Trans Tokyo Bay (TTB) cases referred to earlier. Wen et al. (2023c) and Cathie et al. (2023a) report that broadly comparable static and dynamic shaft capacity trends emerged from these and other cases involving both types of measurement.

Figure 61 summarises the 25 piles' compression shaft capacity-time outcomes, normalised by predictions from ICP-05 and the Unified method in the upper and lower plots respectively. The EoD $Q_s(t)/Q_s^{ICP}$ ratios range from 0.3 to 1.1, with a 0.52 mean which falls below the ≈0.7 indicated for 340mm to 508mm OD piles in Figure 54, and far lower than indicated in Figure 59b) and c) for the 50mm to 60mm OD micro-piles driven in dense Blessington or Dunkirk sands. The average EoD $Q_s(t)/Q_s^{ICP}$ ratios appear to decline systematically with *D*. The aged BoR tests' $Q_s(t)/Q_s^{ICP}$ capacities scatter around the hyperbolic trend curve (see Cathie et al. 2022 for details) which tends, serendipitously, to unity after ≈20 days, indicating less long-term set up than the medium-scale piles in Figure 54.

The equivalent EoD mean $Q_s(t)/Q_s^{UNIFIED}$ ratio is 0.70 at EoD and rises to a steady long term 1.35. Scarfone et al. (2023) explore in greater detail the surprising and systematic difference between the CPT-based methods' predictions for offshore-scale piles.

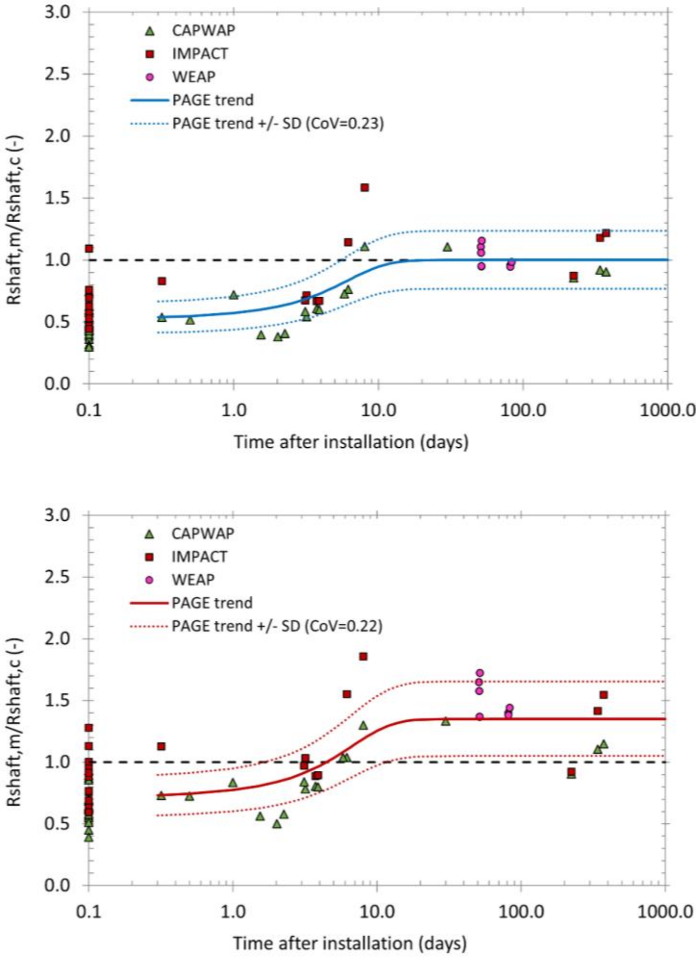

Figure 61. PAGE JIP outcomes: and shaft capacity-time data and hyperbolic trends for 25 offshore piles. ICP $Q_s(t)/Q_s^{ICP}$ sand ratios in upper plot, Unified $Q_s(t)/Q_s^{UNIFIED}$ sand ratios in lower.

The normalised offshore trends are compared in Figure 62 with dynamic and static data from the subset of supplementary cases with $D > 0.45$m and continuous CPT profiles. The two groups of tests show broadly comparable trends up to 20 days, after which the $Q_s(t)/Q_s^{ICP}$ ratios of piles with diameters ≤ 0.76m continues to climb above unity, while the 1.6m and 2.0m TTB shaft capacities fall closer to the lower 'offshore PAGE' plateau. The dynamic testing reported by Bhushan (2004) on 1.37m OD piles from the Los Angeles LAXT port project cannot be plotted in Figure 61 due to a lack of representative CPT data, but their long-term setup ratios fall relatively close to those of the large offshore piles; Cathie et al. (2022).

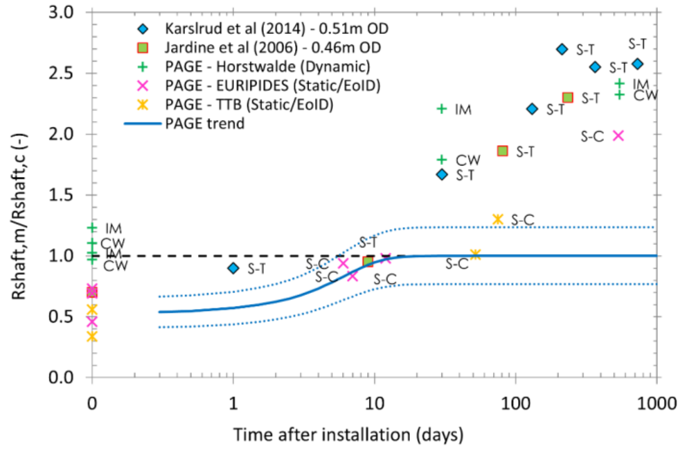

Figure 62. PAGE offshore $Q_s(t)/Q_s^{ICP}$-time trends from Figure 61 with Dunkirk (Jardine et al. 2006), Larvik (Karslrud et al. 2014), EURIPIDES (0.76m OD), Horstwalde (0.71m OD) and TTB (1.6 and 2.0m OD) cases: S = static (C compression, T tension); CW = CAPWAP and IM = IMPACT signal-matches.

It appears that at least two ageing processes are at work. One leads to significant setup for all piles over their first to 20th days after driving. The second leads to significant gains around the piles with D ≤ 0.76m but appears relatively ineffective around the large diameter onshore and nearshore piles.

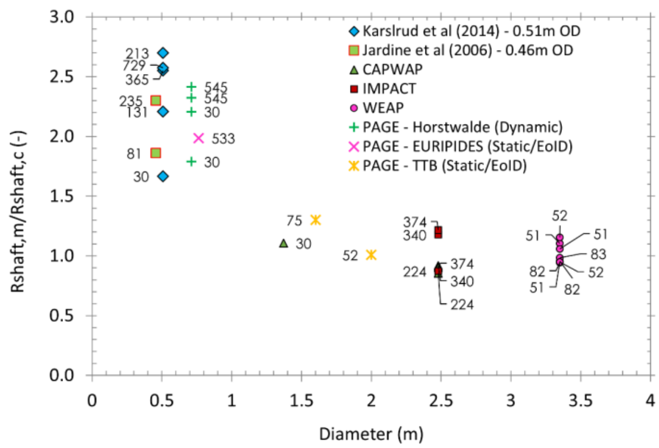

Figure 63. $Q_s(t)/Q_s^{ICP}$ trend with outside diameter for all PAGE supplementary cases with CPT records and large offshore piles tested at ages ≥ 30 days. Test ages shown in days.

The dependency of normalised aged shaft capacity on diameter is explored further in Figure 63, where the Q_s^m/Q_s^{ICP} measured at ages ≥ 30 days are plotted against OD. The piles' Q_s^m/Q_s^{ICP} ratios fall markedly with diameter, as well as growing with age up to the long-term (> 1 year) limits indicated in Figure 62.

Cathie et al. (2023b) explored these features further through a parametric study which adopted the mean geometry of the 25 PAGE offshore piles' (with L = 39.9m, D = 2.7m, D/t_w = 49.8) and its average (86%) relative density. They applied the Baldi et al. (1989) expressions to generate the corresponding 'typical' CPT q_c – depth profile, assuming OCR = 1. ICP-05 calculations were then run with total dilation Δr terms ranging from 0.04mm (double the ICP-05 default value) to 0.4mm, which falls towards the upper range discussed above as resulting from either the long-term corrosion or enhanced dilation mechanisms. Given that predictions are only offered for the average profile, the comparison is indicative rather than rigorously precise for each individual pile test.

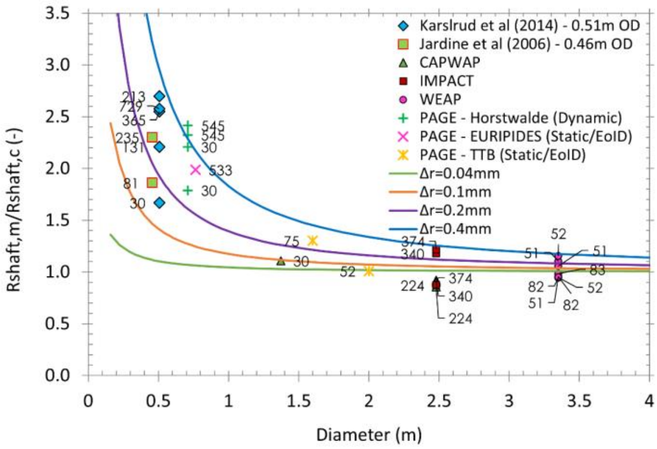

Figure 64. Hypothesised diameter-dependent Q_s/Q_s^{ICP} trends compared to PAGE JIP dataset of 14 offshore piles and 15 supplementary cases tested at ages ≥ 30 days, also showing test ages in days.

The parametric study results, plotted as compressive Q_s/Q_s^{ICP} ratios against D for each Δr case, are compared in Figure 64 with the combined PAGE dataset of 29 dynamic and static tests conducted at ages of 30 or more days. The family of theoretical curves spread widely at smaller diameters and tend to very high Q_s/Q_s^{ICP} ratios. However, adopting the proposed upper bound $\sigma'_{rf}/(\sigma'_{rc})^{ICP}$ = 3.2 limit inferred from the micro-pile tests limits Q_s/Q_s^{ICP} to a credible maximum ≈2.7 for all piles and caps the ratio for any case for which ICP-05 predicts mean $\Delta\sigma'_{rd}/\sigma'_{rc}$ > 0.25, including the micro-piles.

As indicated in Figure 62, the 0.45m ≤ D ≤ 0.71m pile test outcomes also correlate well with age. Tests conducted at ages less than 100 days tend towards the 0.04 and 0.1mm curves in Figure 64, while tests at ages greater than one year after driving scatter mainly between the Δr = 0.2 and 0.4mm theoretical curves. All four predicted curves tend to converge at large diameters to values slightly greater than the Q_s/Q_s^{ICP} = 1 asymptote identified in Figure 62.

It appears that the ICP-05 procedure may be modified to predict the shaft capacities developed by smaller piles with a wide range of diameters at ages greater than 30 days after driving in sand, by (i) imposing the proposed $\sigma'_{rf}/(\sigma'_{rc})^{ICP}$ ≤ 3.2 limit and (ii) substituting Δr values into Equation 11 that reflect site-specific estimates for corrosion and/or enhanced dilation; estimates could also be made through a suitably cautious interpretation of the correlation between Δr and age suggested by Figure 64.

However, for offshore piles driven with D > 2m it may be more representative to simply apply the unmodified ICP-05 method for all ages greater than 20 days after driving. While the offshore PAGE piles' showed shaft capacities that (on average) doubled within 20 days of driving, the available field data suggests that their setup is far slower at greater ages.

3.3.5 *The stress regime around piles driven in sand*

The setup trends identified from the largely uninstrumented pile load tests described above appear to be compatible with the hypothesis that an apparently diameter-independent stress redistribution mechanism leads to marked setup over the first 20 days around open driven piles (made from steel or concrete), after which a pile diameter-dependent mechanism becomes more important. The latter involves radial cavity expansion due to enhanced dilation and (for mild-steel piles) corrosion product growth.

This paper has emphasised the importance of seeking direct field measurements to support any such conjectures. As the ICP tests at Labenne and Dunkirk imposed only short ageing periods after installation, and showed only modest set-up, reliance has to be placed on other observations.

Gavin et al. (2012), (2015) summarise the mixed results obtained with various sensing systems in field studies reported by Ng et al. (1988), Axelsson (2000) and others who noted rises in σ'_{rc} around solid reinforced concrete piles (of modest scale) over more extended periods, as well as marked gains in the dilatant stress changes $\Delta\sigma'_{rd}$ developed during pile axial loading tests. However, Kirwan (2015) and Gavin and Igoe (2021) noted both σ'_{rc} gains and losses around field piles, as well as more impressive gains in the $\Delta\sigma'_{rd}$ components of shaft capacity.

It is important when considering these mixed data, to recall the great difficulties of measuring soil stresses accurately, especially in stress fields that have steep spatial gradients and extreme magnitude ranges, as develop around driven piles. This is even more difficult when the sensors have to be designed sufficiently robustly to withstand percussive impact driving.

Bond et al. (1991) and Jardine et al. (2009) describe the very stiff ICP surface 'pillar' stress transducers they developed to measure to σ'_r on jacked closed-ended piles, including the steps they took to enable cross-checking between independent systems. Zhu et al (2009) report the difficulties of making local stress measurements in sand masses with more conventional strain-gauged diaphragm cells, focussing on cell-action factors that may not always be appreciated. Representative sand mass calibration experiments with diaphragm cells indicate the normal stress versus micro-voltage output characteristics illustrated in Figure 65, where the μV outputs are normalised by the applied bridge input voltage V_{in}. While the cells manifest a conveniently linear response to primary loading, their responses to unloading and reloading are extremely hysteretic. Any given voltage output could signify a wide range of soil normal stresses, whose maxima and minima vary by a factor of up to 3 depending on the loading history, even when considering 'wished in place' sensor installation.

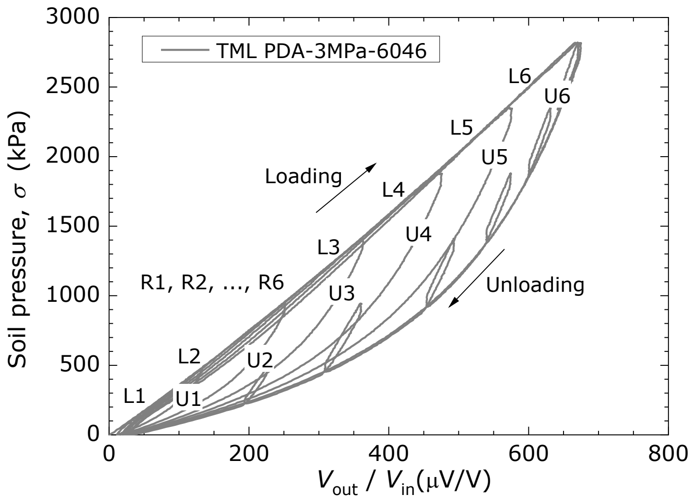

Figure 65. Calibration behaviour of strain- gauge diaphragm stress measuring cells; Zhu et al. (2009).

The cell's outputs are also insensitive to (i) any reductions in applied pressure after a prior loading stage and (ii) any subsequent increase in sand normal stresses that falls short of the maximum prior pressure. Zhu et al. (2009) describe how such hysteresis may be accounted for mathematically when employing diaphragm cells to examine the highly non-monotonic stress paths that around piles penetrating sand.

The Zhu et al. (2009) methodology was applied rigorously in analysing the Grenoble 3S-R calibration chamber experiments, where great emphasis was placed on measuring local stresses faithfully on the surface of the mini-ICP test piles and within the surrounding dense (air-pluviated) Fontainebleu NE34 sand. The piles were advanced by cyclic jacking into a sand mass that had sustained a 150 kPa vertical surcharge under K_0 conditions. Jardine et al. (2013a, b) showed from the local stress measurements that marked circumferential arching developed around the model pile shafts during installation.

Jardine (2020) summarised how the arching regime could be captured through both DEM analyses and representative large-displacement FEM and employing state-dependent elastic-plastic constitutive models that had been carefully calibrated to advanced soil element tests on NE34 sand by Andria-Ntoanina et al. (2010), Yang et al. (2010) and Altuhafi et al. (2018). Comparably close matches with the closed-ended mini-ICP test calibration chamber experiments have been obtained since with a wide range of numerical approaches in joint studies advanced with Zhejiang University (ZJU), as summarised by Xiao et al. (2023) and Ye et al. (2023).

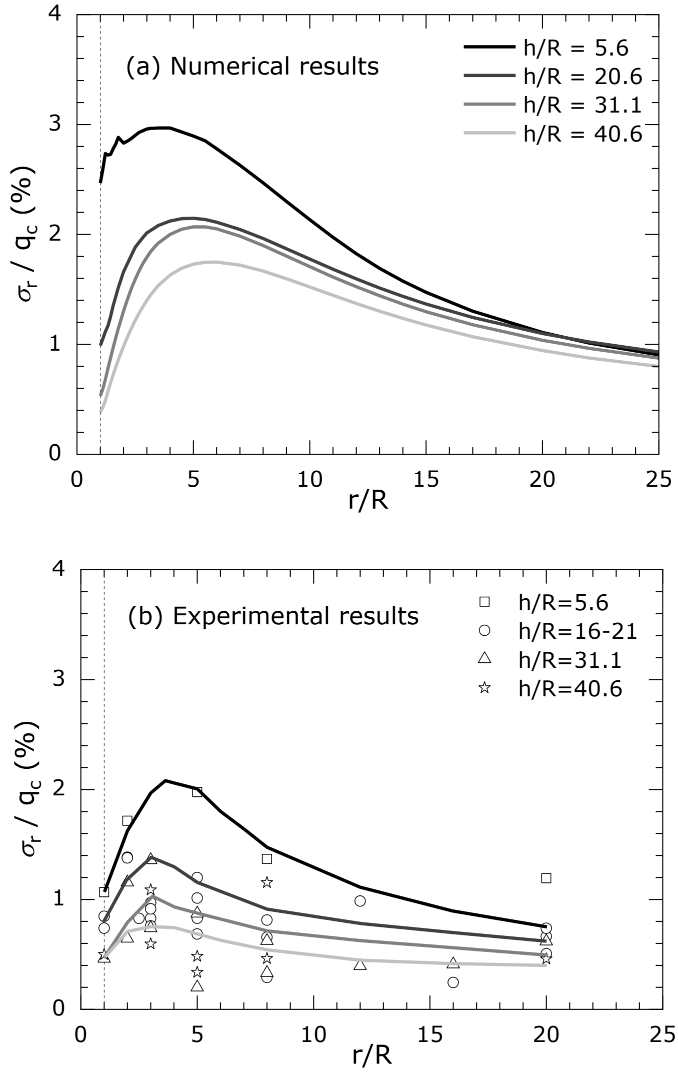

Figure 66. Normalised radial stress σ_r / q_c variation with normalised radial positions (*r/R*) and four heights above the pile tip (*h/R*): (a, above) PFEM predictions; (b, below) experiments from Jardine et al (2013a, b). Normalising CPT q_c values are from PFEM simulations; after Ye et al (2023).

Figure 66 compares, as one example, Ye et al.'s (2023) particle finite element method (PFEM) predictions with the calibration chamber experiments, showing how the local radial effective stresses (normalised by a PFEM predicted CPT q_c profile) varied with normalised height above the pile tip (*h/R*) and radial distance from the pile axis (*r/R*) at the end of installation by cyclic jacking. The sand mass radial stress maxima develop some radial distance out from the shaft. Pile installation leads to relaxation of the near shaft radial stresses through a primarily geometrical mechanism, rather than true 'frictional fatigue'.

While the experimental local radial stress measurements and numerical analyses identify an arching stress regime around the closed-ended jacked mini-ICPs, the 36mm OD calibration chamber test piles showed no significant setup over extended ageing periods, reflecting their corrosion resistant stainless-steel construction and installation by cyclic jacking.

Further research is required to consider the potential influences of other phenomena such as the sand's response to cyclic 'fatigue' loading during driving, grain breakage and flattening, as well as creep and shaft surface abrasion. These phenomena may affect the EoD stresses around open-ended piles and influence how they change over time, potentially in tandem with corrosion in cases that allow this to develop. Advancing such analyses may provide further evidence to support, or dismiss, the currently proposed hypothesis that medium-term stress re-distribution, followed by longer term radial expansion linked to enhanced dilation and steel corrosion, drives field setup, subject to limits on the radial stress growth that can occur related to the cylindrical cavity expansion limit pressures applying around pile shafts.

However, the numerical modelling approaches outlined above also provide a means to examine the proposed limiting cylindrical cavity expansion mechanism. Professor Yang and Rongrong Ye have kindly conducted a preliminary illustrative analysis at ZJU with the PFEM approach that was calibrated to laboratory tests on NE34 sand and gave the mini-ICP installation stress predictions shown in Figure 66.

They considered a mini-ICP pile at the end of its installation into a pressurized sand mass when, as in the Grenoble 3S-R calibration chamber tests, it had developed the stress regime illustrated in Figure 66a). They then expanded the pile radius incrementally. The numerical results are presented in Figure 67 in terms of the average normalised shaft radial stresses σ'_r/q_c plotted against $\Delta r/R$, where the maximum $\Delta r/R$ plotted corresponds to Δr = 1.8mm, exceeding the maximum radial expansion of ≈0.5mm expected around steel piles after 2 years of burial in the field.

While the predicted radial loading response only remains approximately linear up to $\Delta r/R$ ≈0.01, the σ'_r/q_c traces continue to rise in a non-linear fashion until they reach maxima at $\Delta r/R$ levels that increase with *h/R* from around 0.05 (or 0.9mm) for *h/R* up to 20.6 to 0.1 at h/R = *46.6*. Expanding a cylindrical cavity out from the displacement pile shaft invokes a non-linear radial effective stress response on the shaft that is clearly subject to limiting σ'^{max}_r/q_c values.

The predicted σ'^{max}_r/q_c ratios may be compared with the post-installation σ'_{rc}/q_c values shown on the pile shaft in Figure 66 to assess how the cavity expansion limit pressures limit the increases in σ'_{rc} or σ'_{rd} that might develop on the shaft due to stress redistribution, corrosion or enhanced dilation. The post-installation σ'_{rc}/q_c ratios fall from 2.4 to 0.4 with increasing *h/R* and have a simple average of 1.1, while the 'cavity expansion' analysis indicates σ'^{max}_r/q_c ratios that reduce more gently from 5.4 to 3.9 with increasing *h/R* and indicate a simple mean of ≈ 4.2. An average ratio of around 4 is therefore predicted between σ'^{max}_r/q_c and post-installation σ'_{rc}/q_c which is comparable to, but higher than, the $\sigma'_{rf}/(\sigma'_{rc})^{ICP} \leq 3.2$ field limit identified earlier from the open-ended micro-pile tests.

However, it is important to note that corrosion and dilation appear likely to generate smaller field radial displacements than were required to reach the maxima indicated by the PFEM analyses, which employed a relatively simple treatment of pre-failure stiffness that may have over-estimated the movements. In addition, the experimental and 'virtual' calibration chambers' diameters were 33.3 times those of the mini-ICP pile. Salgado et al. (1998) show that cylindrical cavity expansion conducted with such chamber dimensions over-estimate the response of equivalent unconstrained field pressuremeter tests due to the confining effects of the chamber's rigid radial boundary conditions. The model and field piles also had different pile-end conditions; these features all merit further exploration in future analyses.

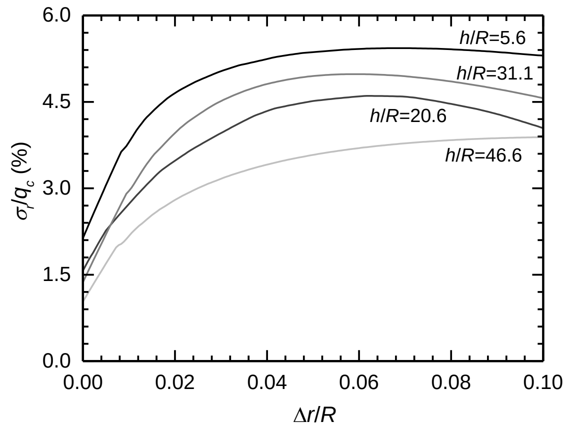

Figure 67. Normalised shaft radial effective stress σ'_r / q_c variation with cylindrical radial $\Delta r/R$ predicted by PFEM numerical analyses, considering four heights above the pile tip (*h*/*R*).

Undertaking fully representative analyses of open-ended piles remains a significant challenge; see for example Ko et al. (2016) or Staubach et al. (2022). Sun et al. (2023) have undertaken initial 3D modelling of open-ended steady pile penetration in sand, employing a high-performance graphics processing unit (GPU) and an accelerated DEM framework to make their DEM analyses practically feasible. Their initial analyses of idealised open-ended model piles appear to confirm that circumferential arching also develops around open piles, although it may be confined to a far smaller annular region (as expressed by its r/R limits) than around closed-ended piles.

3.3.6 *Setup mechanisms for piles driven in sand*

Considering the four setup mechanisms set out previously for clays and chalks, consolidation may be discounted as only being significant at sand sites immediately beneath advancing pile tips and over very short durations after driving: Cathie et al. (2020).

Moving to stress re-distribution mechanism, the calibration chamber experiments and numerical modelling both show that displacement pile installation generates a circumferential arching stress regime around pile shafts in dense sand. As with high φ' clays and chalks, redistribution leading to shaft radial stress increases over time through creep offers an attractive potential mechanism for the setup shown by concrete and steel piles over their first 20 days after driving in sand. This mechanism appears likely to be enhanced by low-level axial cyclic loading. However, the challenge of making reliable long-term shaft radial effective stress measurements on field-driven piles has limited, so far, any unequivocal experimental verification or falsification that this mechanism applies to large open-ended offshore driven piles.

Turning next to the potential roles of soil fabric and enhanced dilation, the laboratory and field and observations summarised above confirm that a densified crushed sand interface shear zone develops around pile shafts whose properties and stress state govern their axial resistance. Interface shear tests indicate that the dilative response to axial loading is likely to grow with time, even around chemically inert piles, as the grains creep, adjust and re-morph their contact force systems and shapes under load.

The products of any corrosion reactions are likely to further fill void spaces and so enhance the dilative behaviour, as well as expand out radially and force shaft shear failure towards soil-soil, rather than soil-steel mechanisms. These changes appear able to generate the 0.03 to 0.4mm radial movements required to explain the field piles' diameter-dependent long term ageing trends. The maximum radial stresses that can develop are, however, limited by a cylindrical cavity expansion mechanism which can be explored through representative numerical analysis.

Moving to consider chemical aspects, the tests on micro-piles made from different steels confirm that corrosion around mild steel pile shafts contributes significantly to their long-term setup, especially with small and medium scale piles.

3.3.7 Practical implications for sand sites

Three extensions are recommended to enable the ICP-05 to capture the diameter-dependent field setup trends of piles driven in sands.

- A cap is required to $\sigma'_{rf}/(\sigma'_{rc})^{ICP}$. While site-specific values can be made by representative numerical analyses, a default ratio of 3.2 is suggested.
- Predictions are needed for how the Δr values substituted into $\Delta\sigma'_{rd} = 2\,G\Delta r/R$ (Equation 11) vary over time. These could be gauged by modelling the given soil, and stress and chemical corrosion conditions etc. However, the trends plotted in Figures 62 to 64 suggest that at onshore test sites Δr may grow semi-logarithmically from 20 µm a few days after driving to perhaps 30 µm at 30 days and 0.3mm over the next two years. Ohsaki's (1982) data plotted in Figure 33 suggest that corrosion rates may slow sharply after this age. In addition, any time-dependent increases in the dilative Δr ial movements invoked by shaft shearing may cease or slow once a sand-sand mechanism is established.
- Finally, non-linear treatments may be required in place of Equation 8 for small diameter piles whose $\Delta r/R$ values exceed 0.01.

3.4 *Overall conclusions for driven piles*

Twelve key conclusions follow regarding piles driven in clays, chalk and sands.

1. Shaft resistance is fundamentally controlled by effective stress processes and a Coulomb failure law. The soil-to-interface δ' angles can be measured in appropriate ring-shear tests.
2. Driving generates potentially large excess pore pressures in clays and chalks. The shaft local radial effective stresses vary as the pressures equalise towards σ'_{rc} values that depend on the geomaterials' initial states, as represented by cone resistances q_t (or other laboratory measured parameters values for clays) as well as relative pile tip depth h/R^* or h/R and the sets per blow achieved during driving.
3. Piles of similar sizes driven at different sites, and with different diameters may show consolidation t_{95} times ranging from minutes to many years around large offshore piles driven in low permeability clays. CPTu dissipation tests give good indications of potential t_{95} durations for post-driving pore pressure dissipation.
4. The set-up values associated with the 'consolidation' stages of the considered dataset spanned from $\Lambda \approx 1.2$ with high YSR, insensitive clays to more than 4 for low-to-medium density chalks.
5. Other set-up processes can operate before or after full pore pressure equalisation that contribute significantly to the capacities predicted by practical axial capacity design methods. The short-to-medium term setup trends of low I_p, high φ' clay, chalk and sand sites are compatible with circumferential arching developing during driving and weakening over the following days and being potentially accelerated by low-level cycling.

6. Enhanced dilation also contributes to longer term setup around steel and concrete piles driven in sands, delivering sub-millimetre additional radial displacements Δr whose impact on shaft radial stresses (and capacity) reduce inversely with pile diameter D when $\Delta r/R$ is small and so have less impact with large offshore piles than with smaller piles, including as those employed in the considered onshore pile ageing research campaigns.
7. Corrosion also contributes to long-term setup for steel piles driven in all three geomaterials through reactions that become established within a few weeks of driving. The gains produced by radial 'cylindrical cavity expansion' are also expected to reduce with pile diameter.
8. Overall, the above setup processes lead to Λ ratios exceeding 3 for medium-scale piles (with 0.3m $\leq D \leq$ 0.7m) piles driven in sands. Long-term Λ values around 2 apply to large diameter (D > 2m) piles and similar, or lower factors, to piles with diameters less than ≈300mm.
9. Comparisons between field measurements and 'total-stress' Unified-CPT predictions in clays show a spread of outcomes, with some not being achieved before pore pressures equalize fully. ICP-05 clay method predictions showed less dispersion for the cases considered, with most predicted capacities being achieved within ≈6 months. However, the ICP-05 approach significantly over-predicts the capacities shown by piles driven in some low I_p, low YSR clays, even years after their installation.
10. The new ALPACA-SNW approach provides good predictions for driving and long-term axial resistances at chalk sites.
11. The ICP-05 sand method provided, at mainly dense sand sites, fortuitously good matches to the long-term capacities of offshore piles with D>2m, as assessed by field re-strikes. However, ICP-05 underpredicted the long-term capacities of most piles driven with D<2m, except for micro-piles (with D = 50mm) driven in loose sand.
12. Modifications are proposed that allow ICP-05 to capture more faithfully the time-dependent shaft capacity trends of piles with D<2m, driven in loose-to-very dense sands. These include imposing an upper limit on $\sigma'_{rf}/(\sigma'_{rc})^{ICP}$ and allowing for the additional outward radial displacements Δr developed along the pile shafts due to corrosion product growth in-situ and additional, age-enhanced, dilation occurring in response to shaft shearing.

Finally, although technically challenging and costly, well-executed and interpreted field tests may offer cost effective guidance for large projects sited in difficult ground conditions for which field experience is limited and pile capacities are uncertain. Barbosa et al (2017) and Shonberg et al (2023) attest to the considerable benefits that can flow in terms of reducing offshore windfarm project risks, pile and structural steel weights, installation costs and environmentally damaging noise, as well as embodied CO_2 tonnages.

Figure 68 illustrates the scale of engineering required to advance a recent highly instrumented, static and dynamic pile testing Taiwan Strait campaign successfully. A bespoke guide frame, which rested on three 5.5m OD suction buckets, is shown being lowered at the start of a campaign which characterized the axial capacity trends of six, 1.5m OD, up to 80m long, piles at two sites at three ages, in potentially problematic loose, possibly micaceous, Taiwan Strait sands, silts and low YSR, very low I_P clays. The testing also established the piles' field monotonic lateral and axial cyclic behaviour.

Figure 68. Deployment of suction-bucket supported pile guide frame required for driving of 1.5m diameter offshore piles in potentially loose Taiwan Strait sands, silts and low YSR very low I_P clays. Photograph courtesy of Ørsted.

4 Concluding remarks

This paper has considered the vertical bearing behaviour of shallow foundations and piles driven at clay, chalk and sand sites. It emphasised the strengths, when studying complex problems and natural geomaterials, of combining field experiments and full-scale monitoring with high quality site characterisation, element testing and representative numerical modelling.

The field, model and theoretical studies considered were selected to demonstrate under which circumstances ageing may: (i) enable optimized foundation design, (ii) allow greater-than-anticipated loads to be borne safely at later stages of service life and (iii) affect the procedures chosen for any final decommissioning uplift, pullout or push-over operations.

The observations reported in Part 1 for shallow foundations, and driven piles in Part 2, provide vital checks and benchmarks for modelling. They also identified important physical processes, that were broadly grouped under the headings of consolidation, creep straining, geomaterial micro-to-macro fabric and in-situ chemical reactions, that were shown to contribute to the time-dependent field bearing behaviour of offshore foundations.

Field tests such as those described provide highly valuable benchmarks against which design methods and alternative analyses may be tested. Advanced numerical analyses employing constitutive models calibrated to high quality stress-path triaxial tests were shown capable of matching key aspects of some long-term shallow foundation field tests accurately. Treatments were also proposed to model driven pile ageing processes. Further development is, however, necessary to enable reliable analyses of prolonged loading cases covering a wider range of foundation systems and geomaterial types.

5 Acknowledgements

The Author acknowledges gratefully the contributions made by many current and former colleagues, particularly Pedro Barbosa, Andrew Bond, Yves Canépa, Clive Dalton, Michael Harte, Gerwyn Price, Avi Schonberg, Kai Wen, Robert Whittle, Rongrong Ye and Drs Andrew Bond, Róisín Buckley, Pasquale Carotenuto, David Cathie, Livia Cupertino Malheiros, Christophe Dano, Roselyn Carroll, Fiona Chow, Liana Gasparre, Tingfa Liu, Robert Overy, Ross McAdam, Alastair MuirWood, Adam Pellew, Siya Rimoy, Felix Schroeder, Philip Smith, Fabian Schranz, Rui Silvano, Emil Ushev and Ken Vinck as well as Professors Byron Byrne, Pierre Foray, Ken Gavin, Barry Lehane, Stavroula Kontoe, Kenny Sorensen, Jamie Standing, Zhongxuan Yang, Lidija Zdravkovic and Bitang Zhu. The vital contributions made by technical staff at Imperial College and Socotec, particularly Steve Ackerley, Alan Bolsher, Angus Campbell, Graham Keefe and Steve Turner are also emphasized. Considerable engineering input by Aarsleff, Bilfinger, NGI and others was essential to the offshore testing. The Author also acknowledges the crucial funding that enabled the research. Recent grants include UK Innovate 101968, UK EPSRC EP/P033091/1 and UK Royal Society NA160438, as well as the National Natural Science Foundation of China (NSFC) project 52020105003. Industrial sponsors who made valuable practical and financial contributions to the most recent projects include Atkins, BP, Cathie Group, DEME Offshore, EnBW, Equinor, Fugro, GCG, Jan de Nul, Lankelma, LEMS, Ørsted, Parkwind, RWE, Siemens-Gamesa, Scottish Power Renewables, Van Oord and Vattenfall.

References

Addis, M. & Jones, M. (1990). Mechanical behaviour and strain rate dependence of high porosity chalk. In Chalk: Proc. International chalk symposium, Thomas Telford, London: pp. 239–244.

Albert, C., Zdravkovic, L. and Jardine, R.J. (2003). Behaviour of Bothkennar clay under rotation of principal stresses. Int workshop on Geotechnics of soft soils – theory and practice. Vermeer, Schweiger, Karstunen and Cudney eds. VGE, Essen. pp. 441-447.

Altuhafi, F., Jardine, R.J., Georgiannou, V.N., and Sim, W. (2018). Effects of particle breakage and stress reversal on the behaviour of sand around displacement piles. Geotechnique. 68 (6): pp. 546-555.

Amar, S., Baguelin, F., Canepa, Y., and Frank, R. (1985). Long term behaviour of shallow foundations: predictions and observations. Proc 11th ICSMFE, San Francisco, Pub. Balkema, Rotterdam. Vol 4, pp 2155-2158.

Amar, S., Baguelin, F., Canepa, Y., and Frank, R. (1994). Experimental study of the settlement of shallow foundations. Proc 13th ICSMFE, New Delhi, Pub. Balkema, Rotterdam. Vol 2, pp 623-626.

Andersen, K. H. (2015). Cyclic soil parameters for offshore foundation design. Third McClelland Lecture. Proc. Frontiers in Offshore Geotechnics III – Meyer (Ed.) Taylor & Francis Group, London, pp 5-82.

Andria-Ntoanina J, Canou J, and Dupla JC. (2010). Caractérisation mécanique du sable de Fontainebleau NE34 à l'appareil triaxial sous cisaillement monotone. Laboratoire Navier - Géotechnique (CERMES, ENPC/LCPC).

API (2014). American Petroleum Institute, ANSI/API recommended practice 2GEO. RP2GEO, 1st ed. API, Washington, D.C.

Argiolas, R. and Jardine, R.J. (2017). An integrated pile foundation re-assessment to support life extension and new build activities for a mature North Sea oil field project. Proc 8th Int. Conf. on Offshore Site Investigations and Geotechnics, SUT London. Vol. 2, p. 695-702. doi:10.3723/OSIG17.695

Axelsson, G. 2000a. *Long term set-up of driven piles in sand*, PhD Thesis, Dept. of Civil and Environmental Engineering. Stockholm: Royal Institute of Technology.

Baldi, G., Belotti, R., Ghionna, V.N., Jamiolkowski, M. and Lo Presti, D.L.F. (1989). Modulus of sands from CPTs and DMTs. Proc 12th Int. Conf. Soil Mech. and Foundation Engg. Rio de Janeiro, 1, pp 165-170.

Baligh, M. M. (1985). Strain Path Method. ASCE Journal of Geotech. Engng. 111 (9), pp 1108-36.

Barbosa, P., Geduhn, M., Jardine, R.J., Schroeder, F.C. & Horn, M. (2015). Offshore pile load tests in chalk. *Proc. 16th Eur. Conf. Soil Mech. Geotech. Eng.* Edinburgh, Scotland: ICE Publishing.

Barbosa, P.M., Geduhn, M., Jardine, R.J. & Schroeder, F.C. (2017). Large scale offshore static pile tests-practicality and benefits. *Proc. 8th Int. Conf. on Offshore Site Investigation and Geotechnics.* London, UK: Society for Underwater Technology.

Battacharya, S., Carrington, T. and Aldridge, T. (2009). Observed increases in offshore pile driving response. Proc ICE Geotechnical Engineering, 162, GE1, pp. 71-80. doi: 10.1680/geng.2009.162.1.71

Bialowas, G. A. (2017). Time and stress dependent mechanical properties of reconstituted chalk. PhD Thesis, University of Bristol.

Bodas Freitas, T.M., Potts, D.M. and Zdravkovic, L. (2015). Numerical study on the response of two footings at Bothkennar research site. Geotechnique, 65 (3): pp 155-168.

Bogard, D. and Matlock, H. (1998). Lateral Pressure Measurements During a 2.5 Year Period of Consolidation and Setup. *Proceedings*, 1998 Offshore Technology Conference, Houston, Texas, May 1998, Paper No. OTC 8765, pp 433-444.

Bolton, M.D. (1986). The strength and dilatancy of sands. Geotechnique. 36 (1), pp. 65-78.

Bond AJ. (1989). Behaviour of displacement piles in an overconsolidated clay. PhD Thesis, University of London, Imperial College.

Bond, A., Jardine, R. and Dalton, C. (1991). The design and development of the Imperial College Instrumented Pile. ASTM Journal of Geotechnical Testing, Vol 14, No 4, pp 413-424.

Bond A.J. and Jardine R.J. (1991). The effects of displacement pile installation in an overconsolidated clay. Geotechnique, Vol 41, No 3, pp 341-363.

Bond, A.J. and Jardine R. J. (1995). Shaft capacity of displacement piles a high OCR clay. Geotechnique, 45, No 1, pp 3-24.

Brosse, A. M., Jardine, R. J. & Nishimura, S. (2017). The undrained shear strength anisotropy of four Jurassic to Eocene stiff clays. Géotechnique 67, No. 8, pp 653–671

Buckley, R.M., Jardine, R.J., Kontoe, S. & Lehane, B.M. (2018a). Effective stress regime around a jacked steel pile during installation ageing and load testing in chalk. *Can. Geotech. J.*, 55, 1577-1591.

Buckley, R.M., Jardine, R.J., Kontoe, S., Parker, D. & Schroeder, F.C. (2018b). Ageing and cyclic behaviour of axially loaded piles driven in chalk. *Géotechnique*, 68**,** 146-161.

Buckley, R.M., Jardine, R.J., Kontoe, S., Barbosa, P. and Schroeder, F.C. (2020). Full-scale observations of dynamic and static axial responses of offshore piles driven in chalk and tills. Géotechnique, 70**,** 657-681.

Buckley R.M., Byrne, B.W., Jardine, R.J. and Turner, S. (2023). Large-scale pile testing research to advance offshore driven pile design. Keynote Paper. Proc. 9th Int. Conf. on Offshore Site Investigations and Geotechnics, SUT London.

Bullock, P.J., Schmertmann, J.H., McVay, M.C. and Townsend, F.C. (2005). Side shear setup II: Results from Florida test piles. J of Geotec, Geoenviron. Engng., ASCE, 131(3), 301-310.

Burland J.B., Burbidge M.C. (1984) *Settlement of foundations on sand and gravel*. Proc. ICE, Part 1, Dec. 1985, 78, pp 1325-1381.

Burland, J. B. (1990). On the compressibility and shear strength of natural clays. Rankine Lecture. Geotechnique 40, No. 3, pp 329-378

Butterfield, R. & Bannerjee, P. K. (1970). The effect of porewater pressures on the ultimate bearing capacity of driven piles. Proc. 2nd Southeast Asian Conf: Soil Mech. Fndn Engng, Singapore, pp. 385--394.

Bhushan, K, (2004). Design & installation of large diameter pipe piles for LAXT wharf. Proc. ASCE Conference in Honor of George G. Gobel, Los Angeles. https://doi.org/10.1061/40743(142)21

Byrne, B.W., McAdam, R.A., Burd, H.J. Houlsby, G.T., Martin, C.M. Beuckelaers, W.J.A.P, Zdravkovic, L., Taborda, D.M.G, Potts, D.M., Jardine, R.J, Ushev, E., Liu, T.F., Abadias, D., Gavin, K., Igoe, D., Doherty, P., Skov Gretlund, J., Pacheco Andrade, M., Muir Wood, A., Schroeder, F.C, Turner, S and Plummer, M. (2017) PISA: New Design Methods for Offshore Wind Turbine Monopiles. Keynote. Proc 8th Int. Conf. on Offshore Site Investigations and Geotechnics, SUT London. Vol. 1, pp. 142-161.

Canépa, Y. (1998). Le comportement des foundations superficielles sous charge constante - Analyse des données expérimentales; Application aux calculs des ouvrages. *LCPC CT24 – 2.24.19.4 - Dossier LREP 1.4.0.9889*, (in French) 104 p.

Canépa Y. and Garnier J. (2003). The behaviour of shallow foundations. Keynote. Proc. Fondsup 2003 International symposium on shallow foundations. Ed. J.P. Magnan and N. Dronuic, Pub. Presses des Ponts et Chausées, pp 1-102.

Carotenuto, P., Meyer, V., Strøm, P.J., Cabarkapa, Z., St. John, H. & Jardine, R.J. 2018. Installation and axial capacity of the Sheringham Shoal offshore wind farm monopiles – a case history. *Engineering in Chalk.* London, UK: ICE. pp. 117-122

Carroll, R., Carotenuto, P., Dano, C., Salama, I., Silva, M., Gavin, K. and Jardine, R.J. (2020). Field experiments at three sites to investigate the effects of age on steel piles driven in sand. Geotechnique. 70 (6), pp. 469-489.

Cathie, D., Jaeck, C., Ozsu, E. and Raymackers, S. (2020). Insights into the driveability of large diameter piles. Proc 4th Int. Symposium on Frontiers in Offshore Geotechnics, Austin, Texas, ASCE DFI Institute. Ed: Z.Westgate.

Cathie D., Jardine, R. J, Silvano, R., Kontoe, S. and Schroeder. F (2022). Pile setup in sand – the "PAGE" joint industry project. Proc. 11th International Conference on Stress Wave Theory and Design and Testing Methods for Deep Foundations. Rotterdam. Sept 2022. Pub. KVI, The Hague, The Netherlands. https://zenodo.org/record/7148625#.Y9eN7HbP2Ul

Cathie, D., Silvano, R., Zarouras, O., Prearo, C., Ozsu, E. and Jardine, R.J. (2023a). Pile setup in sand: analysis of the large diameter pile testing data from Trans Tokyo Bay Highway. 9th Int. Conf. on Offshore Site Investigations and Geotechnics, SUT London.

Cathie, D., Jardine, R.J., Silvano, R., Kontoe, S., Schroeder, F.C. (2023b). Axial capacity ageing trends of large diameter piles driven in sand. Submitted to Soils and Foundations.

Chandler R J, Crilly M S & Montgomery-Smith G. (1992). A low-cost method of assessing clay desiccation for low-rise buildings. *Proc. ICE*, 92 (2) pp 82-89.

Chow, F.C. (1997). Investigations into the behaviour of displacement piles for offshore foundations. PhD Thesis, University of London, Imperial College.

Chow F.C., Jardine, R.J., Brucy, F. and Nauroy, J.F. (1998). The effects of time on the capacity of pipe piles in dense marine sand. ASCE, JGE, Vol 124, No. 3, pp 254-264.

Ciantia, M., O'Sullivan, C. and Jardine, R. J. (2019). Pile penetration in crushable soils: Insights from micromechanical modelling. XVII European Conf. Soil Mech. and Geotechnical Engg. Reykjavik, Iceland. Pub. ECSMGE. ISBN 978-9935-9436-1-3, Vol 1. pp 298-317. doi: 10.32075/17ECSMGE-2019-1111

Ciavaglia, F., Carey, J. & Diambra, A. (2017). Time-dependent uplift capacity of driven piles in low to medium density chalk. *Géotechnique Letters*, 7**,** 1-7.

Clarke, J., Rigden, W.J. and Senner, D.W.F. (1985). Reinterpretation of the west Sole platform 'WC' pile load tests. Geotechnique, 35 (4), pp 393-412.

Clayton, C. R. I., Gordon, M. A. & Matthews, M. C. (1994). Measurements of stiffness of soils and weak rocks using small strain laboratory tests and field geophysics. In Pre-failure deformation of geomaterials (eds S. Shibuya, T. Mitachi and S. Miura), Rotterdam, the Netherlands: Balkema, pp. 229–234.

Clayton, C. R. I., Matthews, M. C. & Heymann, G. (2002). The chalk. In Characterisation and Engineering Properties of natural soils (eds T. S. Tan, K. K. Phoon, D. W. Hight and S. Leroueil), vol. 2, pp. 1402–1434. Rotterdam, the Netherlands: Balkema.

Clukey, E.C. (2022). The role of physical modelling in offshore geotechnical engineering. Proc. International Symposium on Frontiers in Offshore Geotechnics (ISFOG), Austin, Texas. Pub 2020 by US Deep Foundations Institute: https://www.proceedings.com/deep-foundations-institute-dfi 58p.

Cotterill, C., Dove, D., Long, D., James, L., Duffy, C., Mulley, S., Forsberg, C.F. and Tjelta, T.I. (2012) Dogger Bank – A Geo Challenge. Proc 7th Int. Conf. on Offshore Site Investigations and Geotechnics. SUT London, pp. 101-111.

Davis, E.H. and Booker, J.R. (1973). The effect of increasing strength with depth on the bearing capacity of clays. Geotechnique, 23 (4), pp 551-563.

Di Benedetto, H., Tatsuoka, F. and Lo Presti, D. (2005). Time effects on the behaviour of geomaterials. Deformation Characteristics of Geomaterials. Ed. Di Benedetto et al, CRC Press, London, pp 59-124.

Di Benedetto, H. (2015). Advanced Testing and modelling of granular materials with and without viscous glue: Research and practical implication. Third Bishop Lecture. Proc. 6th International Symposium on Deformation Characteristics of Geomaterials. Buenos Aires, IOS Press Amsterdam. Eds Rinaldi, VA; Zeballos, ME; Claria, JJ, pp 3-39.

Doughty, L.J., Buckley, R.M. and Jardine, R.J. (2018). Investigating the effect of ageing on the behaviour of chalk putty. Engineering in Chalk; Eds Lawrence, J.A, Preene, M., Lawrence, U.L. and Buckley, R. Pub. ICE London, pp. 695-702. doi/abs/10.1680/eiccf.64072.695

Durning, P.J., Rennie, I.A., Thompson, J.M. and Ruckstuhl, E.J. (1978). Installing a piled foundation in hard overconsolidated North Sea clay for the Heather platform. Proc. European Offshore Petroleum Conference. Pub. SPE, London, Vol 1., pp 375-382.

Erbrich, C.T, O'Neill, M.P, Clancy P. and Randolph, M.F. (2010). Axial and lateral pile design in carbonate soils. Proc. Frontiers in Offshore Geotechnics II – Gourvenec & White (eds). Taylor & Francis Group, London, pp. 125-154.

Evans, T. G. (2011). A systematic approach to offshore engineering for multiple projects in geohazardous areas. Proc. 2nd International Symposium on Frontiers in Offshore Geotechnics (ISFOG). Eds Gourvenec, S. and White, D. Pub. Tayor and Francis (London) pp. 3-32.

Fellenius, B.H., Harris, D.E. and Anderson, D.G. (2004), Static loading test on a 45m long pipe pile in Sandpoint, Idaho. Canadian Geotechnical. Journal 41, pp 613-628

Flaate, K. (1968). Baereeven av friksjonspeler i leire. Veglaboratatoriet (in Norwegian).

Gasparre, A. (2005). Advanced laboratory characterisation of London clay. PhD Thesis, Imperial College London.

GEO (2011). Geotechnical Data Report, GDR 18.0-005. Project No 32599 Fehmarnbelt, Advanced laboratory testing: Clays of Palaeogene origin. GEO Copenhagen. 46p.

Gavin, K.G., Igoe, D.J.P. and Kirwan, L., (2013). The effect of ageing on the axial capacity of piles in sand. Proc. ICE – Geotech. Eng. 166 (2), pp. 122–130.

Gavin, K., Jardine, R.J., Karlsrud, K. and Lehane, B.M. (2015) The Effects of Pile Ageing on the Shaft Capacity of Offshore Piles in Sand. Keynote paper. Proc. international Symposium Frontiers in Offshore Geotechnics (ISFOG), Oslo. CRC Press, London, Vol. 1, pp. 129-152.

Gavin, K. and Igoe, D. (2021). A field investigation into the mechanisms of pile ageing in sand. Geotechnique, 70 (2), pp. 120-131.

Gibbs, C., McAuley, J., Mirza, U. & Cox, W. (1993). Reduction of field data and interpretation of results for axial load tests of two 762 mm diameter pipe piles in clays. Large-scale pile tests in clay. Thomas Telford Publishing, London.

Gourvenec, S. (2020). Whole-life geotechnical design: what is it? What's it for? So what? And what next? Keynote paper. Proc. International Symposium on Frontiers in Offshore Geotechnics (ISFOG) 2022, Austin, Texas. In Press. p 41. Pub. 2020 Deep Foundations Institute: https://www.proceedings.com/deep-foundations-institute-dfi .

Hampson, K., Evans, T.G., Jardine, R.J., Moran, P., Mackenzie B. and Rattley, M.J. (2017). Clair Ridge: Independent foundation assurance for the capacity of driven piles in very hard soils. Proc 8th Int. Conf. on Offshore Site Investigations and Geotechnics, SUT London. Vol. 2, pp. 1299-1306. doi:10.3723/OSIG17.1299

Heerema E.P. (1980). Predicting Pile Driveability: Heather as an Illustration of the Friction Fatigue Theory. Ground Engineering, April 1980, pp. 15–37.

Heilmann-Clausen, C., Nielsen, O. B., & Gersner, F. (1984). Lithostratigraphy and depositional environments in the Upper Paleocene and Eocene of Denmark. Bulletin of the Geological Society of Denmark, 33, pp. 287–323.

Hight, D.W., Böese, R., Butcher, A.P., Clayton, C.R.I. and Smith, P.R. (1992). Disturbance of the Bothkennar clay prior to laboratory testing Geotechnique, 42 (2), pp. 199–217

Hight, D.W. and Higgins, K.G., (1995). Stiffness of hard soils and rocks in engineering applications. Proc 1st International Conference on Pre-failure Deformation Behaviour of Geomaterials. Sapporo, Japan, 1994, Eds S. Shibuya, T. Mitachi and S. Miura, Pub. Balkema, Rotterdam, Vol. 2, pp. 909-946

Hight, D.W., Gasparre, A., Nishimura, S., Anh-Minh, N., Jardine, R.J. & Coop, M.R. (2007). The London clay at T5: An overview of the characterisation study. Géotechnique, 57(1), pp. 3-18.

Hight, D.W., Paul, M.A., Barras, B.F., Powell, J. J.M., Nash, D.F.T., Smith, P.R., Jardine, R.J and Edwards, D.H. (2003). The characterisation of Bothkennar clay. Characterisation and Engineering Properties of Natural soils, Tan et al eds, Pub. Swets & Zeitlinger, Lisse, Netherlands, pp. 543-598.

Ho, Y.K., Jardine, R.J and Anh-Minh, N. (2011). Large displacement interface shear between steel and granular media. Geotechnique, Vol 61, No. 3, pp. 221-234.

Hosseini Kamal, R., Coop, M.R., Jardine, R.J. and Brosse, A. (2014). The post-yield behaviour of four Eocene-to-Jurassic UK stiff clays. Geotechnique. 64, No. 8, pp. 620–634.

Japsen, P. & Bidstrup, T. (1999). Quantification of late Cenozoic erosion in Denmark based on sonic data and basin modelling. *Bulletin of the Geological Society of Denmark*, Vol. 46, pp. 79–99. Copenhagen. https://doi.org/10.37570/bgsd-1999-46-08

Jardine, R. J., Symes, M. J. & Burland, J. B. (1984). The measurement of soil stiffness in the triaxial apparatus. Géotechnique 34, No. 3, pp. 323–340.

Jardine, R. J. (1985). Investigations of pile-soil behaviour, with special reference to the foundations of offshore structures. PhD thesis, University of London, (Imperial College).

Jardine, R. J., Brooks, N. J. & Smith, P. R. (1985). The use of electrolevel transducers for strain measurements in triaxial tests on weak rock. Int. J. Rock Mech. Min. Sci. & Geomech. Abstr. 22, No. 5, pp. 331–337.

Jardine, R.J. Potts, D.M. Fourie A.B. and Burland, J.B. (1986). Studies of the influence of non-linear stress-strain characteristics in soil-structure interaction. Geotechnique, 36 (3), pp. 377-396.

Jardine, R.J. and Potts, D.M. (1988). Hutton Tension Leg Platform foundations: an approach to the prediction of driven pile behaviour. Geotechnique, 38 (2) pp. 231- 252.

Jardine, R. J., St. John H. D., Hight, D. W. and Potts, D. M. (1991). Some applications of a non-linear ground model. Proc. 10th ECSMFE, Florence, Vol.1, pp. 23-228.

Jardine, R.J. and Smith, P.R. (1991). Evaluating design parameters for multi-stage construction. Geo-coast '91 Int. Conf., Yokohama, Port and Harbour Research Institute, Yokosuka, Vol 1, pp .197-202.

Jardine, R.J. (1992). Observations on the kinematic nature of soil stiffness at small strains. Soils and Foundations, Vol 32, No 2, pp. 111-124.

Jardine R.J. and Potts D.M. (1993). Magnus foundations: Soil properties and predictions of field behaviour. Proc. Conf. Large scale pile tests in clay. Thomas Telford, London, pp. 69-83.

Jardine, R. J., Lehane, B. M., Smith, P. R. and Gildea, P. A. (1995). Vertical loading experiments on rigid pad foundations at Bothkennar. Geotechnique, 45, No 4, pp. 573-599.

Jardine, R.J. and Chow, F.C. (1996). New design methods for offshore piles. MTD Publication 96/103, MTD, London.

Jardine, R.J. (2002). Stability and Instability: soft clay embankment foundations and offshore continental slopes. Keynote Paper. International Symposium on Coastal Geotechnical Engineering in Practice. Yokohama, Volume 2, Balkema, Rotterdam. Pp. 99-118.

Jardine, R.J, Gens, A., Hight, D.W. and Coop, M.R. (2004). Developments in understanding soil behaviour. Keynote paper. Advances in Geotechnical Engineering. Proc Skempton Memorial Conference. Pub Thomas Telford, London, pp. 103-207.

Jardine, R.J., Standing, J.R and Kovacevic, N. (2005a). Lessons learned from full scale observations and the practical application of advanced testing and modeling. Keynote paper, Proc International Symposium on Deformation Characteristics of Geomaterials, Lyon, Vol 2, pub Balkema, Lisse, pp. 201-245.

Jardine, R. J., Chow, F. C., Overy, R. F. & Standing, J. R. (2005b). ICP design methods for driven piles in sands and clays. Thomas Telford Ltd. London.

Jardine, R. J., Standing, J. R. & Chow, F. C. (2006). Some observations of the effects of time on the capacity of piles driven in sand. Géotechnique 55 (4), pp. 27–244.

Jardine, R.J., Zhu, B.T., Foray, P. and Dalton, C.P. (2009). Experimental arrangements for the investigation of soil stresses developed around a displacement pile. Soils and Foundations; Vol. 49, No 5. Pp. 661-673.

Jardine, R.J., Andersen, K. and Puech, A. (2012). Cyclic loading of offshore piles: potential effects and practical design. Keynote Paper. Proc 7th Int. Conf. on Offshore Site Investigations and Geotechnics, SUT London, pp 59-100.

Jardine R.J., Zhu B.T., Foray P., and Yang Z.X. (2013a). Measurement of stresses around closed-ended displacement piles in sand. Géotechnique, 63(1), pp. 1-17.

Jardine R.J, Zhu, B.T., Foray, P. and Yang, Z.X. (2013a) Measurement of Stresses around Closed-Ended Displacement Piles in Sand. Geotechnique 63 (1), pp. 1–17.

Jardine R.J., Zhu B.T., Foray P., and Yang Z.X. (2013b). Interpretation of stress measurements made around closed-ended displacement piles in sand. Géotechnique, 63(8), pp. 613-627.

Jardine, R.J., Brosse, A., Coop, M.R. and Hosseini-Kamal, R. (2015). Shear strength and stiffness anisotropy of geologically aged stiff clays. Proc. International Symposium on Deformation Behaviour of Geomaterials. Buenos Aires. IOS Press. Amsterdam. DOI: 10.3233/978-1-61499-601-9-156, pp. 156 – 191.

Jardine, R. J., Buckley, R. M., Kontoe, S., Barbosa, P. & Schroeder, F. C. (2018). Behaviour of piles driven in chalk. In Engineering in chalk: proceedings of the chalk 2018 conference (eds J. A. Lawrence, M. Preene, U. L. Lawrence and R. M. Buckley), pp. 33–51. London, UK: ICE Publishing.

Jardine, R.J. (2020). Geotechnics, Energy and Climate Change. 56th Rankine Lecture, Géotechnique. 70 (1), pp. 3-59.

Jardine, R.J., Buckley, R.M., Liu, T.F., Andolfsson, T., Byrne, B.W., Kontoe, S., J., McAdam, R. A., Schranz, F. and Vinck, K. (2023a). The axial behaviour of piles driven in chalk. Geotechnique. Published Ahead of Print. https://doi.org/10.1680/jgeot.22.00041

Jardine, R.J., Buckley, R.M., Liu, T., Byrne, B.W., Kontoe, S., McAdam, R.A., Schranz, F. and Vinck, K. (2023b). Driven pile behaviour in low-to-medium density chalk: the ALPACA JIP outcomes. 9th Int. Conf. on Offshore Site Investigations and Geotechnics, SUT London.

Jeanjean, P. (2017). A framework for monotonic p-y curves in clay. Keynote. Proc 8th Int. Conf. on Offshore Site Investigations and Geotechnics, SUT London. SUT London. Vol. 1, pp. 108-141.

Karlsrud K. and Haugen T. (1985). Axial static capacity of steel model piles in overconsolidated clay. Proc. 11th Int. Conf. Soil Mech. & Fdn Engng, San Francisco, 3, pp.1401-1406.

Karlsrud K, Nowacki F and Kalsnes B. (1993). Response in soft clay and silt deposits to static and cyclic loading based on recent instrumented pile load tests. In Society for Underwater Technology (SUT). Offshore Site Investigation and Foundation Behaviour. Dordrecht: Kluwer, pp. 549–584.

Karlsrud, K., Jensen, T.G., Lied, E.K.W., Nowacki, F., (2014). Significant ageing effects for axially loaded piles in sand and clay verified by new field load tests. Proc 46th Offshore Technology Conference, Houston, TX, USA, pp. 1–19.

Karstunen, M., Krenn, H., Wheeler, S.J., Koskinen, M., Zentar, R. (2005). Effect of anisotropy and destructuration on the behaviour of Murro test embankment, Int. Jnl. Geomechanics 5 (2), pp. 87-97.

Karstunen, M., Yin, Z.Y. (2010). Modelling time-dependent behaviour of Murro test embankment, Géotechnique 60 (10), pp. 735-749.

Kavvadas, M. (1982). Non linear consolidation around driven piles in clay. PhD Thesis, Massachusetts Institute of Technology.

Kirwan, L. (2015). Investigation into Ageing Mechanisms for Axially Loaded Piles in Sand, PhD Thesis, University College Dublin

Ko J., Jeong S. and Lee J.K. (2016). Large deformation FE analysis of driven steel pipe piles with soil plugging. Computers and Geotechnics 71: pp 82-97.

Kolk, H., Vergobbi, P., and Baaijens, A. (2005). Results from axial load tests on pipe piles in very dense sands: the EURIPIDES JIP, in: International Symposium on Frontiers in Offshore Geotechnics: ISFOG 2005, Perth, Pub Taylor and Francis, pp. 661-667.

Kovacevic, N., Hight, D.W. and Potts, D.M. (2007). Predicting the stand-up time of temporary London Clay slopes at Terminal 5, Heathrow Airport. Geotechnique. Vol. 67, No. 1, pp. 63-74.

Kovacevic, N., Jardine., R, Potts, D. Clukey, E. Brand, J.R. and Spikula, D. (2012). A numerical simulation of progressive slope failures generated by salt diaiprism combined with active sedimentation. Geotechnique. Vol. 62, No. 9, pp. 777-786.

Kuwano, R. and Jardine R.J. (2002). On measuring creep behaviour in granular materials through triaxial testing. Canadian Geotechnical Journal, Vol 39, No 5, pp. 1061-1074.

Kvalstad, T. J., Nadim, F., Kaynia, A. M., Mokkelbost, K. H. & Bryn, H. P. (2005). Soil conditions and slope stability in the Ormen Lange area. Mar. Petrol. Geol. 22, No. 1–2, 299–310.

Ladd, C.C. (1991). Stability evaluation during staged construction. 22nd Karl Terzaghi Lecture. ASCE Journal of Geotechnical Engineering. 117 (4), pp. 540-116.

Lambson, M.D., Clare, D.G., Senner, D.W.F. and Senner, R.M. (1993). Investigation and interpretation of Pentre and Tilbrook Grange soil conditions. Large-scale pile tests in clay. Thomas Telford Publishing, London.

Leddra, M. J., Jones,M. E. & Goldsmith, A. S. (1993). Compaction and shear deformation of a weakly-cemented, high porosity sedimentary rock. In The engineering geology of weak rock (eds J. C. Cripps, J. M. Coulthard, M. G. Culshaw, A. Forster, S. R. Hencher and C. F. Moon), Rotterdam, the Netherlands: Balkema. pp. 45–54.

Lehane, B.M. (1992). Experimental investigations of displacement pile behaviour using instrumented field piles. PhD Thesis. University of London, Imperial College.

Lehane, B.M., Jardine, R.J., Bond, A.J. and Frank, R. (1993). Mechanisms of shaft friction in sand from instrumented pile tests. ASCE Geot. Journal. Vol 119, No 1, pp. 19-35.

Lehane, B M, Jardine, R J, Bond, A J and Chow, F C (1994). The development of shaft resistance on displacement piles in clay. Proc. XIII ICSMFE, New Delhi, India, pp. 473-476.

Lehane, B M and Jardine, R J (1994a). Displacement pile behaviour in a soft marine clay. Canadian Geotechnical Journal, Vol 31 (2), pp. 181-191.

Lehane, B M and Jardine, R J (1994b). Displacement pile behaviour in glacial clay. Canadian Geotechnical Journal, Vol 31 (1), pp. 79-90.

Lehane B.M., Schneider J.A. and Xu X. (2005). CPT based design of driven piles in sand for offshore structures, GEO:05345, The University of Western Australia.

Lehane, B.M. and Jardine, R.J. (2003). Effects of long term preloading on the performance of a footing on clay. Geotechnique, 53, (8), pp. 689-697.

Lehane, B.M., Lim, J.K., Carotenuto, P., Nadim F., Lacasse, S., Jardine, R.J. and Dijk, B.F.J. (2017) Characteristics of unified databases for driven piles. Keynote. Proc 8th Int. Conf. on Offshore Site Investigations and Geotechnics, SUT London. SUT London. Vol. 1, pp. 162-194.

Lehane, B.M., Liu, L., Bittar, E., Nadim, F., Lacasse, S., Jardine, R.J., Carotenuto, P., Rattley, M., Jeanjean, P., Gavin, K., Gilbert, R., Haavik, J.B., Morgan, N. (2020). A new 'unified' CPT-based axial pile capacity design method for driven piles in sand. Proc. International Symposium on Frontiers in Offshore Geotechnics (ISFOG), Austin, Texas, pp. 462-477.

Leroueil, S., Lerat, P., Hight, D. W. & Powell, J. J. M. (1992). Hydraulic conductivity of a recent estuarine silty clay at Bothkennar. Geotechnique 42 (2), pp. 275-288

Liao, H. R. and Yu, H. S. (2005) Morphology, hydrodynamics and sediment characteristics of the Changyun Sand Ridge offshore Western Taiwan. Terrestrial Atmospheric and Oceanic Sciences 16(3), pp. 621-640.

Lim, J.K. & Lehane, B.M. (2014). Characterisation of the effects of time on the shaft friction of displacement piles in sand. *Géotechnique*, 64(6), pp. 476-485.

Lings, M.L. and Dietz, M.S. (2005). The peak strength of sand-steel interfaces and the role of silation. Soils and Foundations. 45 (6), pp. 1–14.

Liu, T.F, Ahmadi-Naghadeh, R., Vinck, K., Jardine, R.J., Kontoe, S., Buckley, R.M and Byrne, B.W. (2022). An experimental investigation into the behaviour of de-structured chalk under cyclic loading. Geotechnique; published Ahead of Print: https://doi.org/10.1680/jgeot.21.00199

Liu, T.F., Ferreira, P., Vinck, K., Coop, M.R., Jardine, R.J. and Kontoe, S.K., (2023). The behaviour of a low-to-medium density chalk under a wide range of pressure conditions. Soils & Foundations. Published online January 5th 2023. https://doi.org/10.1016/j.sandf.2022.101268.

Lord, J. A., Clayton, C. R. I. & Mortimore, R. N. (2002). Engineering in chalk, C574. London, UK: CIRIA.

Masters, T., Senthilkumar, M., Woodyard, G. (2017). Variations and Limitations of Curve Fitting Methods for Small Strain Shear Modulus in Sands Using the ICP Design Methodology. OSIG 2017, Society for Underwater Technology, London, UK, pp. 464-471.

McAdam, R.A., Byrne, B.W., Houlsby, G.T., Beuckelaers, W.J.A.P., Burd, H.J., Gavin, K.G., Igoe, D.J.P., Jardine, R.J., Martin, C.M., Muir Wood, A., Potts, D.M., Skov Gretlund, J., Taborda, D.M.G. and Zdravković, L. (2020). Monotonic laterally loaded pile testing in a dense marine sand at Dunkirk. *Géotechnique*, 70 (11), pp. 986-998.

McClelland, B. (1956). Engineering properties of soils on the continental shelf of the Gulf of Mexico. Proc 8th Texas Conf. on Soil Mechanics and Foundation Engineering. Bureau of Engineering Research, University of Texas, Austin.

Merritt, A., Schroeder, F., Jardine, R., Stuyts, B., Cathie, D., Cleverly, W. (2012) Development of pile design methodology for an offshore wind farm in the North Sea. Proc 7th Int. Conf. on Offshore Site Investigations and Geotechnics, SUT London, pp. 439-448.

Mesri, G., and Vardhanabhuti, B. (2006) Discussion of "Secondary Compression". ASCE Journal of *Geotechnical and Geoenvironmental Eng*., 132 (6), pp. 817-818.

Matthews, M. C. and Clayton, C. R. I. (2004). Large diameter plate tests on weathered in-situ chalk. Quarterly Journal of Engineering Geology and Hydrogeology, 37 (1), pp 61–72.

Moore, R., Usher, N. and Evans, T.G. (2007). Integrated multi-disciplinary assessment and mitigation of West Nile Delta geohazards. Proc 6th Int. Conf. on Offshore Site Investigations and Geotechnics. SUT London, pp. 33-42.

Mortimore, R. N. (2012). The 11th Glossop Lecture: making sense of chalk: a total-rock approach to its engineering geology. Q. J. Engng Geol. Hydrogeol. 45, (3), pp. 252–334.

Muir Wood, A., Mackenzie, B., Burbury, D., Rattley, M., Clayton, C. R. I., Mygind, M., Andersen, K. W., Le Blanc Thilsted, C., Liingaard M. C., (2015). Design of large diameter monopiles in chalk at Westermost Rough offshore wind farm. Proceedings of the 3rd International Symposium on Frontiers in Offshore Geotechnics (ISFOG 2015) Oslo, Norway: CRC Press, pp. 723-728.

Murff, J.D. (2012). 1st ISSMGE McClelland Lecture. Estimating the capacity of Offshore Foundations. Proc 7th Int. Conf. on Offshore Site Investigations and Geotechnics. SUT London, pp. 9-44.

Narayana, M. (2010). A study of the residual shear strength characteristics of remoulded UK mudrocks. MSc Dissertation. Imperial College, London.

Nash D. F. T., Sills, G. C. & Davison, L. R. (1992). One-dimensional consolidation testing of soft clay from Bothkennar Geotechnique 42 (2), pp. 241-256.

Ng, E., Briaud, J. L. & Tucker, L. M. (1988). Field testing of 5 axially loaded single piles in sand at Hunter's point, research report to FHWA. San Francisco, CA, USA: Geo Resource Consultants Inc.

Nicholson, D.P. and Jardine, R.J. (1981). Performance of Vertical drains at Queenborough bypass. Geotechnique, 31 (1), pp. 76-90.

Ohsaki, Y. (1982). Corrosion of steel piles driven in soils. Soils and Foundations. 22 (3), pp. 57-76.

Ove Arup and Partners (1986). Research on the behaviour of piles as anchors for buoyant structures. Dept of Energy, Offshore Technology Report, OTH 86 215. HMSO, London, 80pp.

Overy, R. (2007). The use of ICP design methods for the foundations of nine platforms installed in the UK North Sea. Proc 6th International Conference on Offshore Site Investigations

and Geotechnics. Society for Underwater Technology (SUT), London, pp. 359–366.
Panayides, S., M. Rouainia, and D. Muir Wood. 2012. Influence of degradation of structure on the behaviour of a full-scale embankment. Can. Geotech. J.49 (3), pp. 344–356.
Pedone, G., et al. (2023). Numerical modelling of laterally loaded piles drivin low-density fractured chalk. Computers and Geotechnics. January 2023, 18p. https://doi.org/10.1016/j.compgeo.2023.105252
Peire, K., Nonneman, H. and Bosschem, E. (2009). Gravity Base Foundations for the Thornton Bank Offshore Wind Farm. Terra et Aqua, 115, pp. 19-29
Pellew A. L., (2002) Field investigation into pile behaviour in clay. *PhD thesis*, Univ. London (Imperial College)
Pellew, A. and Jardine, R.J. (2008). Aged steel displacement and bored concrete piles in London clay. Proc 2nd Int Conf on Foundations. Dundee, Vol 1, pp 269-282. Eds. Brown, Bransby, Brennan and Knappet, Pub. IHS BRE Press, Bracknell.
PISA (2015). PISA Field Test Factual Report. Report No. 2260925.
Potts, D.M., Dounias, G.T., and Vaughan, P.R. (1987). Finite element analysis of the direct shear box test. Geotechnique, 37 (1), pp. 11-23. https://doi/10.1680/geot.1987.37.1.11
Ramsey, N., Jardine, R. J., Lehane, B. M. and Ridley, A. (1998). A Review of soil-steel interface testing with the ring shear apparatus. Int Conf on Offshore Site Investigations and Foundation Behaviour, SUT, London, pp. 237-258.
Randolph, M. F. (1993). Analysis of stress-wave data from pile tests at Pentre and Tilbrook. Large-scale pile tests in clay. Thomas Telford Publishing, London.
Randolph, M. F., Carter, J. P. & Wroth, C. P. (1979). Driven piles in clay-the effects of installation and subsequent consolidation. Geotechnique 29 (4), pp. 361-393.
Randolph, M.F. (2013). 2nd ISSMGE McClelland Lecture. Analytical Contributions to Offshore Geotechnical Engineering. Proc. 8th Int. Conf. on Soil Mechanics and Geotechnical Engineering, Paris, Eds Delage, P. et al., Vol 1., pp 85-106.
Rattley, M. J., Costa, L., Jardine, R. J. & Cleverly, W. (2017). Laboratory test predictions of the cyclic axial resistance of a pile driven in North Sea soils. Proceedings of 8th International Conference on Offshore Site Investigations and Geotechnics, Society for Underwater Technology (SUT), London, Vol. 2, pp. 636–643.
Ridgway, A.E. and Jardine R.J. (2007). A re-evaluation of driven pile capacities for sites involving low plasticity, low OCR clays. Proc. 6th Int Conf on Offshore Site Investigations, SUT London, pp. 347-358.
Rimoy, S.P, Silva, M. Jardine, R.J., Foray, P., Yang, Z.X., Zhu, B.T. and Tsuha, C.H.C. (2015). Field and model investigations into the influence of age on axial capacity of displacement piles in silica sands. Géotechnique 65 (7), pp. 576-589
Robertson, P.K., Sully, J.P., Woeller, D.J., Lunne, T., Powell, J.J., and Gillespie, D.G. (1992). Estimating coefficient of consolidation from piezocone tests. Canadian Geotechnical Journal, **29**: 539–550.
Robertson, P.K. 2009. Interpretation of cone penetration tests - A unified approach. Canadian Geotechnical J., 46 (11), pp. 1337-1355.
Salgado, R., Mitchell, J. K. & Jamiolkowski, M. (1998). Calibration chamber size effects on penetration resistance in sand. J. Geotech. Geoenviron. Engng ASCE 124 (9), pp. 878–888.
Scarfone, R. and Schroeder, F.C., Silvano, R. and Cathie, D. and Jardine, R.J. (2023). Divergence between CPT based method predictions for the axial capacities of large offshore piles driven in sand. Proc. 9th Int. Conf. on Offshore Site Investigations and Geotechnics, SUT London.
ScottishPower Renewables (2019). East Anglia Offshore One: Economic Impact of ICP-05 Design Method. Document EA1-ENG-T-IBR-032375 Rev1, February 2019.
Semple, R. M. and Gemeinhardt (1981). Stress history approach to the analysis of soil resistance to pile driving. Proc 13th Offshore Technology Conference, Houston, 1, pp. 165-172.
Sheil, B.B., McCabe, B.A., Hunt, C. and Pestana, J.M. (2014). A practical approach for the consideration of single pile and pile group installation effects in clay: Numerical modelling. Journal of Geo-Engineering Sciences 2. pp. 119–142.
Shibuya, S., Mitachi, T. and Tamate, S. (1997). Interpretation of direct shear box testing of sands as quasi-simple shear. Geotechnique 47 (4), pp. 769-790. https://doi/10.1680/geot.1997.47.4.769
Shioi Y, Yoshida O, Meta T, Homma M, (1992). Estimation of bearing capacity of steel pipe pile by static loading and stress wave theory (Trans-Tokyo Bay Highway). Application of Stress-Wave Theory to Piles, Eds Barends, Balkema, pp. 325–330.
Shonberg, A., Harte M., Jardine, R.J., Schroeder, F.C., Molyneaux, E.C.M. and Periklious, G. (2023). Full scale pile load testing for an offshore wind farm. Keynote Paper. Proc. 9th Int. Conf. on Offshore Site Investigations and Geotechnics, SUT London.
Skempton, A. W. (1970). The consolidation of clays by gravitational compaction. Q. J. Geol. Soc. 125, pp. 373- 411.
Skempton, A.W. (1986). Residual strength of clays in landslides, folded strata and the laboratory. Geotechnique, 35 (1) pp. 3-18.
Skov, R. and Denver, H. (1988). Time-dependence of bearing capacity in piles. Proc 3rd Int. Conf. on application of stress wave theory to piles. Ottowa, Canada, Editors Niyama, S. et al., pp. 879-888.
Smith, P.R. (1992). Properties of high compressibility clays with reference to construction on soft ground. PhD Thesis, University of London (Imperial College).
Smith P.R., Jardine R.J. and Hight, D.W. (1992). On the yielding of Bothkennar clay. Geotechnique, Vol 41 (2), pp 257-274.
Staubach, P., Machaček, J. Bienen, B. and Wichtmann, T. (2022). Long-term response of piles to cyclic lateral loading following vibratory and impact driving in water-saturated sand. ASCE J. Geotech. Geoenviron. Eng., 2022, 148 (11): 04022097. 17p.
Stock, P., McIntosh, W. and Jardine, R.J., (1992). Foundation monitoring of the Hutton TLP. Proc. Society for Underwater Technology, 3rd Int. Conf. on Offshore site investigations and foundation behaviour. Pub. Kluwer, Dordrecht, pp. 469-492.
Sun, M., Yang, Z.X., Guo, N. and Jardine, R.J (2023). Three-dimensional DEM simulation of plugging behaviour of small-diameter open-ended model piles penetrating into sand. 9th Int. Conf. on Offshore Site Investigations and Geotechnics, SUT London.
Taborda, D.M.G., Zdravković, L., Potts, D.M., Burd, H.J. Byrne, B.W., Gavin, K.G., Houlsby, G.T., Jardine, R.J., Liu, T., Martin, C.M. and McAdam, R.A. (2020). Finite element modelling of laterally loaded piles in a dense marine sand at Dunkirk. *Géotechnique*, 70 (11), pp. 1014-1029.
Tang, W.H., Woodford, D.L. and Pelletier, J.H. (1990). Performance reliability of offshore piles. Proc. 22nd Offshore Technology Conference; Houston, OTC 6379, pp. 299-308.
Tavenas, F. A. and Audy, R. (1972), Limitations of the driving formulas for predicting bearing capacities of piles in sand. Canadian Geotechnical Journal, 9(1), pp. 47-62
Tavenas, F. A. and Leroueil, S. (1980). The behaviour of embankments on clay foundations. Canadian Geotechnical J., Vol. 17 (2), pp. 236-260.
Teh, C.I., and Houlsby, G.T. (1991). An analytical study of the cone penetration test in clay. Geotechnique, 41 (1), pp. 17-34.

Ushev, E. and Jardine, R. J. (2022). The mechanical behaviour of Bolders Bank till. Canadian Geotechnical Journal, Published online 31st May 2022. http://dx.doi.org/10.1139/cgj-2021-0436.

van der Linden M.N, Everts, J.C., van Roij R. and van Blaaderen, A. (2023). Realization of the Brazil-nut effect in charged colloids without external driving. Proc National Academy of Sciences, 120 (9), e2213044120, https://doi.org/10.1073/pnas.2213044120.

Vinck, K., (2021). Advanced geotechnical characterisation to support driven pile design at chalk sites. PhD thesis, Imperial College London.

Vinck, K., Liu, T.F., Jardine, R.J., Kontoe, S., Ahmadi-Naghadeh, R., Buckley, R.M., Byrne, B.W., Lawrence, J., McAdam, R. A. and Schranz, F. (2022). Advanced in-situ and laboratory characterisation of the ALPACA chalk research site. Geotechnique; published Ahead of Print; https://doi.org/10.1680/jgeot.21.00197

Vinck, K., Liu, T.F., Mawcet, J., Kontoe, S. and Jardine, R.J. (2023). Field tests on large scale instrumented piles driven in chalk: results and interpretation. Canadian Geotechnical Journal. Ahead of Print: https://doi.org/10.1139/cgj-2022-0441.

Ward, W. H., Burland, J. B. and Gallois, R. W., (1968). Geotechnical Assessment of a Site at Mundford, Norfolk, for a large Proton Accelerator. Geotechnique, 18 (4), pp. 399-131.

Wardle, I.F., Price, G. and Freeman, T.J. (1992). Effect of time and maintained load on the ultimate capacity of piles in stiff clay. Piling: European practice and worldwide trends. Institution of Civil Engineers, London.

Wen, K., Kontoe, S., Jardine, R.J., Liu, T. and Pan. L (2023a). Non-linear finite-element analysis of axially loaded piles driven in chalk. Proc. 10th European Conference on Numerical Methods in Geotechnical Engineering, London.

Wen K., Kontoe, S., Jardine, R. J. and Liu, T. (2023b). A new load transfer model for axially loaded piles driven in chalk. Proc. 9th Int. Conf. on Offshore Site Investigations and Geotechnics, SUT London.

Wen, K., Kontoe, S., Jardine, R.J., Liu, T., Cathie, D., Silvano, R., Prearo C., Wei, S., Schroeder, F.C. and Stanislas, P. (2023c). Assessment of time effects on capacities of large-scale piles driven in dense sands. Published ahead of print. Canadian Geotechnical Journal, https://doi.org/10.1139/cgj-2022-0060.

White, D.J. and Lehane, B.M. (2004). Friction fatigue on displacement piles in sand. Geotechnique, 54 (10), pp. 645-658.

Whittle A.J. (1987). A constitutive model for overconsolidated clays with application to the cyclic loading of friction piles. PhD Thesis, Massachusetts Institute of Technology, 641pp.

World Forum Offshore Wind (2023). Global Offshore Wind Report 2022. https://wfo-global.org

Xiao, T., Guo, N., Yang, Z.X. and Jardine R.J. (2023). Two-dimensional numerical simulation of displacement pile-wall penetration using a coupled discrete element-finite difference method. 9th Int. Conf. on Offshore Site Investigations and Geotechnics, SUT London.

Yang, Z.X., Jardine, R.J., Zhu B.T., Foray, P. and Tsuha, C.H.C. (2010). Sand grain crushing and interface shearing during displacement pile installation in sand, Géotechnique, Vol 60, No 6, pp. 469-482.

Yang, Z.X., Jardine, R.J., Zhu, B.T. and Rimoy, R. (2014). The stresses developed around displacement piles penetrating in sand. ASCE J. Geotech. Geoenviron. Eng., 130 (3) pp. 04013027-1-13. DOI: 10.1061/(ASCE)GT.1943-5606.0001022

Yang, Z. X., Guo, W. B., Jardine, R. J. & Chow, F. C. (2016). Design method reliability assessment from an extended database of axial load tests on piles driven in sand. Can. Geotech. J. 54 (1), 59–74.

Yang, Z.X. (2023). Personal communication.

Ye, R.R., Yang, Z.X., Guo, N and Jardine, R.J. (2023). Numerical simulations of displacement pile installed in sand based on particle finite element method (PFEM). 9th Int. Conf. on Offshore Site Investigations and Geotechnics, SUT London.

Young, A.G. (2017). Understanding the full potential of an integrated geoscience study. 4th McClelland Lecture. Proc 7th Int. Conf. on Offshore Site Investigations and Geotechnics. SUT London, pp. 28-70.

Zhang, C. Yang, Z.X. Nguyen, G.D., Jardine, R.J. and Einav, I. (2014). Theoretical breakage mechanics and experimental assessment of stresses surrounding piles penetrating into dense silica sand. Geotechnique Letters Vol 4, January to March pp. 11–16, (DOI): 10.1680/geolett.13.00075.

Zdravković, L. and Jardine, R.J. (2001). The effect on anisotropy of rotating the principal stress axes during consolidation. Geotechnique, 51 (1), pp. 69-83.

Zdravković, L., D. M. Potts, and D. W. Hight. (2002). The effect of strength anisotropy on the behaviour of embankments on soft ground. Géotechnique 52 (6), pp 447–457.

Zdravković, L., Potts, D. M. & Jackson, C. (2003). Numerical study of the effect of pre-loading on undrained bearing capacity. ASCE Int. J. Geomech. 3 (1/2): pp 1–10.

Zdravković, L., Jardine, R.J., Taborda D.M.G., Abadias, D., Burd, H.J., Byrne, B.W., Gavin, K.G., Houlsby, G.T., Igoe, D.J.P., Liu, T, Martin, C.M., McAdam, R.A., Muir Wood, A., Potts, D.M., Skov Gretlund, J. and Ushev, E. (2020). Ground characterisation for PISA pile testing and analysis. *Géotechnique*, 70 (11), pp. 945-960.

Zhu, B., Jardine, R.J. and Foray, P. (2009). The use of miniature soil stress measuring cells in laboratory applications involving stress reversals. Soils and Foundations. Vol. 49, No 5. Pp. 675-688.

Zwanenburg, C. and Jardine, R.J. (2015). Full-scale loading, laboratory and in-situ testing to assess foundation stability on peat. Geotechnique 65 (4): pp. 309–326.